Mechanisms of memory consolidation

Analyzing the coordinated activity of concept neurons in the human medial temporal lobe during waking and sleep

Dissertation

zur

Erlangung des Doktorgrades (Dr. rer. nat.)

der

Mathematisch-Naturwissenschaftlichen Fakultät

der

Rheinischen Friedrich-Wilhelms-Universität Bonn

vorgelegt von

Johannes Niediek

aus

Bielefeld

Bonn 2018

Angefertigt mit Genehmigung der
Mathematisch-Naturwissenschaftlichen Fakultät der
Rheinischen Friedrich-Wilhelms-Universität Bonn

1. Gutachter: Prof. Dr. Dr. Florian Mormann
2. Gutachter: Prof. Dr. Horst Bleckmann
Tag der Promotion: 20. November 2018
Erscheinungsjahr: 2018

Summary

Memory consolidation is a process by which memories initially dependent on the hippocampus are transferred to cortical areas, thereby gradually becoming independent of the hippocampus. Theories of memory consolidation posit that memory traces encoding autobiographic episodes are rapidly formed in the hippocampus during waking, and reactivated during subsequent slow-wave sleep to be transformed into a long-lasting form. Concept neurons in the human medial temporal lobe (MTL) are neurons tuned to semantic concepts in a selective, sparse, and invariant manner. These neurons respond to pictures (or written/spoken words) representing their preferred concept (e.g., a person, an animal, an object), regardless of physical stimulus properties. Concept neurons have been speculated to be "building blocks" for episodic memory.

We used whole-night recordings from concept neurons in the MTL of epilepsy patients implanted with depth electrodes for presurgical monitoring to test the hypothesis that the coordinated activity of concept neurons during sleep is a neurophysiological correlate of memory consolidation in humans.

To conduct this study, we developed software methods for artifact removal and spike sorting of long-term recordings from single neurons. In an evaluation on both simulated model data and visual stimulus presentation experiments, our software outperformed previous methods.

Starting from the conceptual analogy between rodent place cells and human concept neurons, we developed an episodic memory task in which patients learned a story eliciting sequential activity in concept neurons. We found that concept neurons preserved their semantic tuning across whole-night recordings. Hippocampal concept neurons were inhibited in rapid-eye-movement (REM) sleep, but not in slow-wave sleep. The activity of concept neurons increased during ripples in the local field potential. Furthermore, concept neurons whose preferred stimuli participated in the memorized story were conjointly reactivated after learning, most pronouncedly during slow-wave sleep. Cross-correlations of concept neurons were most asymmetric during slow-wave sleep. Cross-correlation peak times were often in the range believed to be relevant for spike-timing-dependent plasticity. However, time lags of peak cross-correlations did not correlate with the positional order of stimuli in the memorized story.

Our findings support the hypothesis that concept neurons rapidly encode a memory trace during learning, and that the reactivation of the same neurons during subsequent slow-wave sleep and ripples contributes to the consolidation of the memory episode. However, the consolidation of the temporal order of events in humans appears to differ from what rodent research suggests.

The content of Chapter 3 of this thesis has been published as

J. Niediek, J. Boström, C. E. Elger, and F. Mormann (2016). *Reliable Analysis of Single-Unit Recordings from the Human Brain under Noisy Conditions: Tracking Neurons over Hours*. PLOS ONE 11 (12):e0166598.

Contents

Chapter 1

Introduction

1.1 Memory and the medial temporal lobe

We are able to recall events we experienced, even after decades: the formation and recall of autobiographic memories are among the most important and astonishing cognitive functions of our brains. The modern scientific study of memory arguably started with Hermann Ebbinghaus (1850–1909), who memorized lists of nonsense words to measure the speed of forgetting (Ebbinghaus 1885). Without today's terminology and without any reference to the brain, Ebbinghaus contemplated about the nature of voluntary memory recall: "[…] können wir […] die anscheinend verlorenen Zustände […] willkürlich reproducieren. […] es muss […] irgendwo und irgendwie noch vorhanden gewesen sein" ("[…] we can call back into consciousness […] the seemingly lost states. […] it must have been present somehow or somewhere"; Ebbinghaus 1885, pp. 1–2; translated 1913).

1.1.1 Classifying memory

Clearly, the unspecific term "memory" can refer to a number of different cognitive faculties (Roediger, Zaromb, et al. 2008). Psychologists have established two dimensions of classification for memory: The time span of memory decay, and the nature of the content being remembered. Three different time spans are commonly distinguished: *sensory memory* decays within fractions of seconds, *short-term memory* within seconds or minutes, and *long-term memory* after much longer times, or never. Shiffrin and Atkinson (1969) proposed a model outlining interactions between these different memory systems, see Fig. 1.1. *Short-term memory* is sometimes used interchangeably with *working memory*. More specifically, *working memory* was proposed as a system not merely for the short-term storage, but also for the modification and manipulation of memory contents

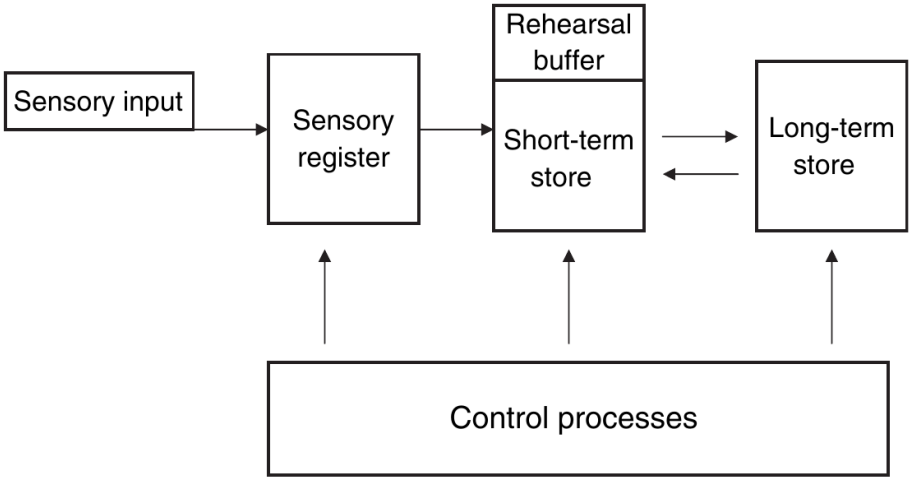

Figure 1.1: **Simple, abstract model of memory systems.** Horizontal arrows denote the flow of information ("copying" in the original presentation), vertical arrows denote processes such as attention, volition, etc., that act on the memory systems, as proposed by Shiffrin and Atkinson (1969). Drawing adapted from Roediger, Zaromb, et al. (2008).

(Baddeley and Hitch 1975; Baddeley 2001).

We will focus on long-term memory. When classifying long-term memory according to the nature of the memory content, two major types are commonly distinguished: *declarative* (or *explicit*) and *nondeclarative* (or *implicit*) memory (Ryle 1945; Graf and Schacter 1985; Squire and Zola-Morgan 1988). Declarative memory is memory for everything that can be explicitly expressed in language, while nondeclarative memory is a broad and heterogeneous category encompassing learned motor skills, habits, and other types of memory.

Further subdividing declarative memory, Tulving (1972) coined the terms *semantic memory* for facts we know (e.g., "Alexander Fleming discovered penicillin"), and *episodic memory* for events we experienced (e.g., a trip to the Sahara). Tulving's original definition of episodic memory reads: "Episodic memory receives and stores information about temporally dated episodes or events, and temporal-spatial relations among these events" (Tulving 1972, p. 385). This purely psychological definition does not involve the nervous system, and neither does it mention recall from memory. Informed by the course of neuroscientific findings (some of which we will discuss below), Tulving published refined definitions of episodic memory several times (Tulving 1985, 2002), mostly to promote the by now well-accepted view that episodic memory constitutes not only an abstract psychological concept, but a memory system of the (human) brain (Schacter and Tulving 1994; Nadel 1994). Following Tulving's most recent definition Tulving (2002, p. 5), we characterize episodic memory as

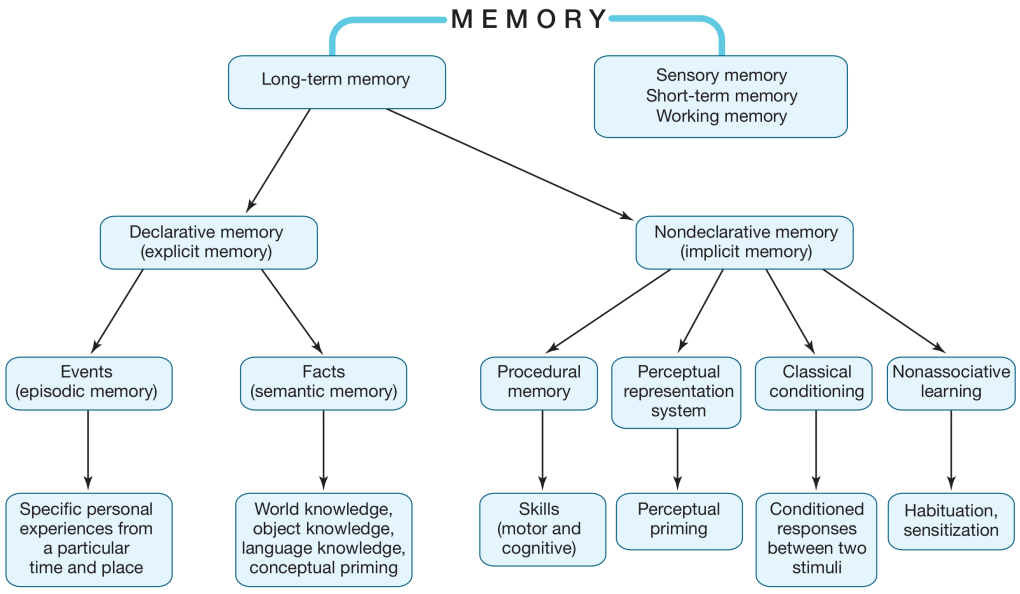

Figure 1.2: **"Tree of memory terms".** The top tier classifies memory according to the relevant time scale, and the second and third tiers classify long-term memory according to its content. The terms *explicit* and *implicit* were introduced by Graf and Schacter (1985), and the term *declarative* was proposed by Cohen and Squire (1980). A tree as the one presented here was first given by Squire and Zola-Morgan (1988). Reproduced from Gazzaniga, Ivry, et al. (2013, p. 381).

> "a recently evolved, late-developing, and early-deteriorating past-oriented memory system, more vulnerable than other memory systems to neuronal dysfunction, and probably unique to humans. It makes possible mental time travel through subjective time, from the present to the past, thus allowing one to re-experience, through autonoetic awareness, one's own previous experiences."

The different forms of memory introduced here are often organized as a tree (see Fig. 1.2). Although this "tree of memory terms" is meaningful even without reference to the brain, its development was largely influenced by clinical and neuroscientific observations (Squire and Wixted 2011).

1.1.2 Neuroscientific approaches to the study of memory

Neuroscientific investigations of declarative memory started with the report by Scoville and Milner (1957) on a case of complete anterograde amnesia after bilateral resection of large parts of the medial temporal lobe (MTL; see Figs. 1.3 to 1.6 and 1.8 for an outline of the relevant anatomy). *Anterograde amnesia* is an impairment of the ability to acquire new declarative knowledge with otherwise normal intellectual capabilities. The patient de-

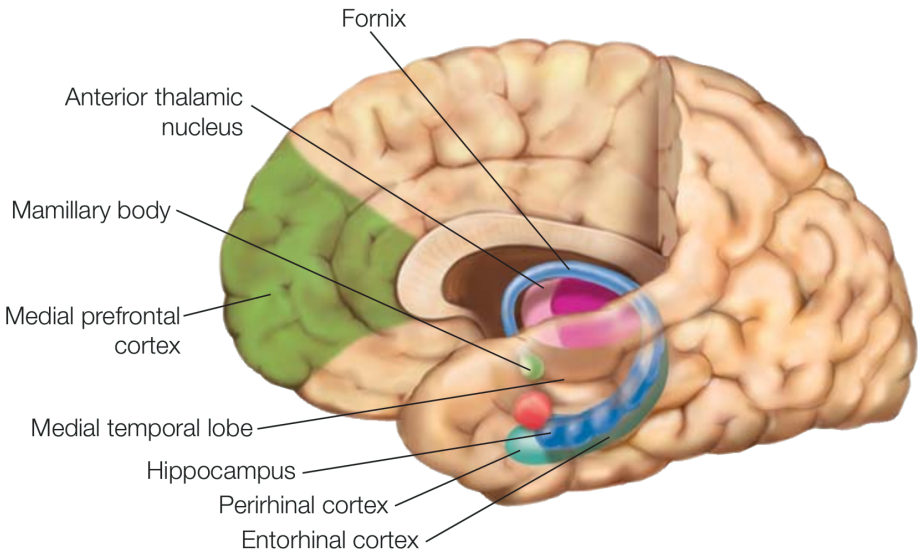

Figure 1.3: **Position of the hippocampal formation within the medial temporal lobe.** Following the terminology of Amaral and Lavenex (2007), we use the name *hippocampal formation* for the hippocampus proper together with the dentate gyrus, subiculum, and entorhinal cortex. The hippocampal formation is crucial for declarative memory. Virtually all information going from cortical regions to the hippocampus (and vice-versa) passes through the entorhinal cortex. Reproduced from Gazzaniga, Ivry, et al. (2013, p. 382).

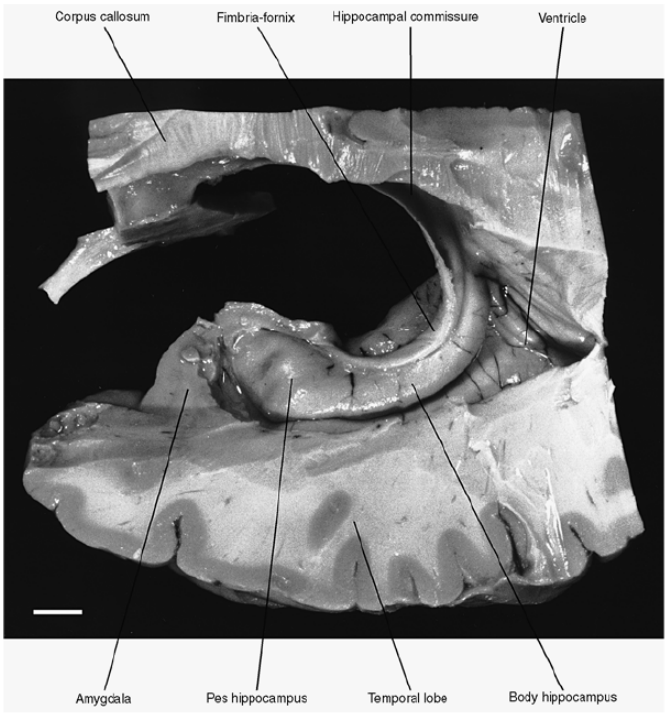

Figure 1.4: **Photography of the human hippocampus in its position in the medial temporal lobe.** Hippocampus literally means sea horse, a name chosen because of its outer appearance. The length of the white bar is 1 cm. Reproduced from Amaral and Lavenex (2007, p. 41).

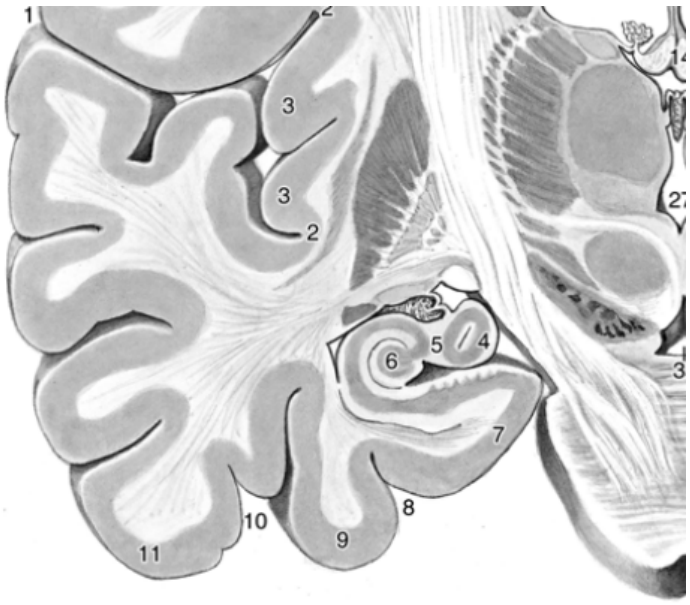

Figure 1.5: **Drawing of a coronal section through the temporal lobe.** The relevant structures are 6, dentate gyrus of the hippocampal formation; 7, parahippocampal gyrus. Reproduced from Nieuwenhuys, Voogd, et al. (2007, p. 146).

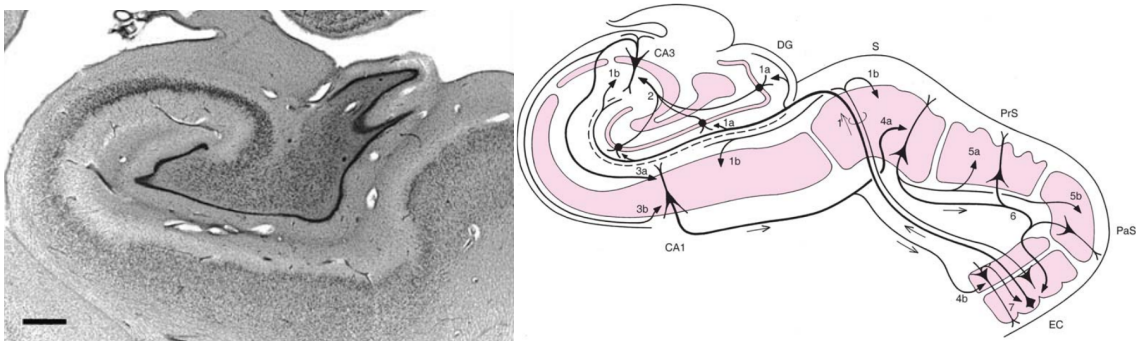

Figure 1.6: **Nissl stained section and drawing of the hippocampal formation. Left:** The systematic regional variation in density of neuronal cell bodies is visible. The length of the bar is 1 mm. Reproduced from Amaral and Lavenex (2007, p. 40). **Right:** Intrinsic connections of the hippocampal formation, see Fig. 1.8 for details. DG, dentate gyrus; EC, entorhinal cortex; PrS, presubiculum; PaS, parasubiculum; Sub, subiculum. Reproduced from Nieuwenhuys, Voogd, et al. (2007, p. 376).

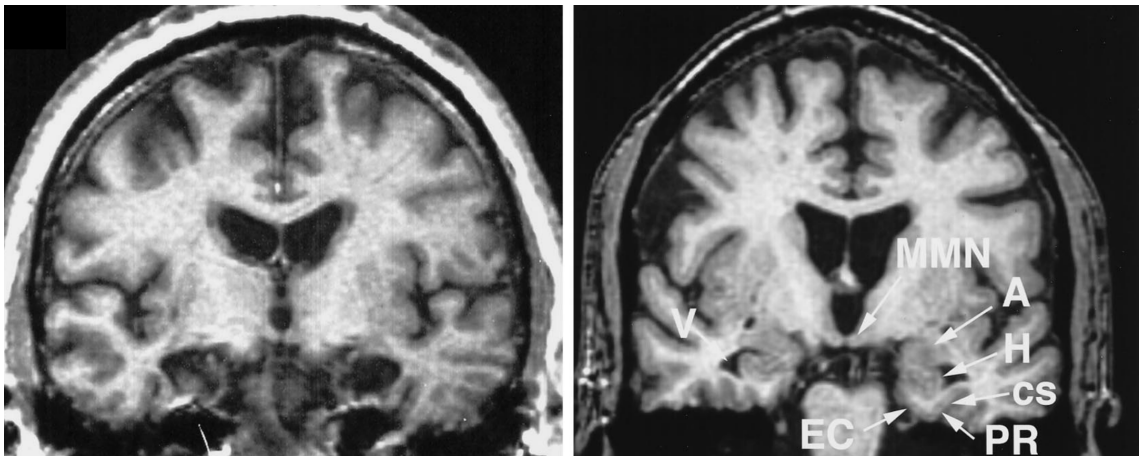

Figure 1.7: **Temporal lobe lesions in patient H. M.** These are T1-weighted MRI coronal sections of H. M.'s brain at age 67 (**left**), and from a 66 year old healthy man who served as a control subject (**right**). The sections show the rostral part of the intraventricular portion of the hippocampus. The hippocampus and entorhinal cortex have been resected from H. M.'s brain bilaterally. A, amygdala; cs, collateral sulcus; EC, entorhinal cortex; H, hippocampus; MMN, medial mammillary nucleus; PR, perirhinal cortex; V, ventricle. Figure reproduced from Corkin, Amaral, et al. (1997).

scribed by Scoville and Milner (1957) was Henry Gustav Molaison (1926–2008), widely known as patient H. M., who had suffered from pharmacologically intractable epilepsy since age 10. In 1953, H. M. underwent surgery in an experimental attempt to ameliorate his severe epileptic seizures (see Chapter 2 for a brief introduction to epilepsy surgery). The decision to resect large parts of the MTL bilaterally was based on the fact that it is a frequent onset zone of epileptic seizures. Fig. 1.7 conveys an impression of the extent of H. M.'s temporal lobe lesion, comprising the medial temporal polar cortex, most of the amygdaloid complex, the entorhinal cortex bilaterally, and the anterior part (approximately 2 cm) of the dentate gyrus, hippocampus, and subicular complex (Corkin, Amaral, et al. 1997). Initial studies on the memory impairment and remaining cognitive abilities of patient H. M. yielded four major insights (Corkin 2002; Squire and Wixted 2011):

- General intelligence and perceptual function are independent of the MTL.
- Integrity of the MTL is necessary for the *acquisition* of new declarative memories, but not for the *recall* of such memories from times long before the lesion.
- Despite the MTL's role in *long-term memory*, it is not necessary for functioning *working memory*.
- Brain structures outside the MTL are sufficient for motor skill learning.

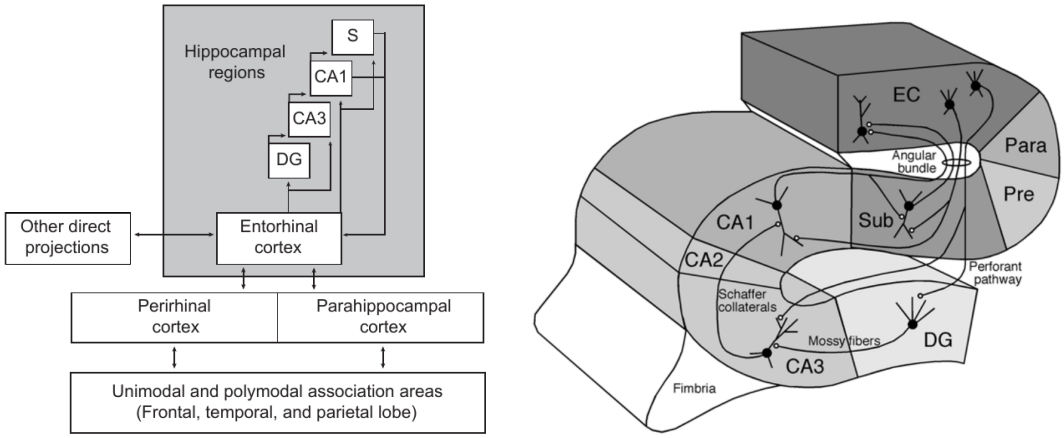

Figure 1.8: **The "MTL memory system".** The entorhinal cortex is the main gateway between cortical areas and the hippocampus. Within the hippocampal formation, information passes through the dentate gyrus (DG), and areas CA3 and CA1 to the subiculum (S), from there back to the entorhinal cortex. **Left:** The perirhinal and parahippocampal cortices are seen as further relay stations between other cortical areas and the hippocampus. This general scheme was first proposed to be a "memory system" by Squire and Zola-Morgan (1991). Graphics reproduced from Morris (2007, p. 594). **Right:** The perforant pathway, mossy fibers, and Schaffer collaterals are the most important projections within the hippocampus. EC, entorhinal cortex; Para, parasubiculum; Pre, presubiculum; Sub, subiculum; DG, dentate gyrus. Reproduced from Amaral and Lavenex (2007, p. 38).

Studies in other amnesic patients confirmed these findings. In patient R. B., postmortem neuropathological analysis of the brain revealed that a complete loss of cells in the CA1 field of the hippocampus bilaterally (sparing CA3, subiculum, alveus, perforant path, and dentate gyrus) sufficed to cause severe anterograde amnesia (Zola-Morgan, Squire, et al. (1986); this study led to the hypothesis that CA1 could be necessary for the integrity of information processing in the hippocampus, which would in turn underlie declarative memory formation). Studies of three additional patients corroborated this notion, and additionally showed that lesions to the hippocampal formation beyond CA1 lead to more severe amnestic symptoms (Rempel-Clower, Zola-Morgan, et al. 1996). Finally, in patient E. P., both extent of the lesion and symptoms strongly resembled the case of H. M. (Stefanacci, Buffalo, et al. 2000).

1.1.3 Declarative memory in animals

In patient studies, the precise location and extent of lesions is not controllable (or even unknown), and the number of patients per type of lesion is low, rendering generalizations across patients unreliable. To overcome these limitations, animal models of amnesia have been developed. Since declarative memory performance is by definition based on lan-

guage, non-language-based declarative memory tasks, such as the *delayed non-matching to sample task* (DNMS task), had to be conceived. In the DNMS task, the subject is presented with an object. After a retention interval during which no object is shown, the subject is presented with the same object again, together with a new one. To obtain a reward, the subject has to indicate the new object (Mishkin 1978; Squire and Zola-Morgan 1991). The DNMS task seemed suitable for animal models of amnesia: severely amnesic human patients performed significantly worse than alcoholics serving as controls, even with a retention interval of merely five seconds (Squire, Zola-Morgan, et al. 1988).

In cynomolgus monkeys (Macaca fascicularis), lesions to the hippocampal formation (including dentate gyrus, subicular cortex, and entorhinal cortex) and portions of the parahippocampal gyrus led to severe deficits in the DNMS task (Zola-Morgan and Squire 1986). Additional resection of the amygdala did not exacerbate the impairment (Zola-Morgan, Squire, et al. 1989a), while additional removal of more anterior parts of the entorhinal cortex and the perirhinal cortex led to more severe impairment (Zola-Morgan, Squire, et al. 1993). Lesions of the perirhinal cortex and parahippocampal gyrus (sparing the hippocampus) also produced severe deficits in the DNMS task (Zola-Morgan, Squire, et al. 1989b), while surgical lesions to the hippocampus alone led to only mild (but significant) impairments (Zola-Morgan, Squire, et al. 1994). Monkeys with cell loss in the CA1 and CA2 fields of the hippocampus were also impaired (Zola-Morgan, Squire, et al. 1992). The effects of lesions on cognition described here modeled human amnesia not only with regard to the memory deficits, but also in that motor learning and working memory were unaffected (for review, see Squire and Zola-Morgan 1991).

Lesion studies were also conducted in rats. Clark, West, et al. (2001) succeeded to transfer the DNMS task to rats with hippocampal lesions, showing that rats with damage limited to the hippocampus bilaterally (CA fields and dentate gyrus) were still able to perform the DNMS task at retention intervals of 4 s, but severely impaired at retention intervals of 1 min and 2 min.

Taken together, the findings in amnesic patients, lesioned monkeys, and lesioned rats consistently showed that the hippocampus has a critical role in the formation of declarative long-term memories, and that the adjacent cortices (entorhinal, perirhinal, parahippocampal cortex) contribute to this process, while the amygdala is less relevant (Squire and Zola-Morgan 1991; Squire 1992).

1.2 Systems memory consolidation

The most prominent symptom of severe amnesia is the profound inability to form new declarative memories. At the same time, most amnesic patients also suffer from a *temporally graded retrograde amnesia*, an impairment to recall events from their premorbid life which is more pronounced for events that had happened close to the onset of the amnesia, and less pronounced for earlier events. For instance, patient H. M. could recall childhood events, but had difficulties recalling events from the eleven years prior to his surgery (Sagar, Cohen, et al. 1985). This observation implies that declarative memories become independent of the MTL over time, that is, that the MTL cannot be the "ultimate storage site for long-term memory" (Squire and Wixted 2011; the higher vulnerability of recent versus remote memories to brain damage was described already by Ribot (1881)).

The neural process by which memories initially dependent on the hippocampus are transformed into long-lasting memories, which are then independent of the hippocampus, is called *systems memory consolidation* (Squire and Alvarez 1995; Squire, Genzel, et al. 2015); not to be confused with *synaptic consolidation* (Frankland and Bontempi 2005; Kandel, Dudai, et al. 2014). Evidence showing that declarative memories gradually become independent of the hippocampus comes from observations in amnesic patients and from animal models.

1.2.1 Evidence from amnesic patients

Several patient studies described temporally graded amnesias. Kopelman, Wilson, et al. (1989) analyzed temporally graded retrograde amnesias in 23 patients with different pathologies, using the categories "childhood", "early adult life", and "recent". Manns, Hopkins, et al. (2003) found impairments of semantic memory for time spans up to ten years before onset of amnesia in six patients with lesions limited to the hippocampus. Bayley, Hopkins, et al. (2006) reported retrograde amnesia for autobiographical events extending up to five years before the onset of amnesia in six patients with lesions limited to the hippocampus, and extending up to fifty years before the onset of amnesia in two patients with extended MTL damage. Childhood memories were spared in all patients. Bright, Buckman, et al. (2006) described severe impairments in both semantic and autobiographic remote memories in seven patients with bilateral damage to the temporal lobe including lateral parts, and impairment limited to recent memories in five patients with damage restricted to the MTL. This study also reported a positive correlation between the volume damaged and the severity of the retrograde amnesia.

1.2.2 Memory consolidation in animals

In cynomolgus monkeys, a prospective study on retrograde amnesia was conducted in the following way (Zola-Morgan and Squire 1990). Monkeys had to learn pairs of objects. At different time points after learning (two to sixteen weeks), the hippocampal formation (including dentate gyrus and subicular complex) as well as the entorhinal and parahippocampal cortices were removed bilaterally. When tested on the learned pairs of objects, the monkeys who had been given more time between learning and lesioning performed better than those with shorter intervals between learning and surgery, despite the longer total time between learning and testing. Non-lesioned controls performed worse on remote than on recent material.

In rats, Kim and Fanselow (1992) used tone and contextual fear-conditioning with subsequent lesioning of the hippocampus after different time intervals (one to 28 days). Hippocampal lesioning one day after conditioning abolished fear responses to the context but not to the tone, but lesioning after longer time intervals did not abolish fear responses, neither to the context nor to the tone. In a study by Anagnostaras, Maren, et al. (1999), each rat was fear conditioned to a context "A" fifty days before hippocampal lesioning, and to a context "B" one day before surgery. Contextual fear for the recent, but not the remote, context was abolished. Focusing on much shorter consolidation time spans, Tse, Langston, et al. (2007) studied a flavor-place association task in rats. Rats lesioned 3 h after learning performed significantly worse than controls, but rats lesioned 48 h after learning did not differ from non-lesioned controls, showing that the time spans necessary for complete consolidation can be quite short and can vary considerably between species and experimental paradigms.

To summarize, hippocampal lesions can lead to better recall performance for remote compared to recent pre-lesion memories in humans, monkeys, and rats. This is often considered the vital evidence showing that systems memory consolidation exists (Zola-Morgan and Squire 1990; Squire 1992; Frankland and Bontempi 2005; Squire, Genzel, et al. 2015).

1.2.3 Models of systems memory consolidation

Several models of memory consolidation have been developed. Inspired by anatomical studies, Marr (1970, 1971) proposed that memories rapidly encoded by the hippocampus over the course of a day are reorganized and transferred to the neocortex during subsequent sleep.

Squire (1992) proposed that during declarative learning, rapid synaptic changes in the

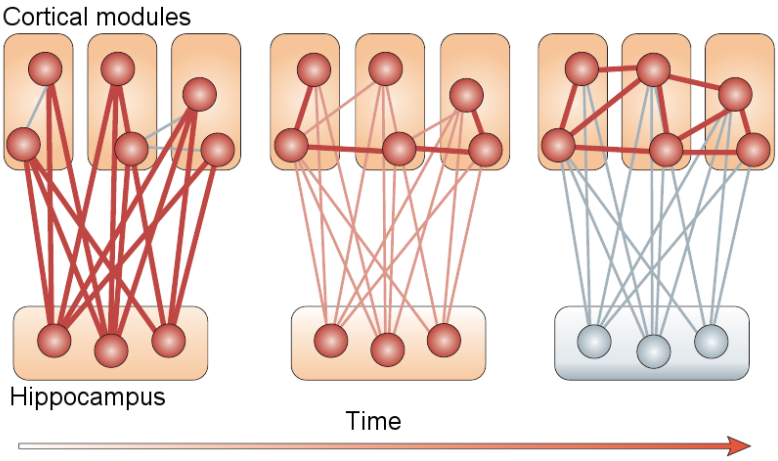

Figure 1.9: **Simple graphical representation of the standard view of systems memory consolidation.** The hippocampus rapidly binds together neocortical representations of an experience. Over time, repeated reactivation of memory traces (especially during slow-wave sleep) leads to a gradual modification and creation of neocortical synapses, which eventually results in a long-lasting memory trace independent of the hippocampus. Adapted from Frankland and Bontempi (2005).

hippocampus (and possibly adjacent cortices) "bind together the areas in neocortex" that are relevant for a specific memory episode, which in turn enables the hippocampus to subsequently retrieve the entire memory from a partial cue. According to this view, a slow reorganization of memory traces in neocortex would gradually enable memory retrieval even without the hippocampus, with the neocortex functioning as the permanent storage site for declarative memories. Alvarez and Squire (1994) added the idea that synaptic modification in neocortex happens "when neural activity within the MTL [repeatedly] coactivates separate regions of neocortex". This idea was incorporated by McClelland, McNaughton, et al. (1995) into a neural-network model of systems memory consolidation that reproduced key experimental observations, such as a temporal gradient in retrograde amnesia. Finally, Squire and Alvarez (1995) proposed that the reactivation of neocortical memory traces by the MTL preferentially takes place during slow-wave, and not REM, sleep. These considerations are together called the *standard view of systems memory consolidation* (Frankland and Bontempi 2005; see Fig. 1.9).

An alternative view (Nadel and Moscovitch 1997) posits that while semantic memories are stored in the neocortex, the hippocampus is the storage site for episodic memories. In this view, consolidation means the creation of "multiple traces" for each episodic memory in the hippocampus by reactivation.

Both views share the idea that reactivation of memory traces in the hippocampus is a key mechanism in systems memory consolidation.

1.3 Neurobiological correlates of systems memory consolidation

Studies in amnesic patients and lesioned animals provided strong support for the existence of systems memory consolidation, and abstract models have proposed possible mechanisms. In this section, we will outline the key neurobiological observations found to correlate with systems memory consolidation, and how these findings were interpreted.

1.3.1 Memory consolidation and sleep in humans

In humans, several studies have found evidence for a role of sleep in memory consolidation. Human sleep can be broadly subdivided into *rapid-eye-movement sleep* (REM sleep) and *non-REM sleep* (NREM sleep; see Section 4.1 for the methodology of polysomnographic recordings). A part of NREM sleep is *slow-wave sleep* (SWS; for details see, e.g. Rama, Cho, et al. 2006; Diekelmann and Born 2010). Plihal and Born (1997) showed significant improvements in declarative but not motor memory after early sleep (i.e., mostly SWS). The opposite pattern emerged after late (i.e., mostly REM) sleep, hinting at the possible importance of SWS for declarative memory consolidation. In this study, declarative memory performance was also enhanced for early sleep versus waking, but not for late sleep versus waking. Using positron emission tomography to monitor hippocampal blood flow, Peigneux, Laureys, et al. (2004) found increased hippocampal activity during SWS after a spatial learning task, and a positive correlation between the amount of hippocampal activity during SWS and memory performance. Marshall, Helgadóttir, et al. (2006) used transcranially applied currents to increase the amount of SWS, showing a performance increase in a declarative memory task for stimulated versus non-stimulated subjects.

An important stride towards causality was made in a study by Rasch, Büchel, et al. (2007), in which an odor was presented during learning, during subsequent SWS, or both. Performance in an object–location task was enhanced only if the same odor was presented during both learning and subsequent SWS. The presence of the odor during SWS was interpreted to trigger hippocampal memory reactivation for the material studied earlier in the presence of the same odor. This study showed no memory gain when odors where presented during learning and subsequent waking or REM sleep, or when the task required procedural instead of declarative memory. Using functional magnetic imaging, the study also demonstrated hippocampal activation during odor exposition in SWS.

Rudoy, Voss, et al. (2009) used an object–location task in which each object was paired with one of two sounds. Subsequently, only one of the two sounds was presented dur-

ing SWS ("cueing"). The study reported improved spatial memory performance for cued versus uncued objects, again interpreting the cues as triggers for hippocampal memory reactivation during SWS. When the cues were presented during waking, performance for cued versus uncued objects did not improve.

1.3.2 Spatial learning in rats

Important contributions to the study of systems memory consolidation came from the investigation of spatial learning in rats. *Place cells* are spatially tuned neurons in the hippocampus, first described in rats by O'Keefe and Dostrovsky (1971): these neurons increase their firing rate whenever an animal traverses a specific location in an environment, and are almost completely silent in other locations. The preferred spatial location of a place cell is called its *place field*. First evidence for a role of place cells in memory-related processes during sleep was presented by Pavlides and Winson (1989), who showed that place cells (in CA1) activated during behavior had elevated firing rates during subsequent sleep (both SWS and REM), compared to place cells not activated during pre-sleep behavior.

1.3.3 Sharp-wave ripples

A hallmark in the electrophysiology of the hippocampus is the *sharp-wave ripple complex* (SPW-R), reflected in recordings of the CA1 local field potential (LFP) as a transient large-amplitude deflection (*sharp wave*), often coupled with a transient, fast, oscillatory pattern (*ripple*). In rats, sharp waves typically last 40 ms to 100 ms, and ripples have a typical central frequency of 110 Hz to 200 Hz (Buzsáki 1986; O'Keefe 1976; Buzsáki, Horváth, et al. 1992; Buzsáki 2015). SPW-Rs are believed to be generated in CA3 and to propagate from there to CA1. Inspired by electrophysiological observations in rats, and preceding some of the models outlined in Section 1.2, Buzsáki (1989) developed a *two-stage model of memory consolidation* that assigns a central role to SPW-Rs. To understand this model, recall that information in the hippocampal formation is predominantly transferred along the pathway entorhinal cortex → dentate gyrus → CA3 → CA1 → subiculum → entorhinal cortex (see Fig. 1.8). The two stages of the model are the following (adapted from Buzsáki 1989, 2015):

1. During exploratory behavior ("learning"), some of the granule cells in the dentate gyrus fire at elevated rates, which transiently raises the excitability of their target pyramidal neurons in CA3. This set of target neurons is specific for the content of the experience. During this phase, recurrent excitation in CA3 is suppressed. Those

place cells in CA1 whose place fields the animal traverses fire, driven by projections from CA3.

2. During SWS (and other quiet states), SPW-Rs "transfer the newly acquired hippocampal information to the neocortex and the repeating SPW-Rs continue to potentiate those same synapses which gave rise to the synaptic changes during the learning process" (Buzsáki 2015, p. 1131). Specifically, during SPW-Rs, recurrent excitation in CA3 leads to firing of exactly those pyramidal cells whose excitability is elevated due to the process described in 1., which entails reactivation of the same pyramidal cells in CA1 and their downstream targets that were activated during learning.

To investigate whether sharp-wave ripples are indeed necessary for memory consolidation, Girardeau, Benchenane, et al. (2009) selectively suppressed SPW-Rs by commisural stimulation during rest and sleep after spatial learning. In a control group, stimulation was delayed by 80 ms to 120 ms to spare SPW-Rs. Performance in spatial memory tests was significantly lower in stimulated rats versus controls, establishing a causal role of SPW-Rs in memory. Similarly, Ego-Stengel and Wilson (2010) used electrical stimulation in rats' CA1 during rest to suppress SPW-Rs. Along with the SPW-R rate, performance in a spatial learning task diminished in comparison to a control task.

1.3.4 Reinstatement of neural activity after learning

One of the most striking features of place cells is that firing patterns occurring during active behavior are reinstated during subsequent SWS. This was observed not only with regard to pairwise correlations (two place cells with correlated activity during behavior have correlated activity also during subsequent SWS), but also when considering sequential activity involving many place cells (firing sequences occurring during behavior are "replayed" during subsequent SWS). As this *neuronal replay* is a potential mechanism of spatial memory consolidation, many studies have been devoted to studying it in detail, the most relevant of which we will now discuss.

Wilson and McNaughton (1994) used parallel recordings from up to 100 CA1 place cells in rats to study the effect of behavior on place cell activity during subsequent sleep. Place cells that were simultaneously active during behavior (because their place fields overlapped) exhibited correlated activity also during subsequent SWS, whereas place cells that were active but not simultaneously active during behavior did not show correlated activity during subsequent SWS (see Fig. 1.10). Furthermore, correlations were higher

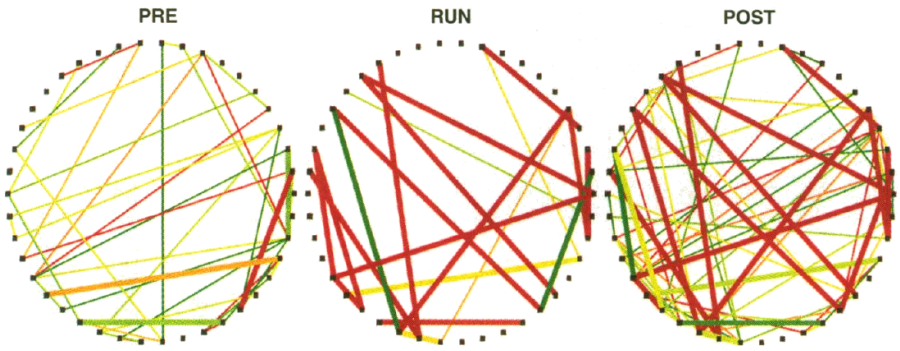

Figure 1.10: **Correlated place cell activity during SWS reflects earlier behavior.** Rat CA1 place cells are shown as dots arranged in a circle. Lines reflect correlations (range, 0.05 to 0.2; cold colors, low values; warm colors, high values) during SWS before (PRE) and after (POST) running (RUN). The structure of correlations during RUN arose as a direct consequence of the arrangement of place fields on the track. The relevant finding was that the structure of correlations was strongly preserved in POST. Reproduced from Wilson and McNaughton (1994).

during SPW-Rs than outside of SPW-Rs.

Skaggs and McNaughton (1996) analyzed the temporal order of activity in pairs of CA1 place cells, reporting that this order was positively correlated between running and subsequent, but not prior, sleep. This study was the first to show that the temporal structure of neuronal activity in the hippocampus during sleep reflects prior experiences. Qin, McNaughton, et al. (1997) confirmed this finding, and reported the same effect for neocortical, and for hippocampal–neocortical pairs of neurons.

Kudrimoti, Barnes, et al. (1999) compared correlations of CA1 place cell activity during running and sleep in a more quantitative manner. The study found that 15% of the variance in firing rate correlations during sleep (POST) could be explained (explained variance, EV) by correlations during previous behavior (RUN), while correlations during previous sleep (PRE) explained only 5% (0.4%) of the correlations during RUN in familiar (novel) environments. Furthermore, place cell firing rates during ripples increased slightly from PRE to POST, and EV during POST ripples was higher than outside of POST ripples. When restricting the dataset to REM sleep, EV was not significantly different from zero, but when restricting the dataset to the awake, motionless state (rich in ripples), EV was 12%, showing that sleep was not necessary for the reinstatement of correlational structure.

Lee and Wilson (2002) reported that the sequence of action potentials fired by CA1 place fields during population bursts in SWS strongly resembled the sequence of action potentials fired during previous spatial learning (hence, it also reflected the arrangement of place fields on the track), see Fig. 1.11. The time interval between action potentials was compressed in time by a factor of twenty. This time-compressed *neural replay* was

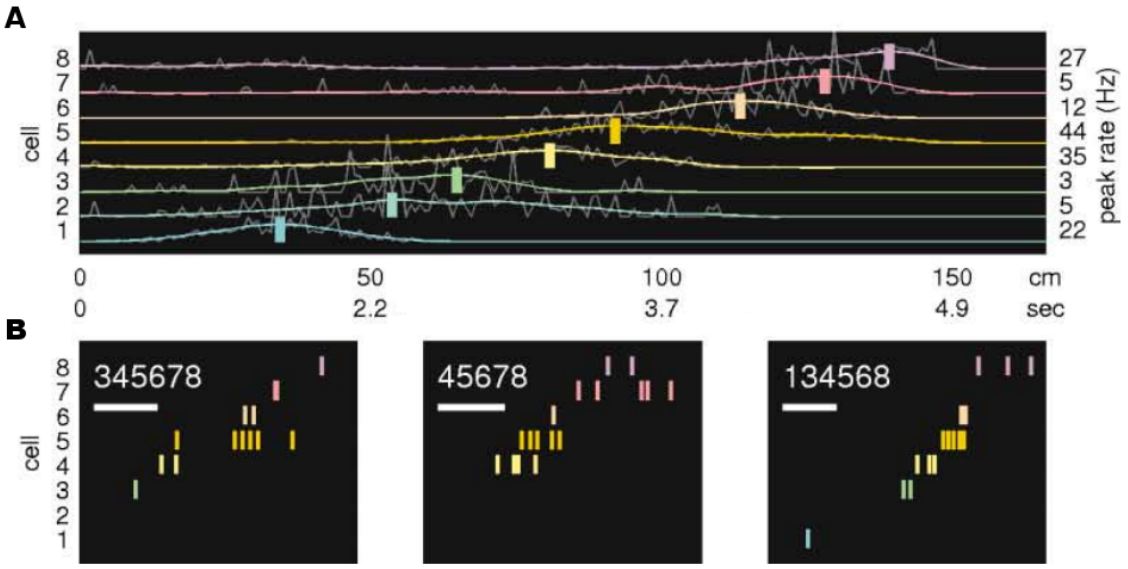

Figure 1.11: **Sequentially ordered reactivation of place cells**. **A,** CA1 place cell firing during running on a linear track. **B,** During population bursts in SWS after running, the neurons fire in the same order as during running. White bar, 50 ms. Adapted from Lee and Wilson (2002).

interpreted as a candidate mechanism for spatial memory consolidation. The study also reported a link between CA1 population bursts and SPW-Rs. Neural replay without time compression and in REM sleep was reported by Louie and Wilson (2001).

Foster and Wilson (2006) observed neural replay also during ripples during rest, but fifteen times more often in the reverse than in the forward direction, hinting at a potentially different mechanisms for awake replay and SWS replay.

Extending the findings on SWS replay, Ji and Wilson (2007) observed that neuronal firing sequences occurring during active behavior were replayed in a time-compressed manner in primary visual cortex and in the hippocampus during subsequent SWS. Replay of sequences corresponding to one behavioral episode concurrently occurred in the two areas. Maingret, Girardeau, et al. (2016) used cortical stimulation at the time points of SPW-Rs to enhance cortico–hippocampal coupling. The study reported a strong enhancement of object–location memory for stimulated animals versus animals receiving delayed stimulation, which was interpreted as evidence for the causal role of SPW-Rs in systems memory consolidation.

Girardeau, Inema, et al. (2017) showed that neurons in the basolateral amygdala of rats were activated during hippocampal SPW-Rs during NREM sleep after learning of the location of an aversive stimulus. This was interpreted as a potential mechanism of emotional memory consolidation.

1.3.5 Memory at the synaptic level

The findings discussed so far mostly concern neuronal activity measured by extracellular electrodes, that is, action potentials and local field potentials. However, studies at the level of synapses, often using intracellular recordings and molecular tools, have contributed enormously to the current understanding of long-term memory. Because this thesis is only marginally concerned with synaptic mechanisms of memory, here we only give a cursory introduction to the most important findings in this realm (for excellent reviews see e.g., Bliss and Collingridge 1993; Dan and Poo 2006; Kandel, Dudai, et al. 2014). The most influential early theory connecting synaptic modifications to learning was formulated by Hebb (1949, p. 70), who famously noted that "the general idea is an old one, that any two cells or systems of cells that are repeatedly active at the same time will tend to become 'associated,' so that activity in one facilitates activity in the other". Among the first experimental results supporting the idea that information can indeed be stored through long-lasting synaptic changes was the discovery of *long-term potentiation* in the hippocampus of rabbits (LTP; i.e., increases in synaptic efficacy, lasting for up to several hours or more, after activity in exactly the same synapses; Bliss and Lømo 1973).

Scrutinizing the role of timing in long-term synaptic modifications, Levy and Steward (1983) showed in rats that the efficacy of initially weak inputs from the entorhinal cortex to the contralateral dentate gyrus increased when an (already effective) ipsilateral input followed within 20 ms. When, on the other hand, the strong, ipsilateral input preceded the weak, contralateral input, the weak input's efficacy further decreased. The principle that the relative timing of synaptic inputs (and postsynaptic action potentials) can determine the direction of synaptic modifications is known as *spike-timing-dependent plasticity (STDP)*.

A study by Wigström, Gustafsson, et al. (1986) corroborated these findings, showing in intracellular recordings from hippocampal slices of the guinea pig that synaptic efficacies increased only when excitatory postsynaptic potentials (EPSPs) were immediately followed by postsynaptic depolarization sufficiently strong to elicited action potential firing. The same study also showed synapse specificity of LTP: the efficacy of synapses that had not been active was not modified. The connection to behavior was made by Morris, Anderson, et al. (1986), who showed that blocking N-methyl-D-aspertate receptors in the hippocampus of rats selectively impaired spatial learning and, at the same time, abolished hippocampal long-term potentiation. In an important contribution to the understanding of STDP, Markram, Lübke, et al. (1997) demonstrated in neocortical slices of rats that synaptic efficacies increased when postsynaptic action potentials followed 10 ms after EPSPs, and decreased when postsynaptic action potentials preceded EPSPs by 10 ms.

No change in synaptic efficacy was observed when the delay was 100 ms, for action potentials following or preceding EPSPs. Bi and Poo (1999) found synapse modifications along polysynaptic pathways by applying paired pulses to cultured rat hippocampal neurons. The study observed large synapse modifications when using short inter-pulse intervals (20 ms to 50 ms), while longer inter-pulse intervals (above 100 ms) did not induce such changes.

Sharp-wave ripples (see Section 1.3.3) appear to constitute a possible link between memory consolidation at the cellular and at the synaptic levels, as the highly synchronous firing induced in CA1 pyramidal cells during sharp-wave ripples could potentially lead to synapse modifications in target neurons (Buzsáki, Horváth, et al. 1992; Buzsáki 1996). However, how precisely sharp-wave ripples might contribute to synapse modification in vivo has as of yet mostly remained elusive (Buzsáki 2015).

1.4 Concept neurons in humans

As we have seen, studies of memory consolidation in rodents have led to detailed models and experimentally testable, concrete hypotheses concerning mechanisms of memory consolidation. How do these findings and predictions relate to studies in humans? Most electrophysiological studies on rodent memory consolidation have investigated place cells. It might seem natural to search for place cells in humans; for some results in this direction, see Section 1.4.3. However, human episodic memory is of course not only concerned with space (the "where" component of episodic memory), but also with the "what" and "when" of a memory episode. Recordings from single neurons in the MTLs of epilepsy patients have yielded the insight that neurons in the human hippocampus represent the "what" in a direct way: in this section, we will explain how single neurons in the human MTL represent semantic content, and how these neurons potentially contribute to memory consolidation.

Concept neurons (sometimes also named *Jennifer Aniston neurons*, *semantic neurons*, or *concept cells*) are neurons in the human MTL that are tuned to the semantic content of a stimulus. Concept neurons were discovered in recordings from the MTLs of epilepsy patients undergoing presurgical monitoring (see Chapter 2 for the method of single-neuron recordings from epilepsy patients). In brief, micro-electrodes with a diameter of 40 µm can be implanted into the MTL to record from individual neurons, along with depth electrodes used as a diagnostic device.

Early studies on recordings of individual neurons from the human MTL reported selective responses to individual words and faces (Heit, Smith, et al. 1988), and faces and

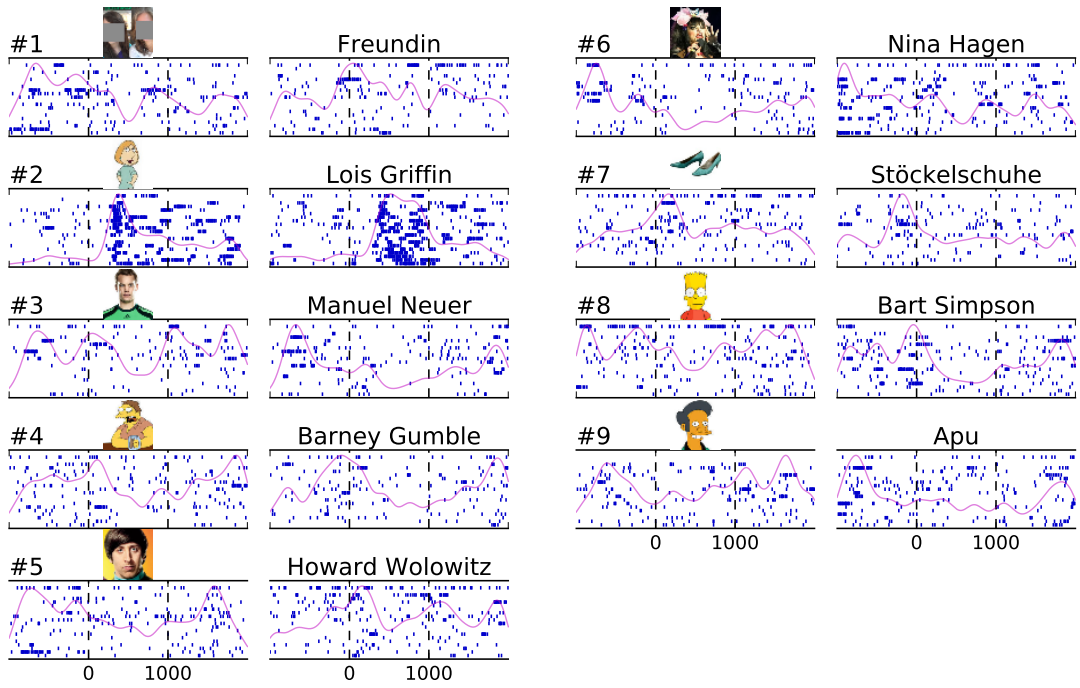

Figure 1.12: **Responses of a concept neuron.** Displayed are raster plots from a neuron in the hippocampus, depicting responses to nine pictures and the corresponding written names, each presented visually twenty times. The neuron responds to the picture and written name of "Lois Griffin". Recorded by J. Niediek.

objects (Fried, MacDonald, et al. 1997). Kreiman, Koch, et al. (2000), using nine stimulus categories (e.g., food items, animals, cars), reported category-specific responses of human MTL neurons.

However, the defining property of concept neurons – their invariance – was first reported by Quian Quiroga, Reddy, et al. (2005): a concept neuron tuned to e.g., Jennifer Aniston, increases its firing rate upon visual presentation of any picture of Jennifer Aniston, independent of physical stimulus properties such as color, viewing angle, size, or position, but not upon presentation of a picture showing a different person. Concept neurons have been found in the hippocampus, amygdala, entorhinal cortex, and parahippocampal cortex. The preferred stimuli of concept neurons can be famous people, personal acquaintances of the subject, animals, landmarks, objects, and others. In a study by Quian Quiroga, Kraskov, et al. (2009), between 35% and 40% of the concept neurons in the hippocampus and entorhinal cortex were reported to exhibit multi-modal invariance: they responded to the written name of their preferred stimulus, and/or to a computer voice pronouncing it. This invariance was observed in 14% (0%) of amygdalar (parahippocampal) concept neurons. Fig. 1.12 shows sample responses of a concept neuron.

1.4.1 Tuning properties of concept neurons

Several studies characterized stimulus–response relationships of human MTL neurons. Waydo, Kraskov, et al. (2006) estimated the probability for a human MTL neuron to respond to a random stimulus to be approximately 0.54%. Viskontas, Quian Quiroga, et al. (2009) subdivided a set of stimulus pictures containing faces into four different categories and reported significantly higher probabilities to elicit a response for pictures categorized as "Self & Family" and "Experimenters" compared to pictures categorized as "Famous people" or "Non-famous people". Mormann, Dubois, et al. (2011) reported preferential responses of neurons in the right amygdala to animals (compared to persons, objects, and landmarks). Rutishauser, Tudusciuc, et al. (2011) found a population of neurons in the amygdala tuned to whole faces, but not parts of faces. Ison, Mormann, et al. (2011) described a higher response selectivity in putative pyramidal cells compared to putative interneurons in visually selective neurons in the amygdala, entorhinal cortex, hippocampus, and parahippocampal cortex. Mormann, Niediek, et al. (2015) reported invariant responses to the identity of persons, but not to their gaze direction, in the amygdala. Mormann, Kornblith, et al. (2017) showed preferential tuning to scenes (compared to people, animals, or objects) in neurons in the parahippocampal cortex. These neurons also responded less selectively than visually selective neurons in other brain regions. Reber, Faber, et al. (2017) demonstrated that the activity of visually selective neurons often, but not necessarily, coincided with conscious perception of the stimulus.

1.4.2 Concept neurons in memory tasks

The findings discussed so far seemingly suggest that concept neurons in the human MTL contribute to invariant object recognition. At least two arguments demonstrate that this is very unlikely. First, the response latencies of concept neurons are slower than object recognition. Mormann, Kornblith, et al. (2008) reported average response latencies of visually selective neurons to be in the 392 ms to 397 ms range in the amygdala, entorhinal cortex, and hippocampus, and 271 ms in the parahippocampal cortex. However, in a study by Kirchner and Thorpe (2006), humans were able to detect the presence of an animal in a scene within 120 ms. Second, patients with extended MTL lesions do not usually show deficits in object recognition (Squire and Wixted 2011).

As discussed in Sections 1.1 and 1.2, converging evidence shows that the hippocampus contributes to declarative long-term memory formation and systems memory consolidation. Accordingly, the idea that sharply and semantically tuned neurons in the MTL could be part of a mechanism for declarative long-term memory was presented already by Heit,

Smith, et al. (1988; for review see Quian Quiroga 2012). Several studies examined the role of concept neurons in various memory tests. Focusing on memory recall, Gelbard-Sagiv, Mukamel, et al. (2008) studied neurons in the hippocampus and entorhinal cortex that selectively responded to the presentation of one out of several video clips. When subjects were asked to freely recall which videos they had watched, a selective neuron's firing rate consistently increased (up to 3 s) before the subjects verbalized the recall of the preferred video of that neuron.

Ison, Quian Quiroga, et al. (2015) asked subjects to memorize person–landscape associations (e.g., "Clint Eastwood" – "Hollywood sign") while recording from visually selective neurons preferentially tuned to one of the persons or one of the landscapes. The study found an increased response to the visual presentation of initially non-preferred, but associated, stimuli after learning, hinting at a potential mechanism of associative learning in the MTL.

Two very recent studies examined the activity of concept neurons in working-memory tasks. Kamiński, Sullivan, et al. (2017) reported that when subjects were instructed to maintain in memory the content of one to three pictures over a period of 2.5 s to 2.8 s, visually selective neurons in the hippocampus and amygdala showed persistent activity during maintenance. This persistent activity was larger in trials with correct subsequent memory of picture identity than in incorrect trials. Kornblith, Quian Quiroga, et al. (2017) presented eight to nine images and used a maintenance period of 2.4 s. The study found that 8% of visually selective neurons were modulated by working-memory content (chance level, 1%), and that these neurons' activity was significantly higher in trials with correct subsequent memory than in incorrect trials.

1.4.3 Other human MTL neurons in memory tasks

It is unlikely that all neurons in the human MTL are concept neurons. However, neurons that are not concept neurons could still contribute to memory-related processes, as was shown in a series of studies by Rutishauser and colleagues. Studying a task in which subjects presented with 100 pictures had to judge if they had seen a picture before ("old") or not ("new"), Rutishauser, Mamelak, et al. (2006) reported on neurons in the amygdala and hippocampus that signaled either familiarity ("old") or novelty ("new") of stimuli, independent of the stimulus identity. Using population decoding from these neurons, the study reported correct decoding of whether a "new" or "old" image was shown in up to 93% of the trials.

Rutishauser, Ross, et al. (2010) reported that 21% of the neurons in the amygdala and

hippocampus were phase-locked to an oscillation in the 3 Hz to 8 Hz range, and that these neurons were much more accurately locked to a particular phase during learning in trials with correct subsequent memory versus subsequently incorrect trials.

Rutishauser, Ye, et al. (2015) showed that the population of familiarity/novelty selective neurons was independent of the population of visually selective neurons recorded in the same areas. The same study showed that familiarity/novelty selective units exhibited a stronger familiarity/novelty signal when the behavioral old/new decision was performed with high confidence.

As outlined in Section 1.3, many relevant contributions to research on systems memory consolidation came from the investigation of place cells in rats. In humans, spatially tuned neurons were described in the hippocampus (Ekstrom, Kahana, et al. 2003; Jacobs, Kahana, et al. 2010). These spatially tuned neurons were described to be activated not only during navigation, but also during memory recall thereof (Miller, Neufang, et al. 2013; for commentary see Niediek and Bain 2014).

1.5 Aim of this thesis

We have discussed theories and possible mechanisms of memory consolidation in Sections 1.2.3 and 1.3, and we have seen in Section 1.4 how concept neurons provide a neuronal representation of semantic content in the human MTL. Concept neurons have been speculated to be "building blocks" for declarative memory (Quian Quiroga 2012). However, a concrete hypothesis on how exactly concept neurons might contribute to memory consolidation has been lacking. Moreover, to our knowledge, no experiments regarding a possible role of concept neurons in a mechanism of memory consolidation have been reported.

The aim of this thesis is to propose and test the idea that *the physiological substrate of "memory traces" is provided by the coordinated activity of concept neurons in the medial temporal lobe.*

More precisely, we propose the following mechanism of memory consolidation:

1. During the experience of an episode, concept neurons in the MTL are activated. Both the ensemble of activated neurons (*which* neurons are active) and the sequential order of activity among the activated neurons (*when* the neurons are active) encode the specific content (the "what" component of episodic memory) and time-course of the episode (the "when" component of episodic memory).

2. During subsequent waking and slow-wave sleep, the very same ensembles in the

MTL that were active during the original experience are repeatedly reactivated in a temporally coordinated manner, thereby creating a long-lasting memory representation.

The model inspires a number of concrete hypotheses (in part related to ideas of Buzsáki 2015, p. 1132):

1. The modality-invariant representation of semantic content by concept neurons is stable over time.

2. Concept neurons in the MTL are active not only during episodic learning, but also during subsequent waking and slow-wave sleep (but not necessarily during REM sleep).

3. The activity of concept neurons increases during ripples.

4. Ensembles of concept neurons with correlated activity during episodic learning also exhibit correlated activity during subsequent slow-wave sleep, and during ripples.

5. The sequential order of events in a memory episode is reflected in the sequential order of neuronal activity during ripples.

This thesis is devoted to testing hypotheses 1.–5. (note that hypothesis 1. can be considered a prerequisite to the others). The thesis is structured as follows: In Chapter 2, we will briefly outline the general method of single neuron recordings in epilepsy patients. In Chapter 3, we will present the spike sorting and data-analysis software *Combinato* that we developed to perform reliable multi-hour single-unit tracking. All results regarding memory consolidation are presented along with specific methods in Chapter 4. Finally, Chapter 5 interprets our results and discusses their relevance in a broader context.

Chapter 2

Single neuron recordings in epilepsy patients

In this chapter, we describe the method of single neuron recordings from the medial temporal lobe of epilepsy patients. More specific methods – in particular regarding experiment design and data analysis – are presented in Chapters 3 and 4.

2.1 Background

An epileptic seizure is "a transient occurrence of signs and/or symptoms due to abnormal excessive or synchronous neuronal activity in the brain" (Fisher, Acevedo, et al. 2014). A modern definition of the disease epilepsy states that a patient has epilepsy if she or he has had at least one epileptic seizure and "demonstrates a pathologic and enduring tendency to have recurrent seizures" (Fisher, Acevedo, et al. 2014). Epilepsy is common: a recent meta-analysis found an incidence of epilepsy of 50.4/100 000 persons/year (Ngugi, Kariuki, et al. 2011). Prevalence reports of epilepsy display considerable variance. A meta-analysis reported the prevalence of epilepsy in developed countries to be 5.8/1000 (5th–95th percentile range 2.7 to 12.4; Ngugi, Bottomley, et al. 2010).

Epileptic seizures are commonly classified as either *focal onset* or *generalized onset* (Fisher, Cross, et al. 2017). Focal-onset seizures start in a small region of the brain (the *seizure focus* or *seizure onset zone*), whereas in generalized-onset seizures no well-defined seizure focus exists: seizures start in both hemispheres simultaneously. Seizure foci can exist in many brain regions, of which the temporal lobe is the most common (*temporal lobe epilepsy*; Téllez-Zenteno and Hernández-Ronquillo 2012).

Temporal lobe epilepsy and other focal epilepsies can often be resolved by pharmaco-

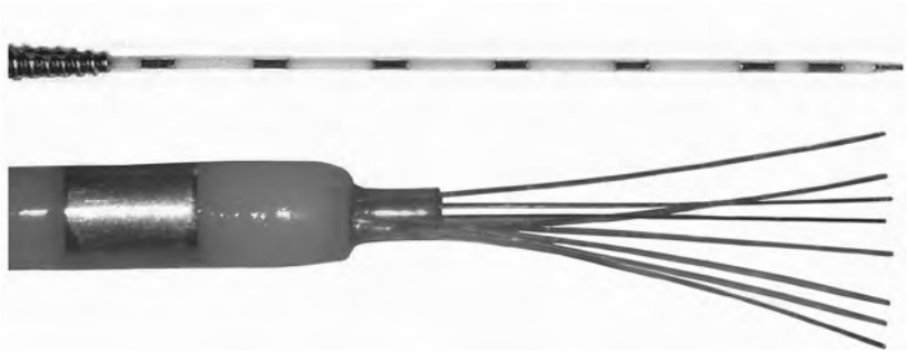

Figure 2.1: **Clinical depth electrodes and microwires. Top,** clinical depth electrode (Behnke–Fried electrode; diameter 1.3 mm, seven contacts) for intracranial EEG recordings. **Bottom,** insulated (except for distal end) platinum–iridium microwires protruding from the tip of the clinical depth electrode. Diameter of each microwire is 40 µm; impedance 100 kΩ to 300 kΩ (Staba, Fields, et al. 2014); ninth wire (uninsulated reference electrode) not displayed. Graphics adapted from Staba, Fields, et al. (2014).

logical treatment. Of those patients whose condition is not resolved pharmacologically, many can undergo *epilepsy surgery*, the surgical resection of the tissue containing the seizure focus from the brain. Epilepsy surgery can only ameliorate seizures when the seizure focus is correctly identified in the brain. In most cases, non-invasive methods suffice for this localization (Fried 2014). These methods include scalp electroencephalography (EEG, often combined with concurrent video monitoring), magnetic resonance imaging (MRI), and neuropsychological tests. However, when these methods fail to unequivocally localize the seizure focus, patients can undergo a procedure known as *invasive presurgical monitoring*. Several approaches for invasive presurgical monitoring exist. A common method is to surgically implant intracerebral depth electrodes into the brain to record an *intracranial electroencephalogram*, which allows for a much more precise spatial resolution of field potentials compared to scalp EEG. A clinical depth electrode with seven recording contacts is displayed in Fig. 2.1 (top). After implantation of depth electrodes, patients have to spend sufficient time in the hospital for epileptic seizures to be registered, typically one to two weeks.

The possibility to record individual neuronal action potentials extracellularly from the brains of patients undergoing presurgical monitoring arises because a bundle of microwires can be inserted into the hollow lumen of clinical depth electrodes (Fried, Wilson, et al. 1999; see Fig. 2.1). The next section outlines this technique in more detail, as relevant to this thesis.

2.2 Surgery and recording procedures

In this section, we outline the procedures relevant for the studies reported in Chapters 3 and 4. Similar procedures have been described by their inventors (Fried, Wilson, et al. 1999).

Depth electrode implantations were performed at the Department of Neurosurgery of the University of Bonn, Germany. Magnetic resonance (MR) images were obtained prior to surgery. After placement of a stereotactic headframe, computer tomography images were obtained and co-registered to the MR images. A target and trajectory for each depth electrode were chosen, carefully avoiding blood vessels. These decisions were based exclusively on clinical criteria. Under general anesthesia, each electrode and microwire bundle were implanted in the following way. A drill hole was made using the stereotactic frame, and a hollow Behnke–Fried depth electrode (Ad-Tech, Racine, WI; MR imaging compatible; top of Fig. 2.1) was inserted using a stylet. A bundle of nine microwires (Ad-Tech, Racine, WI; MR imaging compatible; bottom of Fig. 2.1) was cut to the correct length and inserted into the lumen of the depth electrode. These platinum–iridium microwires had a diameter of 40 µm and protruded from the tip of the depth electrode by approximately 4 mm. Eight microwires in each bundle were insulated except for the cut distal end, and one was not insulated to serve as a reference electrode. A typical implantation scheme consisted of one to three depth electrodes in the hippocampus bilaterally, and one depth electrode in each of the following subregions of the medial temporal lobe bilaterally: amygdala, entorhinal cortex, and parahippocampal cortex.

One day after surgery, patients were transferred to the Department of Epileptology of the University of Bonn for continuous monitoring. Post-operative MR images were obtained to confirm correct electrode placement.

Signals from the microwires were pre-amplified by headstages (Neuralynx, Bozeman, MT) in close proximity to the extracranial end of the depth electrodes within the head dressing, and recorded on a Digital Lynx SX or ATLAS system (Neuralynx, Bozeman, MT) at an effective recording bandwidth of 0.1 Hz to 9000 Hz. Recordings were digitized at 32 000 Hz or 32 768 Hz, and transferred to network-attached storage units for further analysis. Fig. 2.2 shows sample data recorded from microwires implanted into the left hippocampus of a patient, and Fig. 2.3 shows the general setup of the recording system.

For the studies described in Chapters 3 and 4, visual stimuli were displayed on a standard laptop computer (see Fig. 2.3). Experimental paradigms were implemented in the Psychophysics Toolbox 3 (`http://psychtoolbox.org`; Kleiner, Brainard, et al. 2007), running in GNU Octave (`https://www.gnu.org/software/octave`) under Linux.

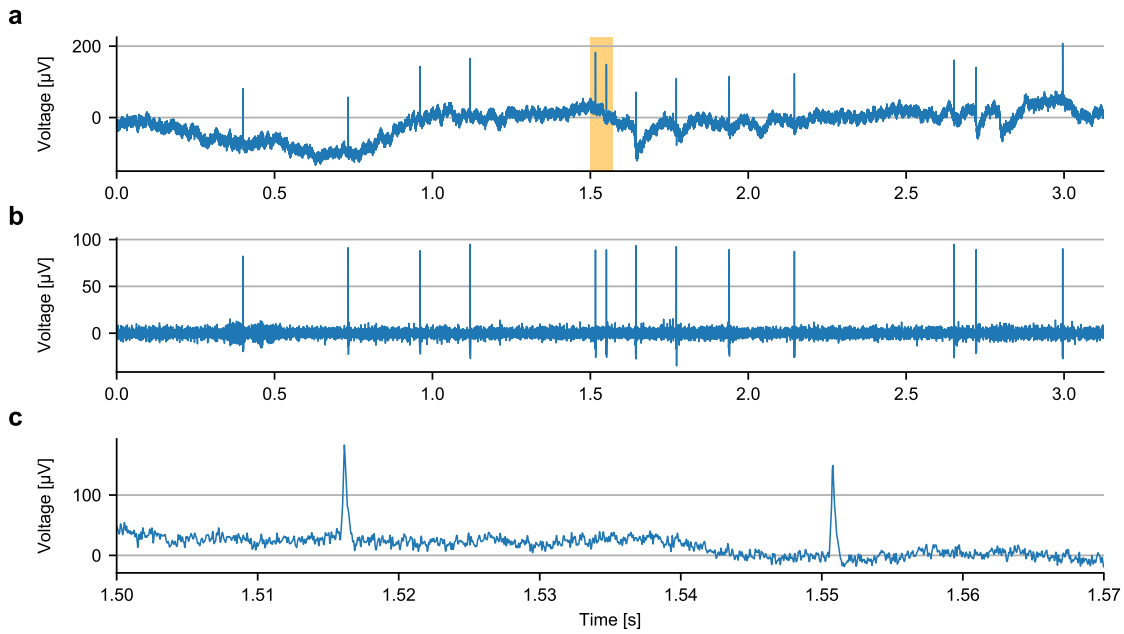

Figure 2.2: **Sample of data recorded with microwires.** Displayed are data from the left hippocampus. **a,** 3125 ms of unfiltered data. Action potentials ("spikes") are clearly visible. **b,** Same data as **a**, but bandpass-filtered for action potential detection (elliptic filter, passband 300 Hz to 1000 Hz). **c,** 70 ms of unfiltered data. The segment displayed here corresponds to the orange box in **a**. The shape of extracellularly recorded action potentials is visible at this time scale. Data recorded by J. Niediek.

Event triggers were sent to the recording system through a USB-1208FS data acquisition device (Measurement Computing, Norton, MA). Further details regarding data analysis etc. are presented in Sections 3.2 and 4.1, respectively.

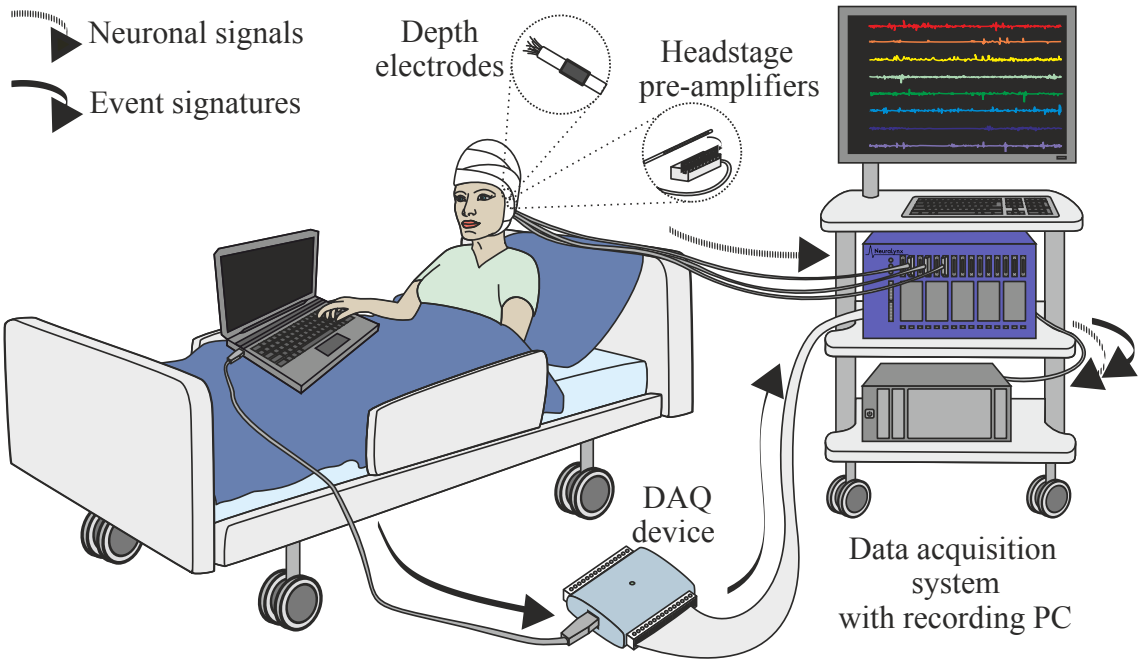

Figure 2.3: **Recording setup for cognitive studies.** Neuronal signals recorded from microwires are transferred to a Neuralynx data acquisition system via headstage pre-amplifiers. Patients perform cognitive studies on a standard laptop computer. Event signatures are transferred to the data acquisition system via a data acquisition (DAQ) device. Graphics adapted from Knieling, Niediek, et al. (2017).

2.3 Ethics statement

All surgical procedures, data recording, and cognitive studies were approved by the Medical Institutional Review Board of the University of Bonn Medical Center (approval number 095/10, implantation of micro-electrodes; approval number 242/11, whole-night recordings and data analysis). All patients gave informed written consent.

Chapter 3

A framework for reliable multi-hour single-unit tracking

The results presented in this chapter have been published as Niediek, Boström, et al. (2016). The text and figures of this chapter correspond closely to the published version.

3.1 Background and overview

Tracking single- and multi-unit activity over hours, possibly during sleep, allows to address important questions regarding neural mechanisms of learning and memory consolidation. For example, a popular theory posits that declarative memory consolidation during sleep depends on the reactivation of neuronal ensembles that were active during earlier behavior, as outlined in Section 1.3.

Over the last years, it has become possible to record from hundreds of channels simultaneously (Berényi, Somogyvári, et al. 2014; Misra, Burke, et al. 2014; Rossant, Kadir, et al. 2016), and modern recording systems allow to record continuously for hours and days, producing datasets that are typically hundreds of gigabytes in size.

Many spike sorting algorithms have been evaluated in the past (Quian Quiroga, Nadasdy, et al. 2004; Rutishauser, Schuman, et al. 2006; Pedreira, Martinez, et al. 2012; Kadir, Goodman, et al. 2014; Friedman, Keselman, et al. 2015; Knieling, Sridharan, et al. 2015; Rossant, Kadir, et al. 2016). The datasets used in these studies were usually simulations or recordings characterized by stationary (constant) noise levels, absence of non-neural artifacts, and short duration.

Even though spike sorting algorithms perform well on small datasets, tracking the activity of individual neurons over many hours has remained a major challenge: spike

sorting algorithms have to be computationally efficient to deal with spike counts in the order of hundreds of thousands per channel, must account for both slow and sudden changes in spike waveform, and have to cope with periods of excessive signal contamination, as inevitable in multi-hour recordings in clinical settings. Furthermore, current spike sorting methods often require manual optimization, a time-consuming task in the case of multi-hour recordings.

In this chapter, we present and evaluate *Combinato*: A software framework for unsupervised spike sorting of noisy long-term recordings. The core of our framework is a novel spike sorting algorithm based on block-wise iterative superparamagnetic clustering (SPC; Blatt, Wiseman, et al. 1996). This core algorithm is accompanied by methods for artifact rejection and tools for the visualization of results.

The importance of ground-truth data for the validation of spike sorting methods is becoming increasingly recognized (Einevoll, Franke, et al. 2012). In Section 3.3.1, we thus present results from a validation of Combinato on a recently published dataset of simulated neural activity (Rey, Pedreira, et al. 2015), showing that our method outperforms state-of-the-art spike sorting methods. This holds true even when the result of our *automated* spike sorting is compared to the published result of *manually optimized* spike sorting results on the same data (Pedreira, Martinez, et al. 2012). When tested on simulated recordings lasting ten hours, our algorithms were capable of recovering on average 74.6% of the simulated neurons, despite drift and high noise levels in the simulations.

We also evaluated the performance of our method in a visual stimulus presentation experiment (Section 3.3.2). The purpose of the experiment was to identify neurons that respond selectively and invariantly to visually presented stimuli (Section 1.4; Quian Quiroga, Reddy, et al. 2005). Without any manual intervention, Combinato identified more neuronal responses than common spike sorting methods that require manual optimization.

Lastly, as presented in Section 3.3.3, an evaluation on eight whole-night recordings from the temporal lobes of epilepsy patients showed that our method tracks visually selective single- and multi-units over more than 12 hours, laying the ground for our study on the role of concept neurons in memory consolidation, presented in Chapter 4.

3.2 Design and implementation

Before describing our spike sorting framework in detail, we will provide a brief outline of its structure; see Fig. 3.1 for an illustration of individual steps. The first two steps are channel selection (Fig. 3.1 **A**) and spike extraction. These steps are conceptually in-

dependent of any specific spike sorting algorithm. The next step is pre-sorting artifact removal (Fig. 3.1 **B**), after which clean spikes are passed to block-wise iterative sorting (Fig. 3.1 **C**). Remaining spikes are then assigned by template matching (Fig. 3.1 **D**), and non-neural clusters are detected and removed (Fig. 3.1 **E**). The last step is to re-combine all clusters from the different blocks (Fig. 3.1 **F**).

Channel selection and spike extraction

In a typical multi-channel setup, not all electrodes record meaningful signals. Reasons for corrupted signals include: bad/broken wiring in the electrodes, inadequate electrode impedance, excessive pick-up of 50/60 Hz power line noise and its higher harmonics. Furthermore, in recordings from the human brain, a micro-electrode bundle sometimes has its tip in white matter or cerebrospinal fluid, where recording of action potentials is impossible.

To exclude unsuitable channels from subsequent analysis, our analysis framework contains a viewer program. The program displays segments of each channel's signal at different temporal resolutions (for a screenshot, see Fig. 3.2 **A**).

Viewing the data at different time scales allows to assess presence of action potentials, contamination by electrical noise, and contamination by low-frequency artifacts. Examples of one selected and one discarded channel are shown in Fig. 3.1 **A**.

Spikes are detected and extracted from all selected channels by the following method, similar to WaveClus (Quian Quiroga, Nadasdy, et al. 2004), but optimized both for speed and large datasets. Raw neuronal recording data are bandpass filtered between 300 Hz and 1000 Hz (second order elliptic filter), and a threshold is determined as $\theta := \frac{5}{0.6745}\text{median}\,(\text{abs}(\mathbf{x}))$, where $\mathbf{x}$ is the filtered signal. This threshold is then used to determine the timepoints of events for extraction. Spikes can occur as both positive and negative voltage deflections. Because event extraction is computationally inexpensive in comparison to data reading and filtering, by default both positive voltage deflections above θ and negative voltage deflections below $-\theta$ are extracted. These positive and negative voltage deflections are stored as two different arrays for later sorting. For each threshold-crossing event, 64 sampling points (corresponding to approximately 2 ms at the sampling rates used here) are extracted from the signal after bandpass-filtering between 300 Hz and 3000 Hz (second order elliptic filter), and aligned to maximum after upsampling using cubic spline interpolation.

The extraction algorithm was implemented in the following, computationally efficient, way: instead of reading and processing data in an alternating manner, one process contin-

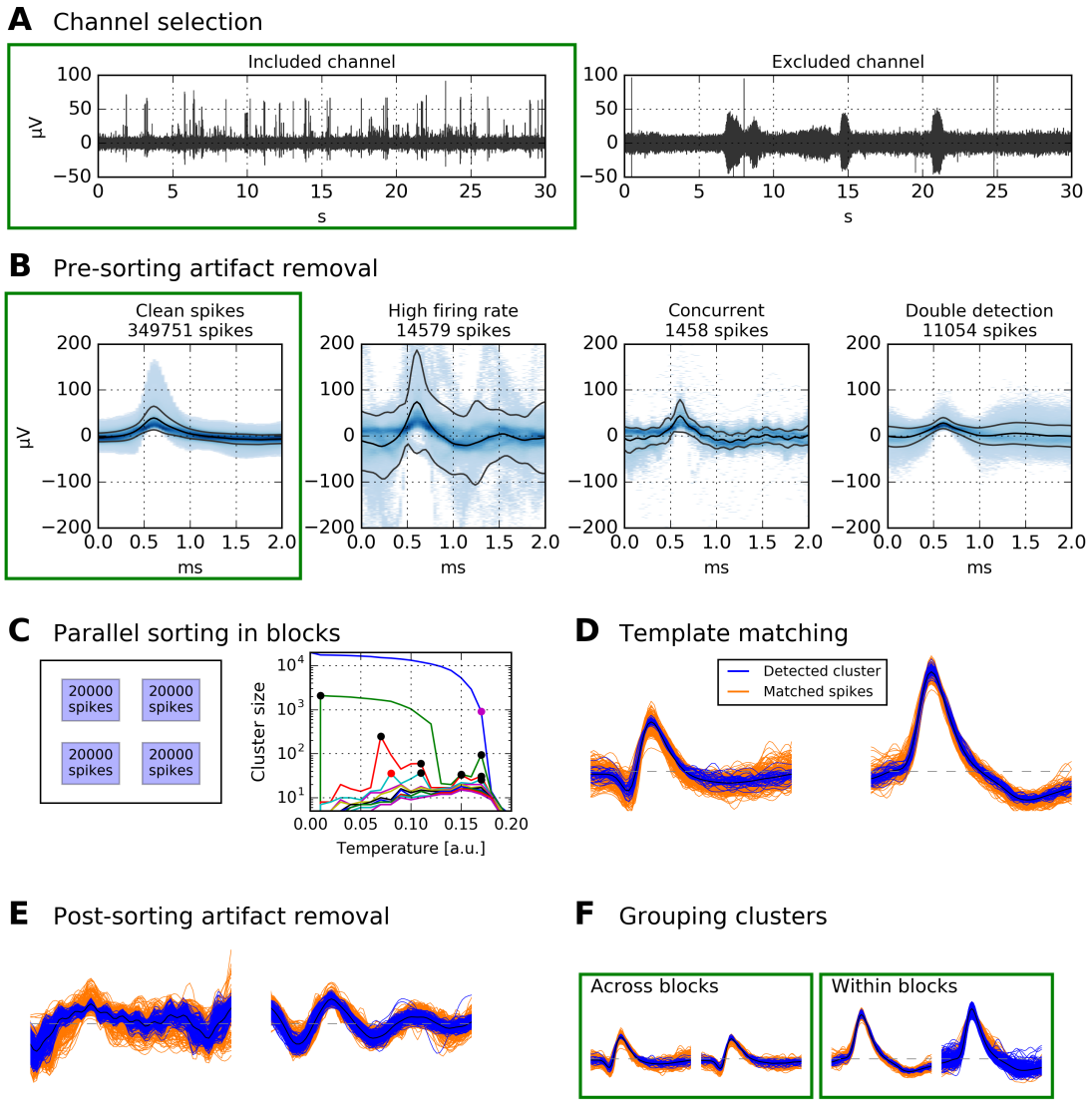

Figure 3.1: **Schematic of data processing. Data displayed in green boxes are passed on to the subsequent stage.** **A** Channels with no unit activity (i.e., broken or empty channels) are discarded. Displayed are bandpass-filtered recordings of two channels in the human MTL (passband 300 Hz to 1000 Hz). **B** After spike extraction, pre-sorting artifact rejection is performed. Displayed are density plots of all spikes extracted from a 12-hour recording (same channel as left panel in A). Artifact rejection removes ≈ 27 000 spikes, and ≈ 350 000 remain. **C** Clean spikes from B are split into blocks of 20 000. In this example, the 350 000 spikes are split into 18 blocks. All blocks are spike-sorted in parallel. For each block, clusters from several "temperatures" are selected. Displayed is an example for one block. Black dots in the temperature plot correspond to clusters that were selected, red dots to clusters that were not selected because their spikes had already been selected at lower temperatures, and the purple dot marks the highest temperature used. Large clusters are again subjected to iterative spike sorting. **D** Template matching is used to assign the remaining spikes to clusters. **E** Artifact clusters are removed. **F** Physiological clusters are grouped, both within each block and across blocks.

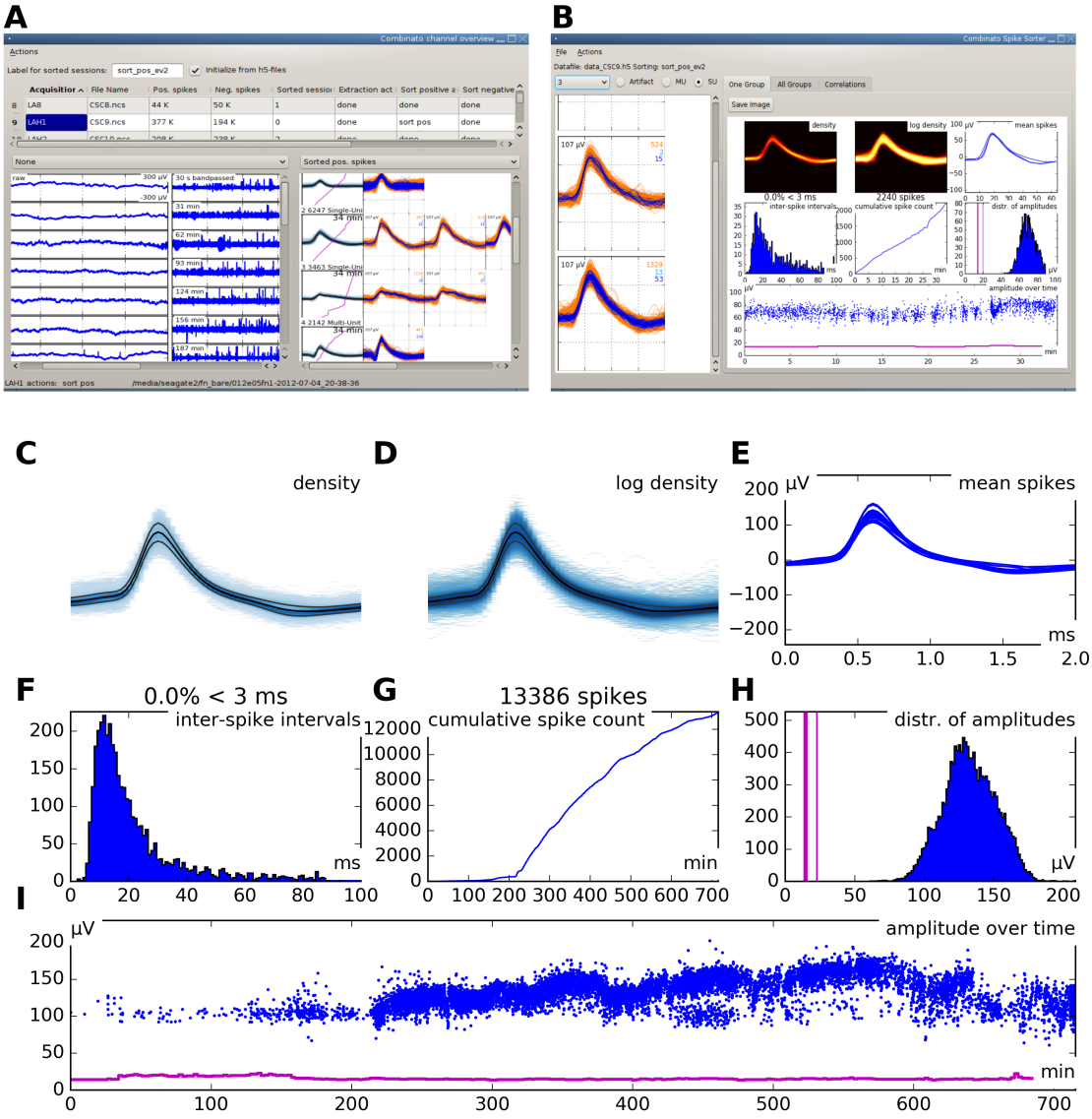

Figure 3.2: **Graphical user interface. A** Screenshot of the graphical user interface (GUI) used for channel selection. Raw and filtered data traces of all channels in a recording session are displayed along with spike sorting results from every channel for which sorting has already been performed. **B** Screenshot of the GUI used for visualization and manual optimization of spike sorting results. The interface shows several informative statistics for one unit. The individual elements are explained in panels C through I. **C** Density plot of all spike waveforms within a cluster group. **D** Same as C, but using a logarithmic scale. **E** Overlay plot of all mean spike waveforms in a group of merged clusters. **F** Histogram of inter-spike intervals. **G** Cumulative spike counts over time (700 minutes in this example). Note that the unit in this example appears to become more active after the first 200 minutes of recording. Detailed inspection of the other cluster groups is necessary to decide whether this is really the case or merely an effect of over-clustering and false re-grouping. **H** Distribution of spike maxima. The three vertical pink lines indicate the minimum, median, and maximum of the detection thresholds over time. Note that in this example, spike maxima are clearly separated from the detection threshold. **I** Spike amplitude maxima over time. The pink line is the extraction threshold. Note that the extraction threshold is relatively stable, while the maxima show considerable drift.

uously reads data segments from disk into memory, while *simultaneously* many processes (typically, one per core of the computer) run in parallel to filter the signal and to extract and store spikes. In this way, our implementation maximizes input bandwidth utilization, thereby minimizing the time processors spend idle (Alted 2010).

The extracted spike waveforms are stored as an array, along with one time stamp per spike. We use the standardized HDF5 data format, which allows for efficient processing of very long recordings.

Pre-sorting artifact rejection

Long-term recordings, especially from human subjects in a clinical setting, inevitably contain periods of excessive noise, e.g. due to subject movement or electrically interfering medical equipment. During such periods, recordings are typically contaminated by events of non-neural origin. We detect such artifacts both before and after spike sorting. Before spike sorting, we use the following procedure, the parameters of which can be modified according to specific demands:

(1) Removal of time periods exceeding reasonable neuronal firing rates. For each recording channel, event counts are calculated in time-bins of 500 ms, with an overlap of 250 ms. Time-bins containing more than 100 events (corresponding to a firing rate of 200 Hz) are excluded from further processing.

(2) Events exceeding a certain amplitude. All events exceeding a threshold of 1 mV are excluded.

(3) Removal of overlapping detections. Because our spike detection algorithm does not impose any artificial refractory period, two extracted spikes can overlap. This happens when the interval between two subsequent threshold crossings is shorter than the extraction window (typically around 2 ms); for example, when there is sinusoidal electrical noise in the range of 2 kHz, or when two different neurons fire action potentials with a very short lag. Depending on the respective scientific question, keeping both waveforms might be desirable (e.g. when analyzing synaptic coupling). When two detections occur within 1.5 ms, our default is to keep the waveform with the larger maximum, and discard the other one.

(4) Events occurring concurrently on many channels. Movement artifacts and periods of excessive electrical noise typically occur simultaneously on many channels, whereas an action potential is typically recorded on one channel only. We thus partition the spike times extracted from all channels into time-bins of 3 ms, with an overlap of 1.5 ms, and count, for each bin, the recording channels with at least one event. A time-bin is excluded

Name	Description	Default value
N_{block}	Number of spikes per sorting block	20 000
$C_{\max}$	Maximum number of clusters at one temperature	5
$S_{\min}$	Minimum number of spikes in a cluster	15
$R_{\min}$	Minimum cluster size for iterative clustering	2000
N_{rep}	Number of clustering iterations	1
f_1	Radius for within-block template matching	0.75
f_2	Radius for across-blocks template matching	3
C_{stop}	Threshold at which merging of clusters stops	1.8

Table 3.1: **Relevant parameters for the proposed spike sorting framework along with their default values.** Parameters and values are explained in the main text.

if it contains an event on 50% or more of the channels.

Note that criteria *(1)* to *(3)* are applied independently on individual channels, whereas *(4)* takes into account all recording channels at the same time.

Segmentation and spike sorting in blocks

After the exclusion of artifact events, the remaining spikes are segmented into independent blocks, such that each block consists of N_{block} consecutive spikes (by default, $N_{\text{block}} = 20\,000$; see Table 3.1 for complete parameter values). These blocks are then spike-sorted independently using parallel processing to make efficient use of modern multi-core computers. The algorithm that processes each block is based on superparamagnetic clustering (SPC; Blatt, Wiseman, et al. 1996) of wavelet coefficients, as introduced to spike sorting in WaveClus (Quian Quiroga, Nadasdy, et al. 2004). However, our procedure differs from WaveClus in the following ways: clusters at several different "temperatures" of the SPC algorithm are selected automatically; clusters are re-clustered in an iterative procedure; similar clusters are merged automatically; template matching is performed at two different stages; unassigned spikes are iteratively re-clustered. What follows is a detailed description of our per-block algorithm.

Feature selection. Similar to WaveClus, a four-level wavelet decomposition is computed for each spike using Haar wavelets. This yields an $(n \times k)$-array of wavelet coefficients, where n is the number of spikes and k the number of sampling points. To reduce feature dimensionality, we select, out of these k dimensions, the 10 dimensions in which the distribution of wavelet coefficients differs most from normality, as quantified by the Kolmogorov–Smirnov test statistic (Quian Quiroga, Nadasdy, et al. 2004).

Clustering. The 10 selected wavelet coefficients are passed on to superparamagnetic clustering (SPC). SPC depends on a parameter T (called "temperature" due to its moti-

vation from statistical physics). For each value of T, SPC partitions the input data in a particular way. Our default is to use $n_T = 21$ different values for T, equally spaced in $[0, 0.2]$. We use these independent n_T data partionings in a combined way to select data clusters.

The idea is to iterate through all temperatures from low to high: at each temperature T_j the clusters present at T_j are sorted by size (i.e., number of spikes). Then, the i-th largest cluster at T_j is selected for later processing if it is larger than the i-th largest cluster at surrounding temperatures T_{j-1} and T_{j+1}. During this iteration over the temperatures, a unique cluster identification number is assigned to each selected cluster, and all spikes belonging to a selected cluster are marked as its members. Importantly, all spikes already marked at lower temperatures $T < T_j$ are not reassigned, but remain members of the clusters selected earlier.

In other words, local maxima of "cluster size" as a function of "temperature" are selected for later processing, and spikes are irreversibly assigned to clusters by moving from low to high temperatures.

The following constraints apply: *(1)* A maximum number of $C_{\max}$ clusters are selected at any given temperature. *(2)* A cluster needs to contain at least $S_{\min}$ spikes in order to be selected, where $S_{\min}$ is defined either as an absolute number or as a fraction of the total number of spikes. *(3)* The cluster assignment procedure begins at the second temperature only, where local maxima are defined.

In this way, at each temperature up to $C_{\max}$ clusters are read out from SPC, such that each cluster contains at least $S_{\min}$ spikes. The cluster selection at different temperatures is illustrated by Fig. 3.1 **C** (right panel). Note that typically a large fraction of spikes is not assigned to any cluster at all, which makes a subsequent template matching step necessary.

Splitting of large clusters. Making use of all available temperatures considerably reduces the chances that a generated cluster contains spikes of two or more neurons (so-called *under-clustering*). To further reduce the risk of under-clustering by splitting clusters into sub-clusters, SPC clustering is run once again on every cluster that contains at least $R_{\min}$ spikes (by default, $R_{\min} = 2000$).

First template matching. After clusters have been generated as outlined above, template matching is used to assign the yet unassigned spikes to existing clusters. For each cluster, its mean spike waveform is calculated, along with a measure of its total variance, $s := \sqrt{\sum_{i=1}^{N} \mathrm{var}(x_i)}$, where $\mathrm{var}(x_i)$ denotes the variance of the cluster at the i-th sampling point. Then, the Euclidean distance between each spike and every cluster is calculated. Each spike is assigned to the cluster closest to it, provided the distance is smaller than $f_1 \cdot s$. Here f_1 is a factor that controls the radius around a mean waveform where template

matching is possible, in units of the variability of that cluster. By default, we use the conservative value $f_1 = 0.75$ for this step, because another template matching step is applied later, when pooling clusters from all blocks.

Re-iteration. After this first template matching step, the clustering procedure can be re-iterated on all spikes that are still not assigned to any cluster. This iteration of clustering and template-matching can be repeated N_{rep} times, but on our data, such iterations were unnecessary (hence by default $N_{\text{rep}} = 1$; see also Section 3.3.2).

Template matching across blocks

After all blocks of spikes from one channel have been independently spike-sorted, template matching is applied across blocks to assign the remaining unclustered spikes, using the same algorithm as for the within-block template matching. Here, we use $f_2 = 3$. Spikes that are still not assigned to any cluster remain in a special "residual" cluster.

Post-sorting artifact rejection

Although our pre-sorting artifact detection algorithm removes large fractions of non-neural events before spike sorting, it is still desirable to decide for each cluster whether it corresponds to neuronal activity or to residual noise in the recording. Often, artifact events appear in a stereotypical manner, e.g. in the case of sinusoidal electrical noise (see right panel of Fig. 3.1 **E** for an example of such an artifact cluster).

Our algorithm designates a cluster as non-neural if it meets any of the three following criteria based on its mean waveform. *(1)* The mean waveform has more than 5 local maxima. *(2)* The ratio of the largest local maximum to the second largest local maximum is less than 2, where only maxima separated by at least 0.3 ms are considered. *(3)* The amplitude range covered in the second half of the mean waveform is greater than the global maximum.

Furthermore, the standard error of the mean at each sampling point is calculated across all spikes in the cluster. A cluster is designated as an artifact if the mean of these standard errors across all sampling points is greater than 2 µV.

Merging of clusters from all blocks

At this stage of processing, each block of spikes has been spike-sorted independently, remaining spikes have been assigned by template matching, and artifact clusters have been identified.

The next step is to create groups of clusters belonging to the same unit. The input to this merging procedure is the pool of all non-artifact clusters from all blocks. The merging procedure has two aims: First, after spike sorting, two or more clusters in one block often correspond to the same unit (resulting from so-called *over-clustering*). Merging highly similar clusters within one block reduces the amount of over-clustering. Second, the same unit typically appears across many blocks (in sufficiently stable recordings, the same units should appear in *all* blocks). Merging highly similar clusters across blocks ensures that units can be tracked over the entire duration of the recording. Guided by empirical testing, we decided to perform both merging procedures – within and across blocks – in parallel. We use a simple hierarchical clustering method for cluster merging, based on the Euclidean distance between mean spike waveforms of the cluster groups. After merging the two clusters whose distance is minimal, the mean waveform is updated, and distances are re-calculated. Merging stops once the minimal distance is greater than a predefined threshold C_{stop} (by default, $C_{\text{stop}} = 1.8$). Importantly, our algorithm saves the original cluster identity of each spike, so that cluster grouping can later be undone if desired. It is also possible to use this cluster identity as a feature for subsequent analyses. Examples of cluster merging both within and across blocks are shown in Fig. 3.1 **F**.

Optional manual verification

Our spike sorting framework comes with a graphical user interface (GUI), which is used to visualize sorting quality, to modify the grouping of clusters, and to mark additional artifact clusters, if necessary. Fig. 3.2 **B** shows a screenshot of the GUI. Different cluster visualization features are explained in Fig. 3.2 **C** through **I**. Some of these features are inspired by a recent publication (Hill, Mehta, et al. 2011). The sparsely firing unit used as an example in Fig. 3.2 **C** through **I** was tracked over the time course of 700 minutes. The total number of spikes in this recording was approximately 330 000. More detailed instructions on how to use the GUI are contained in Appendix A.2.

3.3 Results

Our method proved useful both for spike sorting of short recordings (up to one hour), and for long-term tracking of unit activity over many hours. To demonstrate the broad applicability of our framework, we evaluated it using four different datasets: *(1)* simulated model data (simulated recording duration 10 minutes; Section 3.3.1), *(2)* simulated model data with drift (simulated recording duration 10 hours; end of Section 3.3.1), *(3)* short

recordings from a visual stimulus presentation experiment (Section 3.3.2), *(4)* whole-night recordings from epilepsy patients (Section 3.3.3).

3.3.1 Validation on simulated model data

It is becoming increasingly recognized that in order to estimate the reliability of spike sorting methods, using data with ground-truth is necessary (Einevoll, Franke, et al. 2012). To evaluate our method in a setting where ground truth is available, we used a recent dataset of simulated neural activity. Details regarding this dataset have been published (Pedreira, Martinez, et al. 2012) and the data are available online (`http://bioweb.me/CPGJNM2012-dataset`; Rey, Pedreira, et al. 2015). The dataset consists of 95 simulations, each one representing 10 minutes of continuous recording, sampled at 24 kHz. Each simulation contains the activity of 2 to 20 neurons, superimposed on background noise and multi-unit activity. There are 5 simulations for each number of neurons, resulting in a total of 95 simulations. We chose this dataset because the performance of expert operators of WaveClus on it has been evaluated (Pedreira, Martinez, et al. 2012). Using this dataset, we analyzed our algorithm's reliability by comparing its performance to ground truth, as well as to expert operators' results.

In a first step, spike detection was performed on the simulated dataset. Averaged over the 95 simulations, only 79.2% (SD 8.3%) of all spikes were found, which is indicative of the noise in the simulations (same numbers with WaveClus).

We then used our spike sorting method to spike-sort the extracted spikes. No post-sorting artifact detection was performed because the simulations did not contain any artifacts. We spike-sorted the first of the 95 files several times with various settings to empirically determine suitable parameters based on visual inspection of the spike sorting results, and then used these parameters to evaluate our method on the remaining 94 simulations. We used only one simulated channel for parameter optimization in order to avoid overfitting of parameters. For a more complete evaluation of the various parameters, see the following section.

We used the following parameter values: $C_{\max} = 7$; $C_{\text{stop}} = 1.6$; $N_{\text{rep}} = 2$; $R_{\min} = 1000$; all other parameters were kept at their default values (see Table 3.1 for description of parameters). The deviations from default in $C_{\max}$, C_{stop}, and N_{rep} reflect the relatively large number of true clusters in the simulated data, and the change in $R_{\min}$ accounts for the short overall duration of 10 minutes. We used our algorithm in its completely automatic mode without any manual interaction to strictly avoid a bias of any sort. Fig. 3.3 **A** shows samples of temperature plots with selected clusters marked.

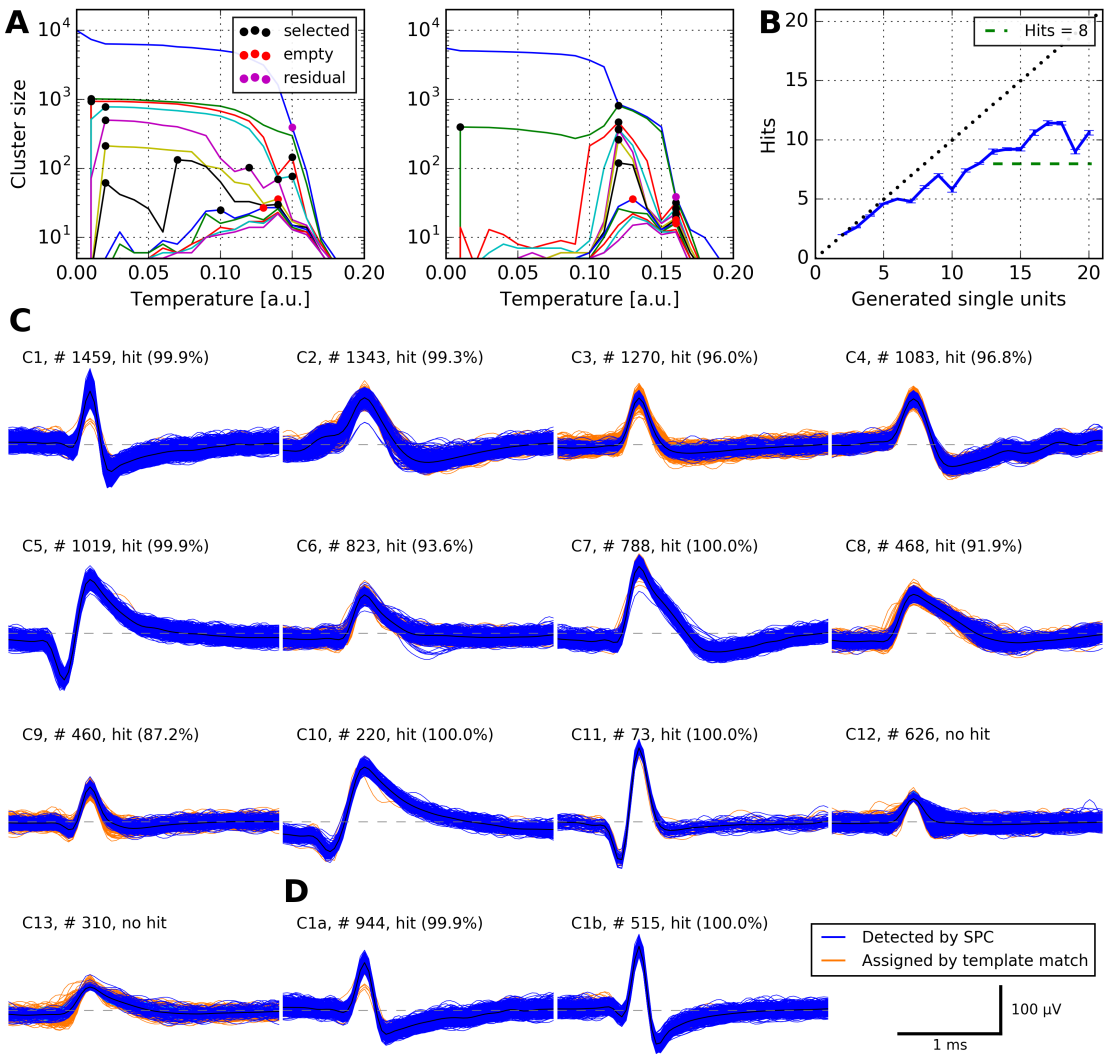

Figure 3.3: **Performance of our algorithm on simulated data. A** Cluster sizes at different temperatures for one of 95 simulations (simulation_5). Each marked location corresponds to an automatically selected cluster; up to $C_{\max} = 7$ clusters are selected at each temperature. Left panel, input to this clustering step were all spikes in one simulated channel. Right panel, input to this clustering step were all spikes not assigned to any cluster during the first clustering step. **B** Performance of our algorithm on all simulated datasets. Each simulated dataset contained action potentials from 2 to 20 neurons. For each simulation, we calculated the number of *hits*: a unit U generated by our spike sorting method was considered a hit if at least 50% of the spikes in U belonged to one neuron and at least 50% of the spikes of that neuron were in U. Displayed is the number of hits as a function of the number of neurons in the simulations (error bars denote s.e.m.). Note that our algorithm is capable of detecting more than eight neurons, a typical maximum for manual operation of WaveClus (Pedreira, Martinez, et al. 2012). **C** All automatically generated clusters from simulation_5. Shown are spike counts and the percentage of spikes in the detected unit that actually belonged to the corresponding neuron in the simulation. Eleven clusters were hits, two clusters were no hits. Note that cluster C11 was perfectly detected despite its low firing rate of 0.12 Hz. **D** Undoing an automatic merge in cluster C1 with our graphical interface generated another hit.

To quantify the success of spike sorting, we used the same score as in Pedreira, Martinez, et al. (2012): A given unit U is considered a *hit* if it fulfills the following two criteria: *(1)* at least 50% of the spikes in U belong to one neuron; *(2)* at least 50% of the spikes of that neuron are in U. See Fig. 3.3 **C** for an example where our algorithm automatically generated 13 clusters, 11 which of were hits. We calculated the number of hits for each of the 95 simulations in the test set. We then grouped the datasets by the number of neurons present, and calculated the fraction of hits for each group (compare Table 1 in Pedreira, Martinez, et al. 2012).

Our algorithm significantly outperformed manual expert operators. In its completely automatic mode, it generated 71.5% (SD 13.8%) hits (percentage of simulated neurons), while Pedreira, Martinez, et al. (2012) achieve 66.7% (SD 18.1%) on the same data with experts manually operating WaveClus ($T = 31.5$, $p = 0.033$; Wilcoxon signed-rank test). Restricting analysis to the more difficult group of simulations with at least 8 neurons, our algorithm generated 64.5% (SD 8.2%) hits, while Pedreira, Martinez, et al. (2012) achieved 58.9% (SD 14.1%) hits ($T = 12.0$, $p = 0.034$; Wilcoxon signed-rank test).

We visualized the proportion of hits for each number of neurons present in the simulations in Fig. 3.3 **B** (compare Fig. 4 in Pedreira, Martinez, et al. 2012). We also verified that the number of hits can be further increased by manually optimizing sorting using our graphical interface. Fig. 3.3 **D** shows an example where manually undoing an automatic merge of two clusters produced an additional hit.

Evaluation at different parameter settings

Having evaluated the performance of our algorithm with one parameter setting, we systematically investigated the influence of the parameters on the sorting result. We analyzed the same simulated dataset using a total of 48 different parameter settings. Specifically, we tested all combinations of the following: $C_{\text{max}} \in \{5, 7\}$, $R_{\text{min}} \in \{500, 1000, 2000\}$, $N_{\text{rep}} \in \{1, 2\}$, $C_{\text{stop}} \in \{1.2, 1.4, 1.6, 1.8\}$. For each of these settings, we quantified the success of spike sorting by counting the number of hits in each simulation. The results are displayed in Fig. 3.4. We used a Wilcoxon signed-rank test in order to compare the number of hits at each parameter setting to the number of hits obtained by manual expert operators in Pedreira, Martinez, et al. (2012). Our method outperformed manual operators for 24 of the 48 different settings used, and in 13 settings, this difference was statistically significant.

At the ranges tested here, R_{min}, C_{stop}, and N_{rep} monotonically influenced the number of hits generated: Increasing C_{stop} above 1.2 always led to a decrease in the number of hits

with all other parameters fixed (12 cases). The same was true when we increased R_{min} above 500 (16 cases), and when we changed N_{rep} from 2 to 1 (24 cases).

The highest fraction of hits was obtained for the setting $C_{\text{max}} = 7$, $R_{\text{min}} = 500$, $N_{\text{rep}} = 2$, and $C_{\text{stop}} = 1.2$. At this setting, 83.6% (SD 8.0%) hits (percentage of simulated units) were generated by our methods (manual operators in Pedreira, Martinez, et al. (2012): 66.7%, $T = 3.0$, $p = 0.0003$; Wilcoxon signed-rank test). The percentage of hits at the best of the 48 parameter settings tested was higher than at the parameter setting we had found by manually optimizing one simulated channel only (83.6% versus 71.5%). At the best of the 48 parameter settings, when including only the more difficult group with at least 8 neurons, our algorithm generated 80.0% (SD 5.8%) hits (manual operators in Pedreira, Martinez, et al. (2012): 58.9%, $T = 0$, $p = 0.001$; Wilcoxon signed-rank test).

Evaluation on multi-hour simulations

To test our algorithm's capabilities at tracking neurons over many hours, we concatenated the simulated data from Pedreira, Martinez, et al. (2012) after extracting spikes. For each number of simulated neurons, ranging from 2 to 20, we chose the first simulation containing this specific number of neurons and concatenated it 60 times, resulting in a total of 19 simulations of 10 hours duration each. In order to make the spike sorting task more difficult, we applied two modifications to each concatenated dataset: *(1)* We simulated electrode drift by multiplying the extracted spikes with a factor that linearly increased from 1 to 1.5 over the course of the 10 hours. *(2)* After this scaling, we added Gaussian noise to each datapoint of the extracted spikes. The noise had a mean of zero and a standard deviation of 20% of the maximum value attained in each simulation.

We then used our algorithm on the concatenated, modified simulations. We tested four different parameter settings: Informed by the systematic parameter evaluation discussed above, we used $C_{\text{max}} = 7$, $R_{\text{min}} = 500$, and $N_{\text{rep}} = 2$. The parameter C_{stop} was set to 1.2, 1.4, 1.6, and 1.8, respectively. An example of a simulated unit that was successfully tracked over 10 hours is shown in Fig. 3.5.

Fig. 3.6 shows the number of hits obtained at each setting and number of neurons. The highest number of hits, obtained at $C_{\text{stop}} = 1.4$, was 74.6% (SD 17.1%).

3.3.2 Validation on a picture presentation experiment

After validating our method's performance on simulated data, we then turned to data recorded from human subjects during a cognitive paradigm. Six epilepsy patients were implanted bilaterally with micro-electrodes in the medial temporal lobes (MTLs) as outlined

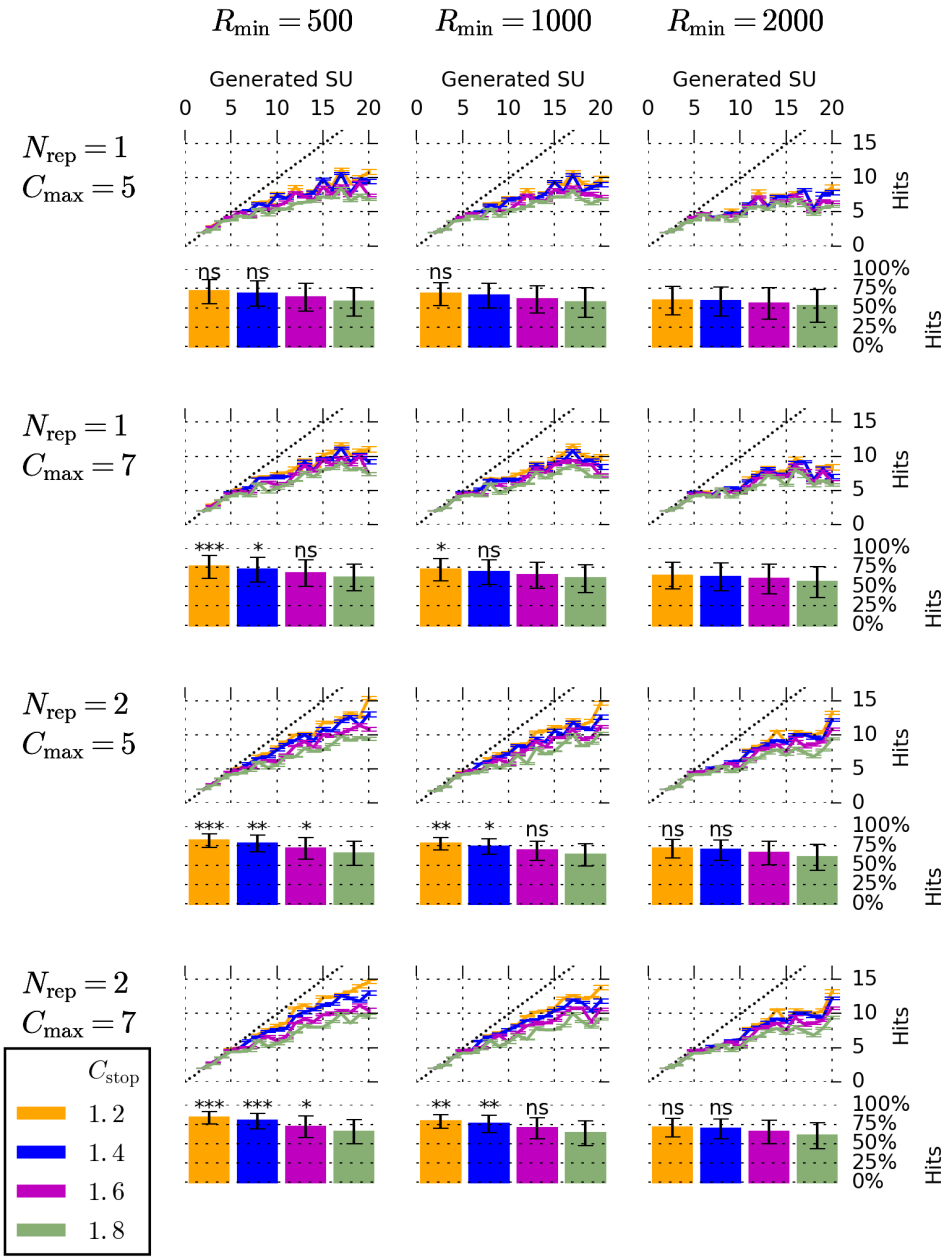

Figure 3.4: **Performance of our algorithm on simulated data at different parameter settings.** Results for a total of 48 different parameter settings are displayed. Each column of panels corresponds to one value of $R_{\min}$ (indicated above each column), and each row of panels corresponds to one pair of values for N_{rep} and $C_{\max}$ (indicated left of each row). Colors correspond to four different values of C_{stop}, as indicated by the legend in the lower left. Each line plot shows the number of hits as a function of the number of neurons in the simulation (error bars denote s.e.m.), compare Fig. 3.3 **B**. Each bar plot represents the number of hits as a fraction of the number of neurons in the simulation (error bars denote standard deviation). The presence of asterisks or 'ns' above each bar indicate that the fraction of hits obtained at this particular choice of parameters is higher than the one obtained by manual expert operators in Pedreira, Martinez, et al. (2012) ('ns' if $p \geq .05$; * if $p < .05$; ** if $p < .01$; *** if $p < .001$). A Wilcoxon signed-rank test was used for all comparisons. Bars without 'ns' or asterisks indicate parameters at which the fraction of hits was lower than the one obtained by manual expert operators.

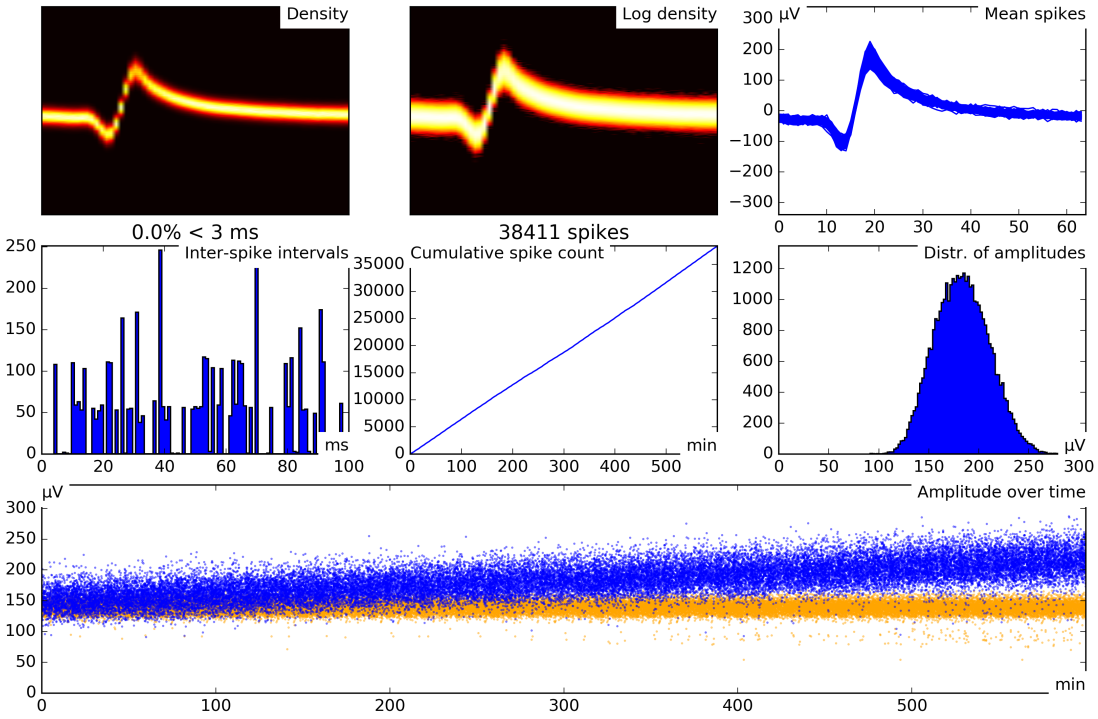

Figure 3.5: **Example of a simulated neuron successfully tracked over 10 hours.** This specific simulation was created by concatenating `simulation_10` 60 times, resulting in a total of 820 800 spikes. Drift was simulated by multiplying the extracted spikes by a linearly increasing factor. Gaussian noise was added to the extracted spikes before sorting. The tracked unit has 38 411 spikes. Of these, 38 012 spikes belong to one unit in the simulation (which consists of 40 200 spikes), and 399 spikes belong to different units. The unit was successfully tracked despite the drift. Each subpanel is labelled according to its content. In the panel *Amplitude over time*, the tracked unit is displayed in blue, and the same unit without drift and without added noise is displayed in orange for comparison. Drift and added noise are clearly visible in the tracked unit.

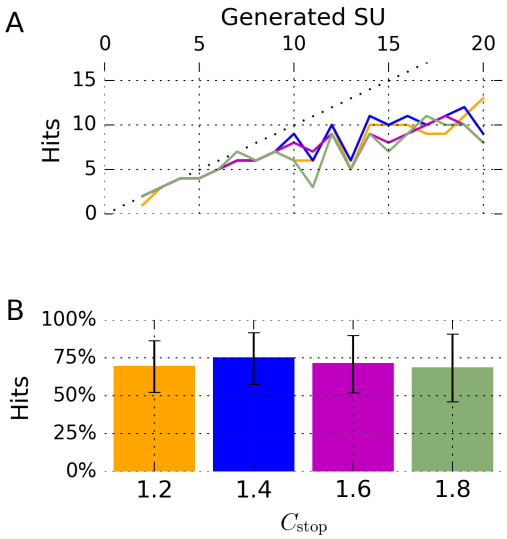

Figure 3.6: **Performance of our algorithm on multi-hour simulated datasets. A** Results for a total of 4 different parameter settings are displayed. The number of hits is shown as a function of the number of neurons in the simulations. See **B** for color legend. **B** Each bar represents the mean number of hits as a fraction of the number of neurons present in the simulation. Error bars denote standard deviation. The colors of the bars correspond to the lines in **A**.

in Chapter 2. We used a picture presentation paradigm to screen for neurons in the MTL that responded selectively and possibly invariantly to a small number of visual stimuli. In these "screening sessions", the six patients were presented with 130 to 150 pictures (mean 138.3) of well-known persons, landscapes, animals, and other objects. Pictures were presented in a pseudorandomized order on a laptop screen. Each picture was presented six times, for a duration of one second. Details of this paradigm have been described previously (Quian Quiroga, Reddy, et al. 2005; Mormann, Kornblith, et al. 2008; Mormann, Dubois, et al. 2011).

We used our viewer program (see Fig. 3.2 **A**) to exclude recording channels that clearly carried no unit activity. Starting from an initial total number of 536 channels, this left us with 409 recording channels (range 36 to 87 per session, median 70) from the amygdala, hippocampus, entorhinal cortex, and parahippocampal cortex.

We used our software in its completely automatic mode to extract spikes, remove artifact spikes, sort spikes, and mark artifact clusters. The pre-sorting artifact rejection removed different fractions of spikes on different channels: 6.3% of all spikes were removed, but on some channels, up to 76.6% of the spikes were removed. See Table 3.2 for details and Fig. 3.7 for an example of a channel on which clean clusters and clear neuronal responses were detected only after our pre-sorting artifact algorithm removed

Artifact type	% chan. aff.	% spikes removed		
		mean (all chan.)	max (aff. chan.)	of all spikes
Firing rate	6.4	13.1	67.2	2.3
Amplitude	30.1	0.5	3.7	0.1
Double detection	96.3	8.7	48.6	3.7
Concurrent	64.3	3.5	41.2	0.3
Any of the above	96.6	12.0	76.6	6.3

Table 3.2: **Effect of pre-sorting artifact removal.** These values show the variability of artifacts across channels. For example, only 6.4% of all channels were affected by the artifact criterion related to high firing rates, but on these affected channels, an average of 13.1% and a maximum of 67.2% of the spikes were removed. See main text for a detailed description of different types of artifacts. chan., channels; aff., affected.

large amounts of noise. Fig. 3.7 **D** also shows examples of a correct post-sorting artifact rejection, as well as an artifact cluster that the post-sorting artifact criterion missed (Cluster 4 in Fig. 3.7 **D**). Table 3.2 and Fig. 3.7 also give an impression of both the amount and characteristics of noise in the data used here.

To test the performance of our automated algorithm against an established standard, we again chose WaveClus. We asked trained operators to analyze the same dataset: operators sorted the data with WaveClus and optimized sorting results manually using its graphical interface. These operators were uninformed about the analyses described here. Manual operation of WaveClus typically resulted in fewer units per channel than application of our automated method, see Fig. 3.8 **D**. We controlled for this difference in further evaluations (see below and Section 3.4).

We tested to which extent the single- and multi-unit responses found by manual spike sorting with WaveClus could be recovered by our automated method.

In the following, we use the term *WaveClus sorting* to refer to the clusters generated by manual operation of WaveClus, and *Combinato sorting* to refer to the clusters generated by our automated method.

To identify response-eliciting pictures and the corresponding single- or multi-units, we used a simple *response score* algorithm (Mormann, Kornblith, et al. 2008; Mormann, Dubois, et al. 2011; Mormann, Niediek, et al. 2015). Briefly, action potentials from all six repetitions of a picture presentation (6×1000 ms) were binned into 19 overlapping time-bins with a duration of 100 ms each and an overlap of 50 ms. The Mann–Whitney U test was applied to each time-bin separately against a baseline distribution consisting of all 500 ms intervals preceding all picture onsets. These 19 p-values were subjected to the Benjamini–Hochberg procedure (Benjamini and Hochberg 1995), yield-

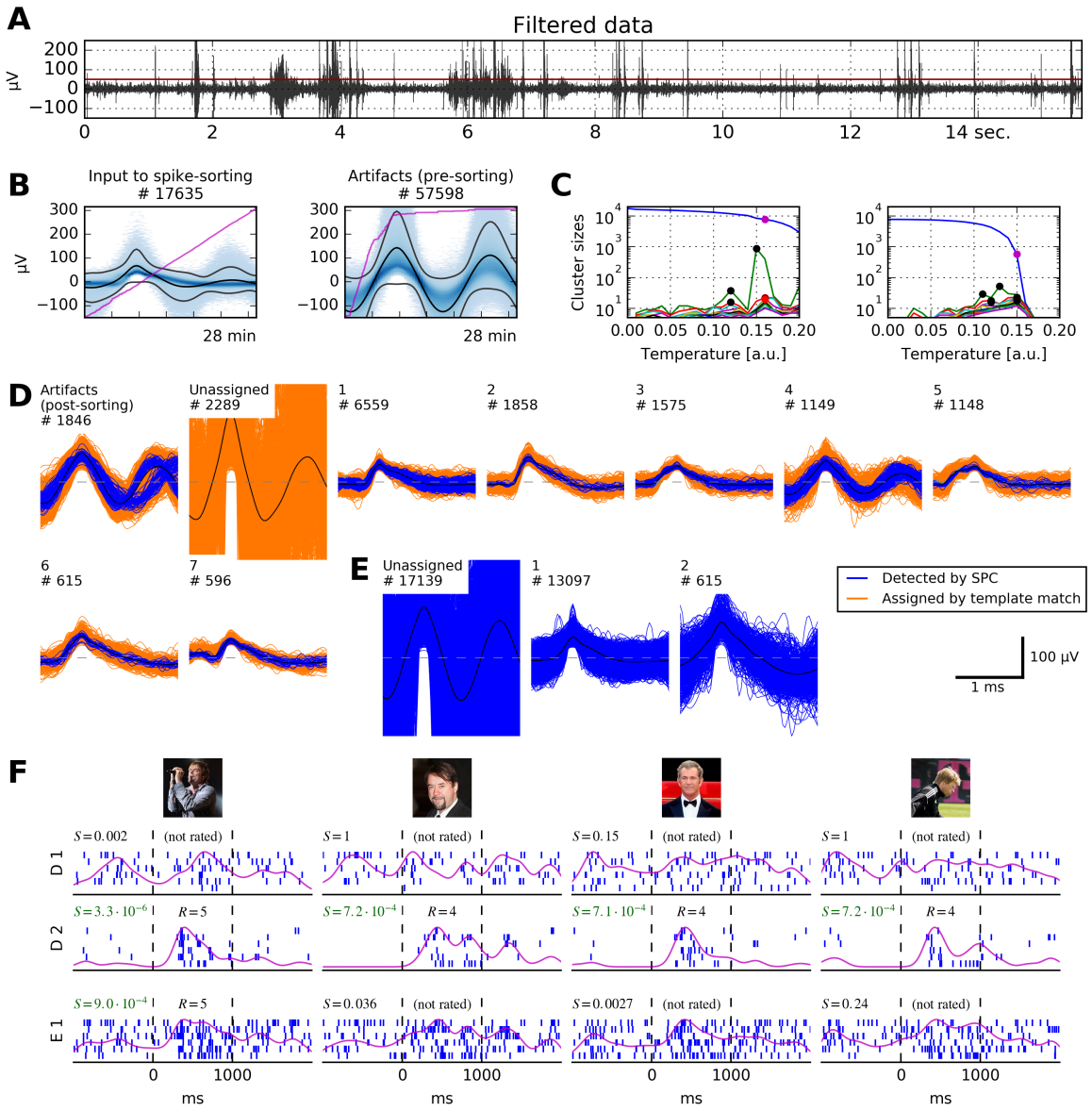

Figure 3.7: **Our algorithm applied to recordings from the human medial temporal lobe (MTL).** **A** 15 seconds of bandpass filtered data (passband 300 Hz to 1000 Hz) from a micro-electrode in the right anterior hippocampus. Extraction threshold is marked in red. Several artifact events are clearly visible. **B** This recording channel is extremely noisy: Our pre-sorting artifact detection removed ≈ 77% of all spikes from the recorded data. The pink lines depict the cumulative count of events over the course of the recording (28 minutes). **C** Cluster sizes at different temperatures. Left panel, input to the first clustering step were all non-artifact spikes. Right panel, input to the second clustering step were residual spikes not assigned to any cluster in the first clustering step. Color code of marked dots as in Fig. 3.3. **D** Output of our sorting algorithm. Post-sorting artifact detection correctly identified several artifact clusters, but missed one (number 4). Six non-artifact clusters remain. **E** Result that expert operators generated manually with WaveClus. Two clusters were identified, ≈ 17 000 spikes were left unassigned. **F** Results of the picture presentation experiment. Displayed are raster plots corresponding to Clusters 1 and 2 from D, and to Cluster 1 from E. Responses to four different pictures are shown. It is clearly visible that Cluster D 2 responds sharply to pictures of four male celebrities, while the responses of Cluster E 1 to the second, third and fourth picture are barely recognizable. No other cluster from D responded to any stimulus. S, score of the response; R, rating given to the response by human raters (see main text for details). Stimulus pictures displayed here have been replaced by similar pictures for legal and privacy reasons.

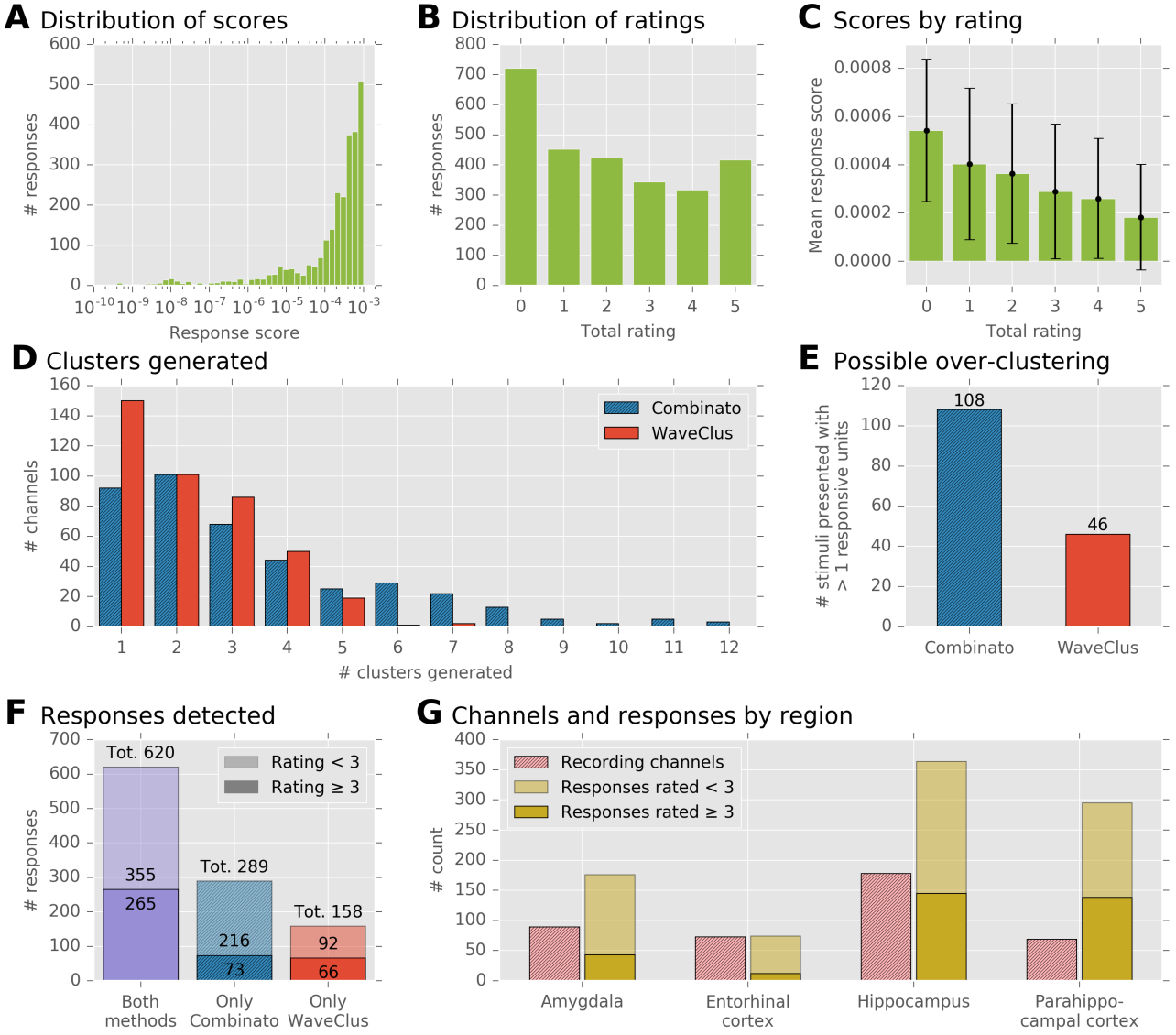

Figure 3.8: **Evaluation of our algorithm on a visual stimulus presentation experiment. A** Distribution of response scores. Some scores are extremely small, but the majority of scores lies in the interval $[10^{-4}, 10^{-3}]$ (1939 out of 2672; 72.6%) **B** Each response's rating is defined as the sum of the binary votes of five human raters. Of all 2672 ratings, 1596 (59.7%) were < 3, and 1076 (40.3%) were ≥ 3. **C** Mean score and standard deviation of responses at each rating. The relationship between mean scores and ratings is strictly monotonic, but the variance of scores at each rating is large. **D** Histogram of the numbers of clusters that were generated, on the same recordings, by Combinato and WaveClus. On average, Combinato generated more clusters. **E** Analysis of possible over-clustering. Displayed is the number of stimuli for which a response was detected in more than one cluster of the same recording channel. **F** Total numbers of detected responses. The numbers were corrected for possible over-clustering: only one response was counted per stimulus and channel, even if the response was detected in multiple clusters. Of all responses, 620 were detected both by Combinato and WaveClus. An additional 289 responses were detected only by Combinato, and further 158 responses only by WaveClus. The opaque parts of the bars correspond to responses that were rated 3 or better by expert raters. **G** Distribution of recording channels and responses across regions. Opaque parts of the bars as in F.

ing one single score. The combination of a neuronal cluster and a stimulus picture was then called a *response* if the p-value obtained by this procedure was below 0.001, and if action potentials were fired during at least four presentations of the picture.

We calculated response scores for all stimuli and all clusters from both sortings. For every channel, we included its unsorted multi-unit activity as an additional cluster. The response score algorithm yielded a total of 2672 numerically identified responses. Fig. 3.8 **A** shows the distribution of all response scores.

Our aim was to compare how WaveClus and Combinato perform in finding responsive neurons. Therefore, we could have compared how many numerically identified responses both methods yielded (WaveClus, 1274; Combinato, 1398). However, this comparison neglects two important aspects stemming from potential over-clustering: First, if Combinato tended to over-cluster the data, would a simple response count not be inflated due to responses from single neurons that would appear in multiple clusters because of over-clustering? Second, would a higher number of clusters not increase the number of detected responses simply because of false-positive detections? In light of these potential pitfalls, we used the following approach to ensure a fair comparison between WaveClus and Combinato.

We asked five expert human raters to rate each of the 2672 identified responses. For each response generated by the algorithm, raters were presented with a raster plot of the neural activity during the six picture presentations, showing spikes from one second prior to picture onset to one second after picture offset. Each rater was asked to assign a value of either one or zero to each raster plot, indicating whether or not it contained the typical pattern of a neuronal response. The total rating of the response was then defined as the sum of all raters' scores, resulting in a number between zero and five. The raters were informed about the purpose of the procedure, but uninformed about the stimulus picture and clustering method that had generated each raster plot. As a measure of inter-rater agreement, we calculated Cohen's κ for each of the ten pairs of raters (Cohen 1960). The median κ was 0.466 (range 0.258 to 0.525).

Fig. 3.8 **B** shows the distribution of ratings. The rating procedure confirmed the high false-positive rate of the numeric response score: of all 2672 numerically detected responses, 1596 (59.7%) received a rating of less than 3, while 1076 (40.3%) were rated 3 or better. As expected, the mean numeric response score at a specific rating was a strictly decreasing function of the rating, see Fig. 3.8 **C**. Spearman's rank correlation coefficient between the ranks and the scores was $\rho = -0.399$ ($p = 10^{-102}$), and Kendall's rank correlation coefficient was $\tau_b = -0.291$ ($p = 10^{-112}$).

We then used the ratings to control for possible over-clustering in the comparison of

WaveClus and Combinato. First, if more than one cluster on a given channel responded to the same stimulus, we kept only the response that had received the highest rating, and dropped all others. This applied to 108 stimulus–channel combinations in the Combinato sorting and 46 stimulus–channel combinations in the WaveClus sorting, see Fig. 3.8 **E**. After removing all but one response for all of these stimulus–channel combinations, 778 responses remained in the WaveClus sorting, and 909 responses remained in the Combinato sorting. By applying this control, we ensured that no stimulus–channel combination could contribute more than once to these counts, which effectively ruled out response count inflations due to over-clustering. Fig. 3.8 **F** depicts the distribution of these responses: 620 responses were detected in both the Combinato and the WaveClus sorting, an additional 289 responses in the Combinato sorting only, and an additional 158 responses in the WaveClus sorting only.

Second, to ensure that the higher response count in the Combinato sorting was not just due to false-positive detections, we restricted our analyses to responses rated 3 or better. Here, 265 responses were detected in both sortings, 73 in the Combinato sorting only, and 66 in the WaveClus sorting only.

Responses were detected in all regions we recorded from. Fig. 3.8 **G** shows the regional distribution of responses as detected in the Combinato sorting.

A number of responses was detected by only one of the methods: 32% of the responses detected by Combinato were not detected by WaveClus, and 20% of the responses detected by WaveClus were not detected by Combinato. When including only responses rated 3 or better, 22% of the responses detected by Combinato were not detected by WaveClus, and 20% of the responses detected by WaveClus were not detected by Combinato.

Fig. 3.9 shows five examples of responses that were detected by only one of the methods. These examples illustrate that several different factors can contribute to the difference in response detection. First, small differences in cluster composition can strongly influence the numeric response score (Fig. 3.9 **B**, **C**, and **E**). In these cases, responses are detected numerically by only one of the methods, despite relatively similar cluster composition. Second, better separation of clusters can render responses detectable that would otherwise go unnoticed (Fig. 3.9 **A**). Third, the fact that we require at least one spike to be fired during at least four picture presentations leads to the exclusion of some clusters that would otherwise have a low numeric response score (Fig. 3.9 **D**).

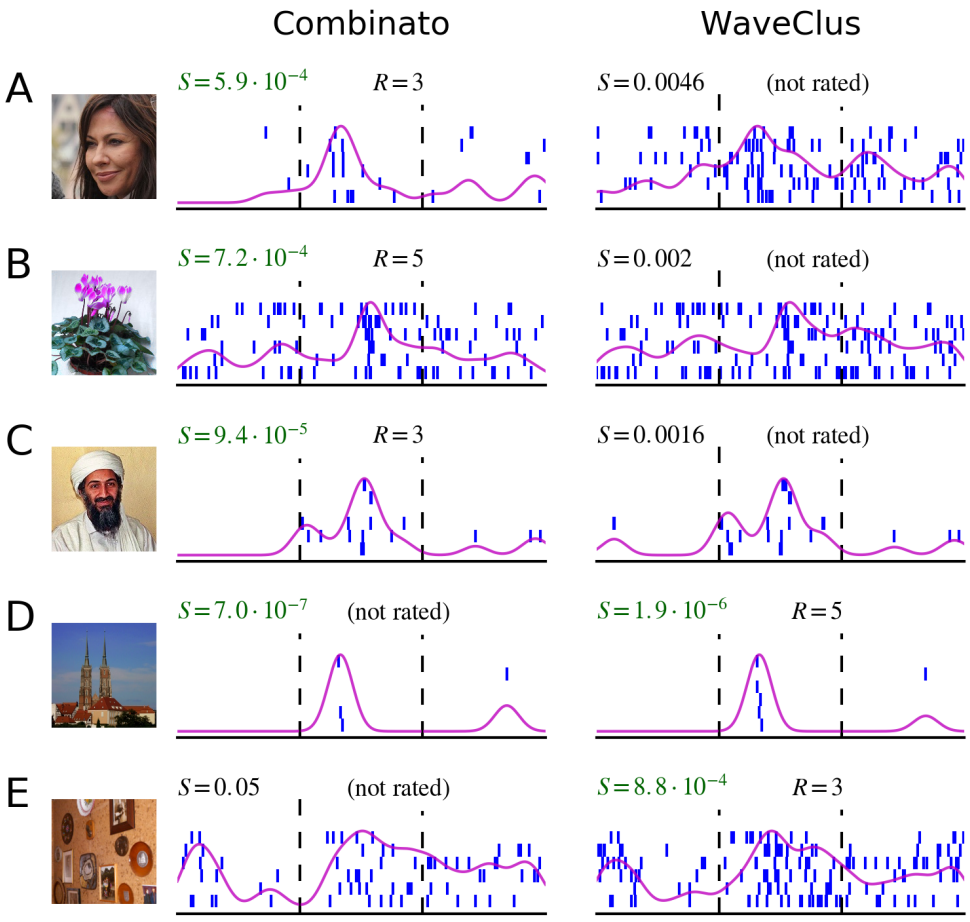

Figure 3.9: **Responses detected by only one spike sorting algorithm.** Displayed are five different visual stimuli, and corresponding neuronal responses. Each row (**A**–**E**) shows the visual stimulus presented and two raster plots. The raster plots on the left correspond to a unit in the Combinato sorting, and the raster plots on the right correspond to a unit in the WaveClus sorting, on the same channel. Differences in spike sorting become apparent. **A** Combinato generated a sparse unit that enabled detection of the neuronal response. The unit generated by manual operators of WaveClus was not detected as a response. **B**, **C** Tiny differences in the units' composition led to a large difference in the numeric response score. **D** The unit generated by Combinato violates the requirement that one spike has to be fired during at least four picture presentations. **E** Differences in unit composition led to a large difference in the numeric response score. S, numeric score of the response; R, rating given to the response by human raters. Stimulus pictures displayed here have been replaced by similar pictures for legal and privacy reasons.

3.3.3 Validation on whole-night recordings

Combinato was designed to work with long, possibly noisy, recordings. To test its performance on such data, we used whole-night recordings from eight epilepsy patients, implanted with depth electrodes for presurgical monitoring and microwires as described in Chapter 2. Recordings started between 18:00 and 21:00 and ended between 8:00 and 11:00 (see middle column in Fig. 3.10 for exact times).

We used selective neuronal responses to images and written names in order to assess whether our method can track the activity of a single neuron over the course of an entire night. For this purpose we conducted a "screening session" at the beginning and end of each whole-night recording. These screening sessions differed only slightly from the experiment described in the previous section: here, eight to eleven pictures were presented to the patients. For each picture, a written representation of the picture's content was also presented (in seven out of the eight patients). Each picture and each written name was presented ten to thirty times.

We used Combinato to extract and sort unit activity from all recordings. We then analyzed the screening sessions at the beginning and end of each recording. To illustrate our findings in a qualitative way, we selected one representative channel from each recording. Fig. 3.10 shows the unit activity recorded in these channels from eight different patients. We chose channels carrying a selective neuronal response in both screening sessions (evening and morning), see columns "Evening" and "Morning" in Fig. 3.10. These responses allowed to analyze whether our method splits one neuron's activity into several different units in whole-night recordings.

The units displayed in Fig. 3.10 exhibit several phenomena: In three cases (Fig. 3.10 **A**, **B**, and **E**), the response to the stimulus was contained in the same cluster both in the evening and morning, and no other cluster showed any response to the same stimulus. In Fig. 3.10 **A** and **B**, the response raster plots from evening and morning are highly similar, whereas in Fig. 3.10 **E**, the response is much more pronounced in the evening than in the morning.

In the five remaining cases (Fig. 3.10 **C**, **D**, **F**, **G**, **H**), more than one of the generated clusters responded to the stimulus. In Fig. 3.10 **C**, a clear amplitude shift over the course of the night is visible in the responsive clusters. The graphical user interface can be used here to merge the two units into one continuous track. In Fig. 3.10 **D**, **G**, and **H**, more than one stable, responsive cluster exists throughout the recording. In each of these cases, one of the tracked clusters creates the majority of the response, with small contributions by the other clusters. All clusters were successfully and independently tracked. Careful

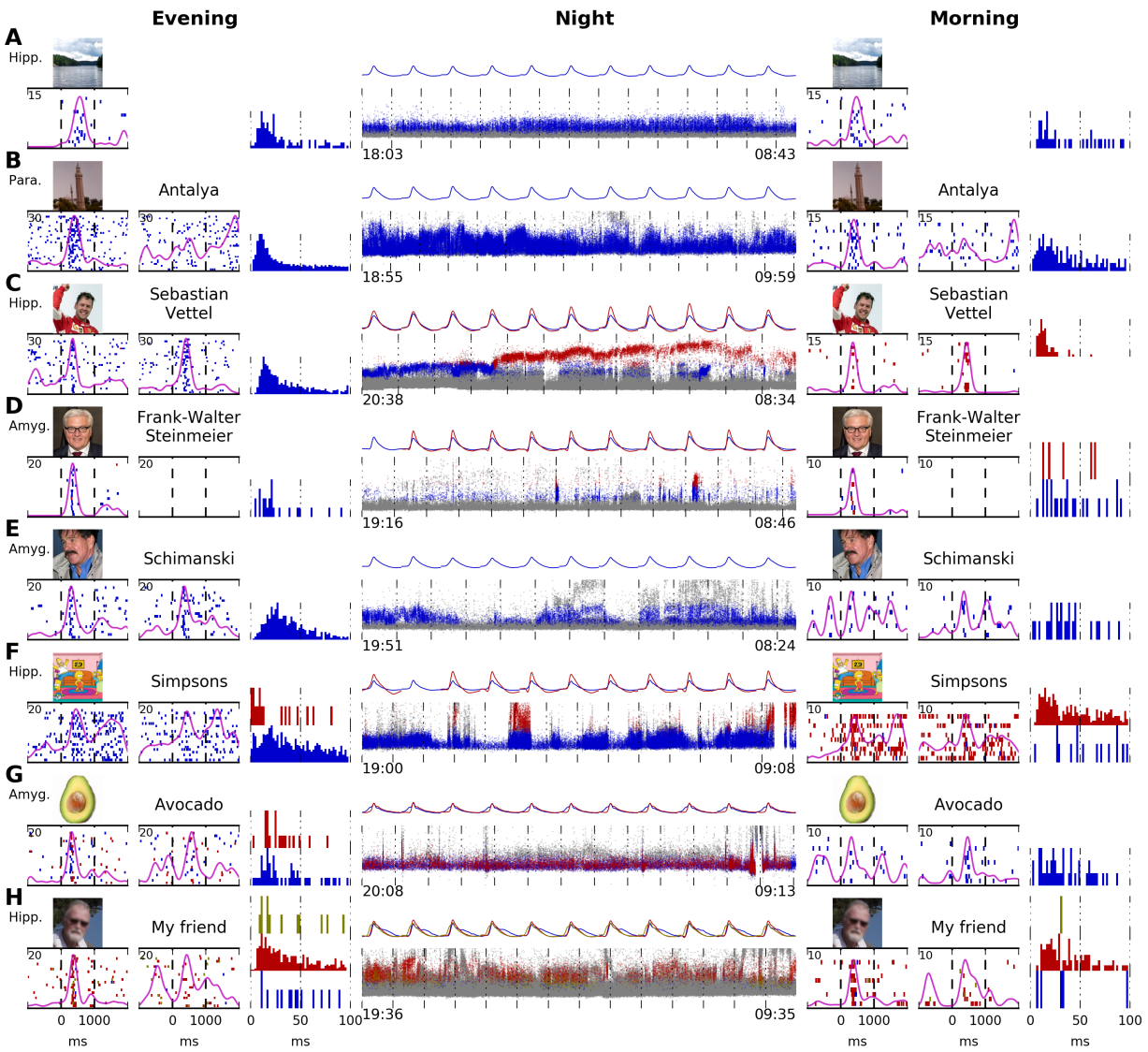

Figure 3.10: **Tracking of selectively responding neurons over an entire night. A–H** show data from eight patients. Continuous unit recordings started in the evening and ended the next morning. "Screening sessions" were performed at the beginning and in the end of each recording. Displayed are raster plots for one stimulus image per screening session, along with inter-stimulus interval histograms. In all patients but A, corresponding written names were presented. The middle column ("Night") shows the activity of units tracked automatically during the entire recording. Each small dot marks the time point and maximal voltage of one action potential. Colors correspond to the raster plots from the screening sessions: units marked in gray do not respond to the images/written names. Units marked in blue, red, or yellow respond to the images/written names as shown in the raster plots. Mean waveforms of all responsive units are displayed for each hour recorded. **A** Stable waveform and response pattern. **B** Amplitude variations are visible. As typical for parahippocampal units, unit does not respond to the written name. **C** An amplitude shift in the responsive neuron (possibly caused by micro-movement of the electrode) results in the detection of two different units, most likely belonging to one neuron. **D** Two responsive clusters are generated. No response to the written name. **E** Stable waveform, but very weak response in the morning. **F** Solid response in the evening and morning, but with separate units. No definite conclusion about the success of tracking can be made. **G** The blue cluster generates most of the response. The red cluster also contributes to the response. Both clusters are tracked with a stable waveform. **H** Similar to G, with three responsive clusters. The red cluster generates most of the response. The blue and yellow clusters contribute to the response. All three clusters have a stable waveform. Hipp., hippocampus; Para., parahippocampal cortex; Amyg., amygdala. Stimulus pictures displayed here have been replaced by similar pictures for legal and privacy reasons.

inspection of waveforms and cross-correlograms using the graphical user interface is necessary to decide whether over-clustering occurred. In the remaining case (Fig. 3.10 **F**), two clusters are tracked throughout the night with a stable waveform, but one cluster responds in the evening, and the other one in the morning. In this case, too, careful inspection of waveforms and cross-correlograms is necessary.

In all eight cases in Fig. 3.10, there is a continuous background of spikes from clusters showing no response to the selected stimulus. Note that in Fig. 3.10 **B** and **D** there was no response to the written names of the pictures. These cells were either selective to a different semantic content of the pictures or not semantically invariant at all.

For eight more examples of units tracked throughout an entire night, see Fig. 3.11.

3.4 Discussion of the new method

Spike sorting has been an important tool in electrophysiological research for decades. Existing algorithms are not optimized to be used with multi-hour datasets and do not handle noisy recordings well. We here presented a complete framework for spike sorting of multi-hour recordings under noisy conditions. Our evaluations showed that our tools outperform current spike sorting methods both on simulated data, and in the analysis of a visual stimulus presentation experiment. Furthermore, our method allows to reliably track single units in the human MTL over the course of an entire night.

Presence of numerous, possibly sparse, neurons Pedreira and colleagues stated that current spike sorting methods – even manually guided ones – can rarely detect more than 8–10 neurons (Pedreira, Martinez, et al. 2012). We have shown that our automated method can reliably detect more than 10 neurons (Fig. 3.3 **B** and Fig. 3.4). Our algorithm copes with the presence of many neurons by selecting many clusters at several temperatures, and by applying SPC iteratively. Pedreira and colleagues also observe that sparsely firing neurons are particularly hard to detect with current spike sorting methods (Pedreira, Martinez, et al. 2012). As our evaluation shows, our method is capable of correctly detecting sparse neurons, e.g. units C10 and C11 in Fig. 3.3 **C**, consisting of 220 and 73 spikes, respectively (2.21% and 0.73% of the 9942 spikes that were the input to clustering).

Large numbers of clusters per channel In many cases, our automated method generated more units than manual operators of WaveClus (Fig. 3.8 **D**). This could be due to several reasons. First, our post-sorting artifact rejection sometimes missed artifact clusters, e.g. unit D 4 in Fig. 3.7 **D**. Such missed artifact clusters artificially increase the unit

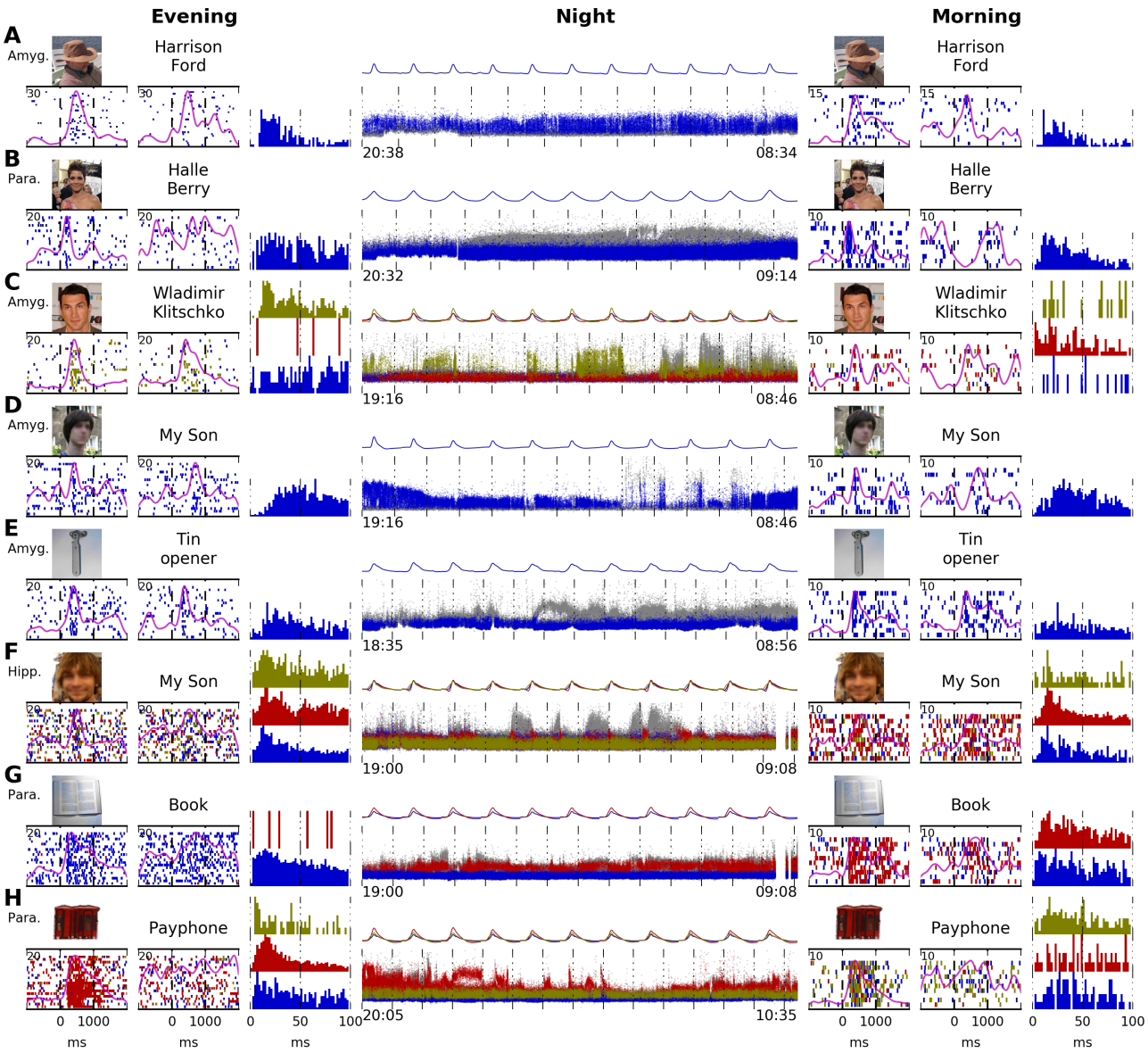

Figure 3.11: **Tracking of selectively responding neurons over an entire night.** **A**–**H** show continuous unit recordings starting in the evening and ending the next morning. "Screening sessions" were performed at the beginning and in the end of each recording. Displayed are raster plots for one stimulus image per screening session. In all sessions, written names corresponding to the images were also presented. Inter-stimulus interval histograms for the evening and morning are displayed. The middle column ("Night") shows the activity of units tracked automatically during the entire recording. Each small dot marks the time point and maximal voltage of one action potential. Colors correspond to the raster plots from the screening sessions: units marked in gray do not respond to the images/written names. Units marked in blue, red, or yellow respond to the images/written names as shown in the raster plots. Mean waveforms of all responsive units are displayed for each hour recorded. **A**, **B**, **D**, **E** One responsive unit was continuously tracked throughout each recording. **C**, **F**, **G**, **H** Two, resp. three responsive units were continuously tracked throughout each recording. However, contributions to visual responses of each unit sometimes differ between evening and morning. As is often the case in the parahippocampal cortex, units do not respond to written names. Hipp., hippocampus; Para., parahippocampal cortex; Amyg., amygdala.

count. Since no ground truth is available for artifact clusters, the accuracy of our post-sorting artifact rejection is difficult to estimate.

Second, there are cases where manual operators of WaveClus failed to separate two or more true units. An example is provided in Fig. 3.7 **D** through **F**: the raster plots (Fig. 3.7 **F**) show that our method correctly separated units D 1 and D 2, while operators of WaveClus generated the under-clustered unit E 1.

Third, as Fig. 3.8 **E** indicates, over-clustering occurred more frequently in our method than with manual operators of WaveClus. To avoid any bias introduced by over-clustering, we counted no more than one responding cluster per stimulus and channel, so that over-clustering could not artificially increase the number of responses. With and without this correction, our method detected more neuronal responses than manual operators of WaveClus. When the goal is to maximize the number of detected responses, a potentially increased likelihood of over-clustering is justified. However, by modifying Combinato's parameters, researchers can systematically shift the balance between over- and under-clustering according to the demands of the respective scientific question, an option (to our knowledge) not available in other spike sorting methods.

As summarized by Pedreira, Martinez, et al. (2012), theoretical considerations predict higher numbers of neurons per recording channel than typically observed with current spike sorting techniques. Thus our result might represent unit counts more realistically than other methods.

Properties of block-wise sorting We segmented spikes into blocks for spike sorting. This has various advantages over spike sorting all spikes at once: First, periods of signal contamination are often confined to short segments of the recording, and thereby affect only a small number of blocks. The remaining, uncontaminated blocks are spike-sorted independently, without the detrimental effects of large numbers of non-neural artifacts.

Second, especially in multi-hour sleep recordings, some units may be active only during short parts of the recording. In a block-wise approach, these units have high chances of being detected in the corresponding blocks, but might be overlooked if spikes from the entire recording were sorted in one step.

Third, the computational time of spike sorting algorithms typically scales super-linearly with the number of spikes sorted. A block-wise approach not only avoids these super-linear computational costs, but also enables us to use a parallelized implementation for the sorting of different blocks.

We used a fixed number of spikes per block (20 000 by default). Other ways of defining blocks are conceivable, e.g. a fixed amount of recording time for each block. There

are two possible problems with a time-based definition of blocks: First, clinical recordings often suffer from short periods of signal contamination, during which a large number of artifactual spikes is generated. In a time-based approach, short periods of signal contamination thus pollute blocks of otherwise uncontaminated recording. In our approach, if large numbers of artifactual spikes are generated, these are confined to blocks that correspond to short amounts of recording time.

Second, in a time-based approach, researchers would necessarily have to adapt the block length to the firing rates of the neurons recorded. Without such an adaptation, there would be the risk of accumulating too few or too many spikes for successful spike sorting in each block. However, even though this adaptation could be performed automatically, it would introduce another algorithmic step without obvious benefits.

Several alternative approaches to the problem of sorting hundreds of thousands of spikes are conceivable. One idea would be to generate clusters from a small random subset of all spikes and use these clusters as templates in a template matching procedure. A possible problem with this approach is that sparse units could be missed if no corresponding template was generated. Furthermore, even short periods of signal contamination can lead to the presence of large amounts of non-neural artifacts, which could in turn compromise the template matching procedure if no templates for the artifacts exist. Another idea is implemented in spike sorting tools that use template matching as the main principle for clustering (Rutishauser, Schuman, et al. 2006; Knieling, Sridharan, et al. 2015). While these methods have the advantage of working online, they continuously have to solve the problem of when to open a new cluster, based on single spikes. This decision problem might become harder in the presence of non-neural artifacts. Further studies are necessary to determine how such methods perform in comparison to our framework.

Applicability to neuroscientific studies The four validation schemes used in this study show that our framework is ready for use in a neuroscientific study. Fig. 3.7 **D** demonstrates our method's ability to spike-sort highly contaminated recordings.

Fig. 3.8 **G** shows response counts for each region we recorded from. Because each response is defined as a pair of a stimulus and a neuronal unit, individual units can contribute more than once to the counts. Several studies report the fraction of units that respond to at least one stimulus (14% of all units in the MTL (Quian Quiroga, Reddy, et al. 2005); 11% of all units in the MTL (Quian Quiroga, Kraskov, et al. 2009); 9–16% of all units in individual MTL subregions (Mormann, Kornblith, et al. 2008)). These studies also report responses by one neuron to more than one stimulus, either by example (Quian Quiroga, Kraskov, et al. 2009) or as a summary statistic: in one study, the average percentage of

stimuli eliciting a response in a responsive neuron was 4.7% in the parahippocampal cortex, 1.7% in the entorhinal cortex and hippocampus, and 2.4% in the amygdala (Mormann, Kornblith, et al. 2008).

An exhaustive analysis of response counts is beyond the scope of the present work. Nevertheless, we report here the response statistics for the Combinato sorting: 11.9–26.7% of all units responded to at least one stimulus, depending on MTL subregions. The average percentage of stimuli eliciting a response in a responsive neuron was 3.7% in the parahippocampal cortex, 1.5% in the entorhinal cortex, 2.3% in the hippocampus, and 2.1% in the amygdala.

The average percentages of response-eliciting stimuli per responsive neuron we observed are in good agreement with the findings of Mormann, Kornblith, et al. (2008). As discussed in Mormann, Kornblith, et al. (2008), a likely reason for the higher average number of response-eliciting stimuli in the parahippocampal cortex with respect to the other regions is that parahippocampal units respond less selectively to the stimulus material used here.

Our evaluation of whole-night recordings demonstrates the feasibility of tracking responsive units in the human MTL over the course of an entire night. In Chapter 4 we use this capability to study a potential mechanism of memory consolidation during sleep at the level of single neurons. Apart from mechanisms related to memory consolidation, processes underlying the generation of epileptic seizures are a relevant topic of research (Mormann, Andrzejak, et al. 2007). A question of particular interest would be how firing patterns of single neurons change in the hours before an epileptic seizure (Gast, Niediek, et al. 2016).

Micro-electrode recordings from the human brain are a novel and still developing technique. Our method can be used to evaluate the stability of multi-hour recordings in order to optimize recording procedures and to identify potential problems and pitfalls. Suitable methods to assess recording stability have been proposed by several authors (Schmitzer-Torbert, Jackson, et al. 2005; Tolias, Ecker, et al. 2007). Another interesting question concerns the activity of visually responsive neurons during sleep, also addressed in Chapter 4. Bondar, Leopold, et al. (2009) addressed questions regarding the response stability of such neurons in the infero-temporal cortex of rhesus monkeys, by comparing responses across different recording sessions.

Future directions We concatenated existing simulated datasets to evaluate our algorithms on multi-hour data where ground truth is available. Despite the fact that we increased the difficulty of the spike sorting task by adding drift and noise, our algorithms

correctly identified 74.6% of the simulated units. For further quantitative evaluations, simulation algorithms as in Martinez, Pedreira, et al. (2009) and Hagen, Ness, et al. (2015) could be used to create multi-hour datasets with ground truth available.

Many spike sorting algorithms employ template matching at some point. Template matching can be performed in many different ways. Our template matching algorithm is based on the Euclidean distance in waveform space. Rutishauser and colleagues use distances based on the Euclidean distance, with the option to use pre-whitened waveforms (Rutishauser, Schuman, et al. 2006). Friedman and colleagues use a more complex matching method ("rebuilding from cores"). Integrating such template matching algorithms into our tools could lead to further improvement (Friedman, Keselman, et al. 2015).

The trade-off between over- and under-clustering deserves further investigation. As we have shown, our methods make it possible to automatically sample a wide range of settings, which directly influence unit counts. Depending on the specific research question at hand, different points along this parameter range will prove optimal.

In contrast to human recordings, animal electrophysiologists have long been using stereotrodes, tetrodes, and multitrodes, which increase both clustering quality and unit yield (Harris, Henze, et al. 2000; Schmitzer-Torbert, Jackson, et al. 2005). As of yet, our software has been tested only with single-wire electrodes. An adaptation to multi-wire electrodes would require only small changes in the code and would certainly broaden the scope of our software.

Availability

We implemented Combinato in Python. The full source code is available as a GitHub repository (`https://github.com/jniediek/combinato`) under the MIT license. Installation instructions for Combinato are contained in Appendix A.1, and a comprehensive user guide is contained in Appendix A.2.

Chapter 4

Reactivation of concept cells during sleep after episodic learning

The aim of this chapter is to test our hypothesis that the coordinated activity of concept neurons is a physiological substrate of "memory traces" in humans, as outlined in Section 1.5. This chapter presents the relevant methods (Section 4.1) and results (Section 4.2). A discussion of the results is presented in Chapter 5.

4.1 Materials and methods

4.1.1 Subjects and Recordings

Twenty-three epilepsy patients (13 female; aged 20 to 62, median 41, years) suffering from pharmacologically intractable epilepsy participated in the study. Subjects were implanted with depth electrodes for intracerebral electroencephalographic monitoring to localize the epileptic focus, as described in Section 2.2.

A total of 57 whole-night recordings (typically lasting from 19:00 to 08:00 of the next day) were performed for this study.

4.1.2 Polysomnography and sleep staging

Polysomnography (PSG) was recorded in 54 of the whole-night recording sessions (Schwarzer EEG system, 23 sessions; Neuralynx ATLAS system, 31 sessions). Electroencephalographic (EEG) electrodes C3, C4, F3, F4, O1, O2, Cb1, Cb2 were recorded along with the electrooculogram (EOG) and electromyogram (EMG) derived at the chin.

Sleep staging was performed in 43 recording sessions (in the remaining 11 sessions,

PSG electrodes were not continuously maintained due to head dressing and other clinical demands). Sleep scoring was performed according to Iber, Ancoli-Israel, et al. (2007) in windows of 30 s, and EEG as well as EOG recording channels were digitally re-referenced to Cb1 or Cb2, whichever gave the cleaner signal. Data were digitally filtered according to Iber, Ancoli-Israel, et al. (2007). Sleep staging was performed with the software Polyman (22 sessions; `http://www.edfplus.info/downloads/`) or with our publicly accessible signal viewer (21 sessions; `https://github.com/jniediek/combinato/tree/master/signalviewer`).

4.1.3 Study design

Each experimental session spanned two days. In the morning of Day 1, a screening session was conducted to identify visually responsive neurons and the corresponding response-eliciting pictures (details below).

In the evening of Day 1, subjects performed an episodic memory task consisting of a learning and a recall part ("Fotonovela", see Fig. 4.1 a; details below). In the morning of Day 2, subjects again performed the recall task. To assess if responsive neurons were stably recorded, and to test for invariance of neuronal responses, subjects performed three short screening sessions: before and after the episodic memory task in the evening of Day 1, and after the recall task in the morning of Day 2. See Fig. 4.1 b for the exact time course of one experimental session.

Note that during Day 1, between the screening session in the morning and the episodic memory task in the evening, some subjects participated in other, unrelated experiments, as is common in human single-unit research.

4.1.4 Identification of visually responsive neurons

Visually responsive neurons and response-eliciting pictures (Section 1.4; Quian Quiroga, Reddy, et al. 2005; Quian Quiroga, Kraskov, et al. 2009) were identified as follows (see also Section 3.3.2): 100 to 150 pictures of famous people, acquaintances of the subjects, animals, landscapes, and objects were presented on a laptop computer (pseudorandomized order, 1 s presentation time, jittered onset, 6 or 10 presentations per stimulus). After automated spike extraction and sorting by either WaveClus (Quian Quiroga, Nadasdy, et al. 2004) or Combinato (Chapter 3; Niediek, Boström, et al. 2016), visually responsive neurons and the corresponding response-eliciting stimuli were identified according to a published response criterion (Mormann, Kornblith, et al. 2008; Mormann, Dubois, et al. 2011; Mormann, Niediek, et al. 2015; Niediek, Boström, et al. 2016): spike times of each

unit during the 6 or 10 repetitions of each picture presentation were binned into 19 overlapping bins (duration 100 ms, overlap 50 ms). A baseline distribution was generated from the intervals preceding each picture onset (−500 ms to 0 ms relative to picture onset). A Mann–Whitney U test against this baseline was applied to each of the bins separately. The 19 resulting p-values were subjected to the Benjamini–Hochberg procedure (Benjamini and Hochberg 1995), yielding a single response score. For each unit, all stimuli were sorted by their response score. Up to 12 response-eliciting stimuli were selected for the episodic memory task.

4.1.5 Episodic memory task: "Fotonovela"

To induce coordinated, sequential activity in a population of concept neurons, we created an episodic memory task ("Fotonovela") involving pictures found to elicit neuronal responses in the screening sessions in the morning.

The Fotonovela task was designed around a simple story to be memorized by the subjects. For each recording session, this story was created from the response-eliciting pictures identified in the morning (Section 4.1.4). The story was presented as a sequence of slides on a laptop computer (see Fig. 4.1 a, "Learning").

Each slide contained one response-eliciting picture in its center, the corresponding written name as a title above the picture, and two to four written sentences beneath the picture. The titles were chosen as follows: for pictures containing a person, e.g. an actress or an acquaintance of the subject, the given name and family name of that person were used. For pictures containing an object, e.g. a food item, the name of the object in German language was used. For other cases, such as buildings or logos, a name was chosen that unambiguously identified the picture for the subject, in some cases by asking the subject to choose a name before the experiment.

The sentences beneath the pictures referred to the picture on the previous slide, the picture on the currently displayed slide, and the picture on the subsequent slide, creating an episodic link between the individual items of the story. Each story consisted of between 6 and 12 (median 9) such slides with pictures and sentences.

The memory task consisted of two parts: learning the story and recalling it (see Fig. 4.1 a). In the learning part ("Learning" in Fig. 4.1 a), subjects were instructed to memorize the story by viewing and reading the slides in a self-paced manner. Subjects proceeded from one slide to the next by pressing a key. A fixation cross was displayed for 15 s after the last slide. Subjects were instructed to repeat this learning part as often as they felt necessary to memorize the story.

When subjects indicated readiness to recall the entire story ("Recall" in Fig. 4.1 a), they were asked to name the first item in the story. Thereafter, the picture of the correct first response was displayed as an indication whether the subject's response was correct. This picture remained visible while the subject recalled the second item. Then the correct second item appeared as feedback, and the first item disappeared. Recall proceeded in this manner until the last picture.

The recall of an item was scored as correct if the correct item was named at the correct position in the story, and as incorrect if the subject named an item at an incorrect position within the story, or was unable to name the correct item. Subjects had to correctly recall the entire story six times. The experimenter logged the time points of all responses by key presses, which also triggered the progression of the feedback pictures. In the morning of Day 2, subjects performed the recall part once, in exactly the same manner.

Details on the implementation of the experiment in software are given in Section 2.2.

4.1.6 Short screening sessions

The purpose of the short screening sessions (conducted in the evening of Day 1 and morning of Day 2, see Fig. 4.1 b) was twofold: to measure neuronal responses to pictures and written names independently of the memory task, and to verify that neuronal responses were present at the beginning and in the end of whole-night recordings. All pictures and written names used in the episodic memory task were presented on a laptop computer (pseudorandom order, pictures and written names randomly interspersed, 1 s presentation time, jittered onset, 10 presentations per picture/written name). In four sessions, only pictures but no written names were presented for technical reasons.

4.1.7 Processing of whole-night neuronal recordings

Neuronal activity was recorded from the evening of Day 1 through the morning of Day 2. We used Combinato (Chapter 3; Niediek, Boström, et al. 2016) to exclude recording channels carrying no neuronal signal, and to extract spikes from all remaining channels. Python 2.7 was used for all data processing steps and all analyses, unless stated otherwise.

Exclusion of highly correlated channels

We sometimes observed nearly identical firing times (lag ≤ 0.5 ms) on two (rarely three) microwires of one bundle. This most likely originated from an imperfect spread/splay of the microwires, with their tips ending in too close proximity. In each such case, we

excluded all but one of the involved microwires from further analysis by the following procedure. For each pair of microwires in one bundle, we computed cross-correlograms of firing times (*before* spike sorting; lags −10 ms to 10 ms, bin size 0.5 ms) in windows of 20 min duration. We excluded one of the two microwires in a pair if 50% or more of the spike-time lags fell into the range −0.5 ms to 0.5 ms in three or more 20 min windows.

Channel selection, recording stability

After automatic removal of non-neural artifacts by Combinato, we used Combinato to perform fully automated spike sorting of all remaining spikes. Default parameters were used, except for setting $S_{\text{min}} := 25$ (minimum number of spikes in a cluster) and $C_{\text{stop}} := 1.6$ (threshold for automatic merging; see Table 3.1 for all default parameter settings).

Raster plots and peri-stimulus time-histograms were plotted and visually inspected for all units and all visual stimuli. Recording channels on which no unit showed a visible response to any stimulus were excluded from further analysis. The remaining channels were processed in Combinato's graphical user interface to manually remove remaining artifacts and to merge highly similar units.

Some units can be recorded only for a part of the recording duration in multi-hour recordings (as discussed in detail in Chapter 3; see also Niediek, Boström, et al. 2016). We thus quantified the recording stability of a unit as the fraction of time-windows of duration 5 min during which the unit's firing rate was at least 5% of its average firing rate across the night. All units with recording stability less than 90% were excluded from further analysis.

Responsive neurons in whole-night recordings

Data from the short screening sessions (Section 4.1.6) were used to identify neuronal responses in an automated way. The following procedure was applied independently to the data from the short screening sessions in the evening of Day 1, and from the short screening session in the morning of Day 2. For the evening data, the short screening sessions before and after the episodic memory task were analyzed as a whole. Note that only the pictures and written names used in the episodic memory task were used as stimuli in these short screening sessions.

For each neuronal unit and each visually presented stimulus, we calculated the average number of spikes fired during all stimulus presentations, denoted by $N_{\text{spk},i}$ for stimulus i.

We defined the *selectivity index* for stimulus i as the following variant of the z-score:

$$\mathrm{SI}_i := \frac{N_{\mathrm{spk},i} - \mathrm{mean}_{j\neq i}\left(N_{\mathrm{spk},j}\right)}{\mathrm{std}_{j\neq i}\left(N_{\mathrm{spk},j}\right)}.$$

By definition, a high selectivity index corresponds to an elevated spike count for one stimulus, compared to the other stimuli. However, the selectivity index alone does not detect typical properties of a response (e.g., a well-defined onset latency). We thus combined the selectivity index with the following response score (Mormann, Kornblith, et al. 2008; Mormann, Dubois, et al. 2011; Mormann, Niediek, et al. 2015; Niediek, Boström, et al. 2016): for a stimulus that had been presented N times ($N = 20$ in the evening of Day 1, $N = 10$ in the morning of Day 2), we subdivided the $N\times$ 1000 ms onset-aligned presentation time into 19 overlapping time-bins (duration 100 ms, overlap 50 ms).

We then used the Wilcoxon signed-rank test to compare the firing rate in each of these bins to a baseline defined as the 500 ms interval before stimulus onset. This generated 19 p-values (one for each bin), which we combined into a single response score by applying the Benjamini–Hochberg procedure (Benjamini and Hochberg 1995). We denote the response score for stimulus i by RS_i.

We defined the following criteria for neuronal responses, based on the selectivity index and the response score.

$$\mathrm{SI}_i \geq 5 \quad \text{and} \quad \mathrm{RS}_i < 1 \tag{4.1}$$

$$\mathrm{SI}_i \geq 3 \quad \text{and} \quad \mathrm{RS}_i \leq .5 \tag{4.2}$$

$$\mathrm{SI}_i \geq 1 \quad \text{and} \quad \mathrm{RS}_i \leq .001. \tag{4.3}$$

A pair of a neuronal unit and a stimulus was defined as a response if it met at least one of the criteria (4.1)–(4.3). We use the term *responsive unit* to refer to a unit that responded to a stimulus picture either in the evening, or morning, or both. A neuronal response was defined as invariant if the unit responded to exactly one stimulus picture and to the corresponding written name, or if it responded to exactly one stimulus picture and had a selectivity index of at least 3 for the corresponding written name. We use the term *invariant unit* to refer to a unit that responded invariantly either in the evening, morning, or both. In particular, invariant units are a subset of responsive units.

Data included in main analyses

Only whole-night recordings with sleep staging and at least one responsive unit were included for analysis, resulting in a total of 40 sessions (out of 57) from 17 patients.

4.1.8 Ripples in the local field potential

For the defining properties and relevance of ripples in the local field potential see Section 1.3.3.

Downsampling and re-referencing to local references

For all analyses of the local field potential (LFP), we downsampled the data recorded from microwires to 2000 Hz (19 sessions) or 2048 Hz (21 sessions). We used the script `ncs2h5.py` from Combinato for downsampling (`https://github.com/jniediek/combinato/blob/master/signalviewer/ncs2h5.py`).

Some microwire recording channels were initially referenced to a reference wire from a different bundle of microwires. For each of these channels, we chose a new, local reference channel, and digitally re-referenced the recording to this new reference, in order to ensure that all analyzed LFP signals originated from tissue in close proximity to the contacts. We used the script `parse_cheetah_logfile.py` from Combinato to read out the physical references of each channel (`https://github.com/jniediek/combinato/blob/master/tools/parse_cheetah_logfile.py`).

Ripple detection and classification

For the detection of ripple events we followed the methodology of Nir, Staba, et al. (2011). For all microwires in the hippocampus, the signal was filtered between 80 Hz and 200 Hz (4th order Butterworth bandpass filter, applied forward and backwards to prevent phase shifts). The Hilbert transform was used to extract the instantaneous amplitude of the signal. The resulting signal was normalized to z-scores (i.e., subtraction of mean and division by standard deviation) in blocks of 5 min duration. A candidate ripple event was defined as a period during which the signal exceeded a z-score of three for at least 10 ms and at most 150 ms. After the detection step, the maximum of the z-score transformed signal within each candidate event was determined. A period of 1 s around the maximum was cut out from the unfiltered, locally re-referenced, downsampled data for each event, and its mean subtracted. Events whose absolute voltage exceeded 750 µV during the 1 s window were discarded.

Following Burnos, Hilfiker, et al. (2014), we used the S transform (Stockwell transform; Stockwell, Mansinha, et al. 1996) to estimate the central frequency of each candidate ripple event. We used the function `tfr_array_stockwell` from MNE (Gramfort, Luessi, et al. 2013, 2014; `https://martinos.org/mne`). The central frequency was defined as the dominant frequency above 60 Hz when averaging the S-transformed event over its entire duration. We discarded all events with central frequency above 150 Hz as potential "fast ripples" and stored the remaining events for further analysis.

4.1.9 Main data analysis

Preprocessing of unit data

To ensure that correlational measures were not artificially inflated by spikes or artifacts recorded on more than one channel, we iterated over all pairs of units in each session. Whenever spikes from two units in a pair had a time difference of less than 0.3 ms, one of the spikes was discarded.

The visual presentation of response-eliciting stimuli by definition leads to neuronal responses (i.e., immediate elevations of firing rates). Since we were interested in memory consolidation subsequent to the actual presentation of visual stimuli, all analyses were restricted to the time after the last experiment subjects performed in the evening (i.e., the last short screening session) and before the first experiment subjects performed in the morning (i.e., the recall task). In particular, all results refer to time periods during which we did not present any of the visual stimuli to the subjects.

Firing rate comparisons

For each unit, we calculated firing rates in bins (bin duration 10 s).

As a measure of effect size for modulation of unit activity by sleep stages, we calculated, for each unit, Hedges' g for the comparison of sleep stages Awake vs. SWS, and Awake vs. REM. *Hedges' g* is a measure of effect size defined as (Hedges 1981, p. 110)

$$g \coloneqq \frac{\mathrm{mean}_1 - \mathrm{mean}_2}{\sqrt{\frac{(n_1-1)\mathrm{var}_1+(n_2-1)\mathrm{var}_2}{n_1+n_2-2}}},$$

where in this case n_1 and n_2 are the counts of 10 s bins in the two sleep stages to be compared, and $\mathrm{mean}_1/\mathrm{mean}_2$ ($\mathrm{var}_1/\mathrm{var}_2$) refer to the mean value (variance) of firing rates calculated across bins, for each of the two sleep stages. We used a two-sided Wilcoxon signed-rank test against zero to determine significant differences from zero in sleep-stage

modulation at the level of neuronal populations, and we used a two-sided Mann–Whitney U test to test for differing sleep-stage modulation of neuronal populations (such as non-responsive vs. responsive neurons).

As a complementary analytic approach, we computed numbers of sleep-stage modulated units, again for comparisons of sleep stages Awake vs. SWS, and Awake vs. REM: a unit was operationally defined as sleep-stage modulated if the p-value of a two-sided Mann–Whitney U test of all 10 s bins from the two sleep stages under comparison was below $\alpha = 0.001$. The direction of modulation was determined by comparing the mean firing rates in the two sleep stages under comparison. We used a two-sided binomial test (chance level 50%) to determine significance of count differences for all sleep-stage modulated units (e.g., to determine if significantly more units were inhibited in REM sleep vs. waking than vice versa).

Analysis of LFP ripples

All hippocampal ripple events with a central frequency below 150 Hz were included in the analysis. Ripple event rates in sleep stages Awake, REM, and SWS were calculated by binning (bin duration 10 s, data from time during cognitive tasks excluded from analysis as explained above).

To analyze the participation of neurons in LFP ripples, we computed, for each unit, Hedges' g for the time periods before ripple events versus during ripple events (before, -375 ms to -125 ms relative to ripple center; during, -125 ms to 125 ms relative to ripple center). We used a two-sided Wilcoxon signed-rank test against zero to assess significance of unit modulation by ripples for neuronal populations, and a two-sided Mann–Whitney U test to compare ripple modulation of different groups of units (e.g., non-responsive vs. responsive units).

Spike-count correlations

For a unit U_i and a time window T subdivided into N bins of equal duration, denote by $v_{i,T}$ the vector of counts of spikes fired by U_i in each bin of T. We defined the *spike-count correlation* of units U_1 and U_2 during T as

$$r_{\mathrm{SC}}(U_1, U_2, T) \coloneqq r_{\mathrm{Pearson}}(v_{1,T}, v_{2,T}),$$

where r_{Pearson} denotes the Pearson correlation coefficient (Cohen and Kohn 2011). To compute spike-count correlations in a time-resolved manner, we divided the time after the

Set	Bin dur. [ms]	Bin overlap [ms]	Window dur. [s]	Window overlap [s]
1	40	20	6	3
2	200	0	30	10
3	1000	0	300	100

Table 4.1: Parameter sets for spike-count correlations. dur., duration.

last evening experiment and before the first morning experiment into overlapping time windows. To analyze the effect of the various analysis parameters involved, we used three different parameter sets for bin duration, bin overlap, window duration, and window overlap (see Table 4.1). For each experimental session, each pair of neurons recorded, and each parameter set, we thus obtained a time series of spike-count correlations. To compare spike-count correlations, we computed, for each pair of units and sleep stages Awake, REM, and SWS, the mean spike-count correlation across all time windows within the said sleep stages. We then used a two-sided Mann–Whitney U test to assess significance of differences between sleep stages and between groups of pairs of neurons (e.g., pairs of non-responsive units vs. pairs of responsive units).

The magnitude of spike-count correlations has been reported to depend, among other factors, on the distance between the two neurons in the brain (Cohen and Kohn 2011). To avoid confounding effects of distance, we report spike-count correlations only from pairs of units recorded on the same bundle of microwires. Additionally, to avoid confounding effects of spike sorting, we excluded pairs of units recorded on the same microwire.

To compute spike-count correlations during LFP ripples for pairs of units, we built vectors of the counts of the units' spikes during ripple events (−125 ms to 125 ms relative to ripple center), and computed the Pearson correlation coefficient of these vectors of counts (i.e., we used each ripple event as a time bin when generating the vector of counts). For each pair, we used the recording channel with the higher ripple rate to define the relevant time points. To minimize the effect of chance correlations, we excluded from this analysis, for each sleep stage separately, channels with less than ten ripple events in that sleep stage. Note that due to the varying numbers of ripple events across channels, the lengths of the vectors of counts used in this analysis necessarily varied, too.

Cross-correlations

To identify stereotypically ordered firing among pairs of concept neurons (i.e., "leader–follower" relations) and to analyze the precise timing of ordered firing, we calculated cross-correlograms for each pair of responsive units (maximum lag 300 ms, bin width 3 ms), for each sleep stage separately. Only units responding to exactly one stimulus were

included in this analysis. To avoid possible confounding effects of spike sorting, pairs of units recorded on the same microwire were excluded from this analysis.

To estimate peak cross-correlation times, we smoothed each cross-correlogram by convolution with a Gaussian window (standard deviation 3 ms) and determined a lag at which the smoothed cross-correlogram attained its maximum (denoted by t_{peak} in the following). We operationally defined the *asymmetry* of a cross-correlogram as

$$\text{asym} := \text{sign}\left(t_{\text{peak}}\right) \cdot \frac{N_{\text{pos}} - N_{\text{neg}}}{N_{\text{pos}} + N_{\text{neg}}},$$

where N_{pos} and N_{neg} denote the numbers of positive and negative lags constituting the cross-correlogram. In particular, this definition entails that cross-correlograms in which peak time and the majority of lags have the same sign ("consistent" cross-correlograms) have *positive* asymmetry, whereas cross-correlograms in which the signs of the peak time and of the majority of lags differ ("inconsistent" cross-correlograms) have *negative* asymmetry.

For a pair of two responsive units recorded in one session and each responding to exactly one stimulus, we defined the *relative (stimulus) position* as the difference of the position numbers of the two units' preferred stimuli in the Fotonovela story. For example, if unit A responded to "Lois Griffin" and unit B to "My brother", and "My brother" immediately followed "Lois Griffin" in the Fotonovela, the relative stimulus position of the pair (unit A, unit B) was -1. We calculated the Pearson correlation coefficient between relative positions and peak cross-correlation times after normalizing to non-negative relative positions (by swapping the sign of peak cross-correlation times for negative relative positions). We computed a linear least-squares fit to the same data for display purposes only.

To account for effects of stimulus order on firing order regardless of precise timing, we defined, for each pair of responsive neurons, the *firing order* as the sign of the peak cross-correlation time, and the *stimulus order* as the sign of the relative stimulus position. A pair of responsive units was defined as a *forward pair* if the firing order and stimulus order coincided, and as a *reverse pair* otherwise. We excluded pairs of responsive neurons from this analysis if the absolute value of their peak cross-correlation time was below 3 ms, because estimating the "true" firing order becomes unreliable at short lags. A two-sided binomial test (chance level 50%) was used to assess significance of count differences of forward vs. reverse pairs.

Estimating the firing order from a cross-correlogram also becomes unreliable when N_{pos} and N_{neg} are either very small or very close, i.e., when either the total number of

lags in the cross-correlogram is low or when its asymmetry is close to zero. To systematically analyze the influence of the number of lags and asymmetry on the counts of forward and reverse pairs, we sorted all cross-correlograms either by number of lags or by asymmetry, and computed the number of forward minus reverse pairs at each step: for $k = 1, \ldots, n_{\text{all pairs}}$, we computed the number of forward versus reverse pairs for the k cross-correlograms with most lags, and for the k cross-correlograms with highest asymmetry. For each k, we computed, from a binomial distribution (chance level 50%), the minimum differences "forward minus reverse pairs" that would be significant at $\alpha = 0.05$ and $\alpha = 0.01$, and compared the observed differences "forward minus reverse pairs" to these hypothetical values.

4.2 Results

Subjects learned a simple story ("Fotonovela"; Fig. 4.1 a; Section 4.1.5) constructed from pictures that had previously been identified as eliciting selective responses in neurons of the hippocampus, amygdala, and parahippocampal cortex ("concept neurons"; Quian Quiroga, Reddy, et al. 2005; Quian Quiroga, Kraskov, et al. 2009; Section 1.4). The purpose of the Fotonovela was to create a well-defined memory episode with an observable correlate ("memory trace") at the level of single neurons: behaviorally, the Fotonovela linked various semantic contents in a fixed sequential order, while neurophysiologically, the activity of concept neurons represented these contents.

In this section, we test Hypotheses 1–5, outlined in Section 1.5, by examining the activity of concept neurons during sleep after learning.

4.2.1 Behavioral results

The Fotonovela stories consisted of a sequence of 6 to 12 slides (median 9). Each slide contained a picture that elicited the response of a concept neuron, a corresponding title, and two to four sentences connecting the content of each slide to the previous and next one, thus creating episodic links between the slides. Each experiment began in the evening. Immediately after self-paced learning, subjects freely recalled the story six times. This recall was repeated once more in the next morning. Subjects correctly recalled 98.7% (SD 3.7%) of all items in the last evening repetition and 93.9% (SD 9.4%) in the morning, see Fig. 4.1 d.

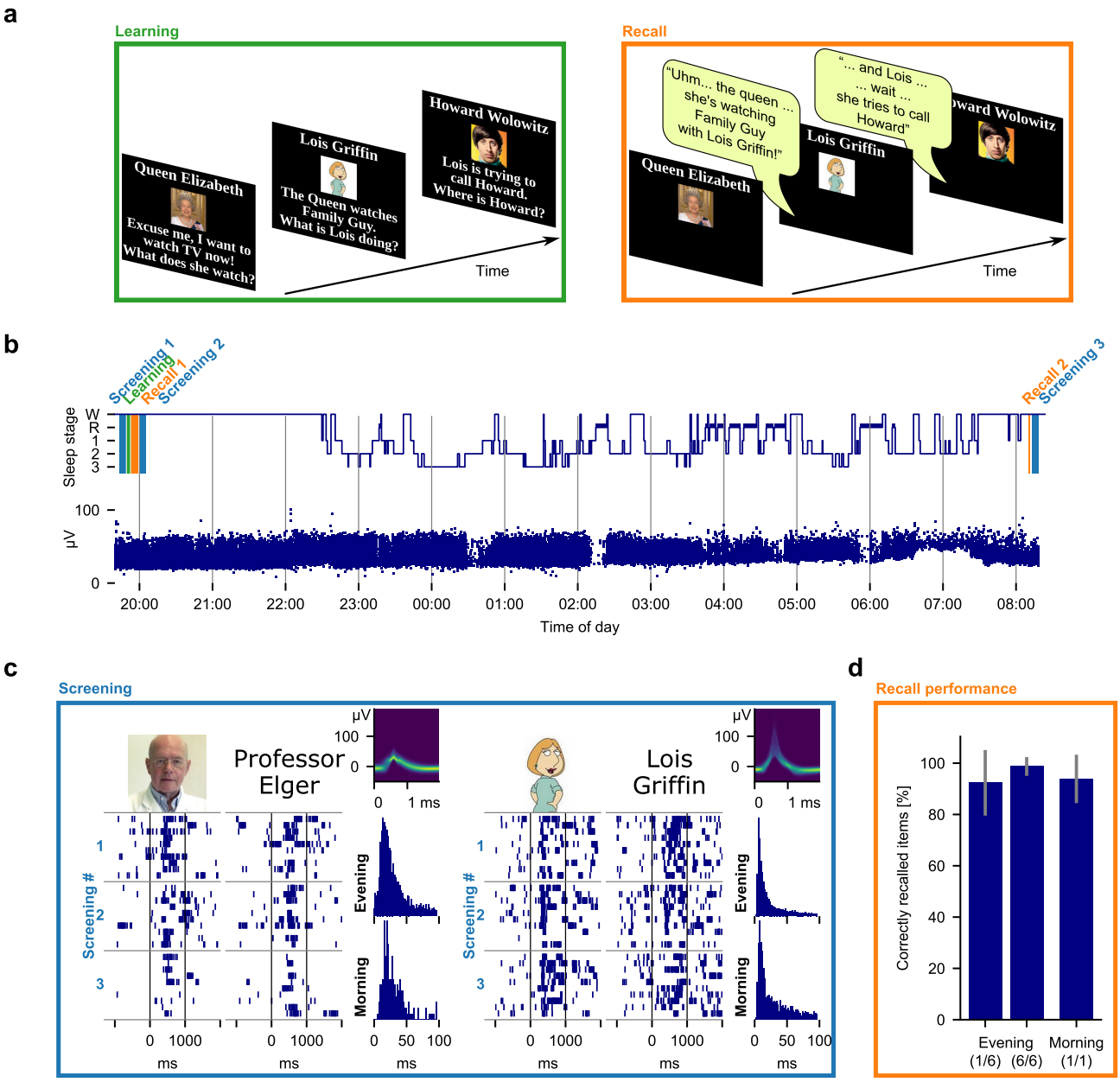

Figure 4.1: **Tracking concept neurons during sleep. a,** Subjects learned a simple story involving up to 12 items (concepts) in a defined sequential order. Subjects first read ("Learning"), then told ("Recall") the story. **b,** Sample time course of an experimental session. Top: Hypnogram from one session along with the times of three Screenings, Learning, and Recall. Bottom: A single unit tracked across the entire night, with time axis corresponding to the hypnogram. Displayed are amplitudes of action potentials over time. **c,** Responses of two invariant single units. Left half: Same unit as in b. The unit responds to visual presentations of the picture and written name of "Professor Elger". The raster plots show responses from all 10 trials in each of the three Screenings. Inter-spike interval (ISI) histograms for the screenings in the evening and morning are also displayed. Note the similarity of raster plots and ISI histograms despite the time gap of approx. 12 h. Waveform of action potentials is displayed as a density plot. Right half: A unit from a different patient, responding to the picture and written name of "Lois Griffin". **d,** Performance in the recall task. Bar plots indicate the fraction (mean ± S.D.) of correctly recalled story items out of all items for the first and last of the six recall runs in the evening, and for the morning run.

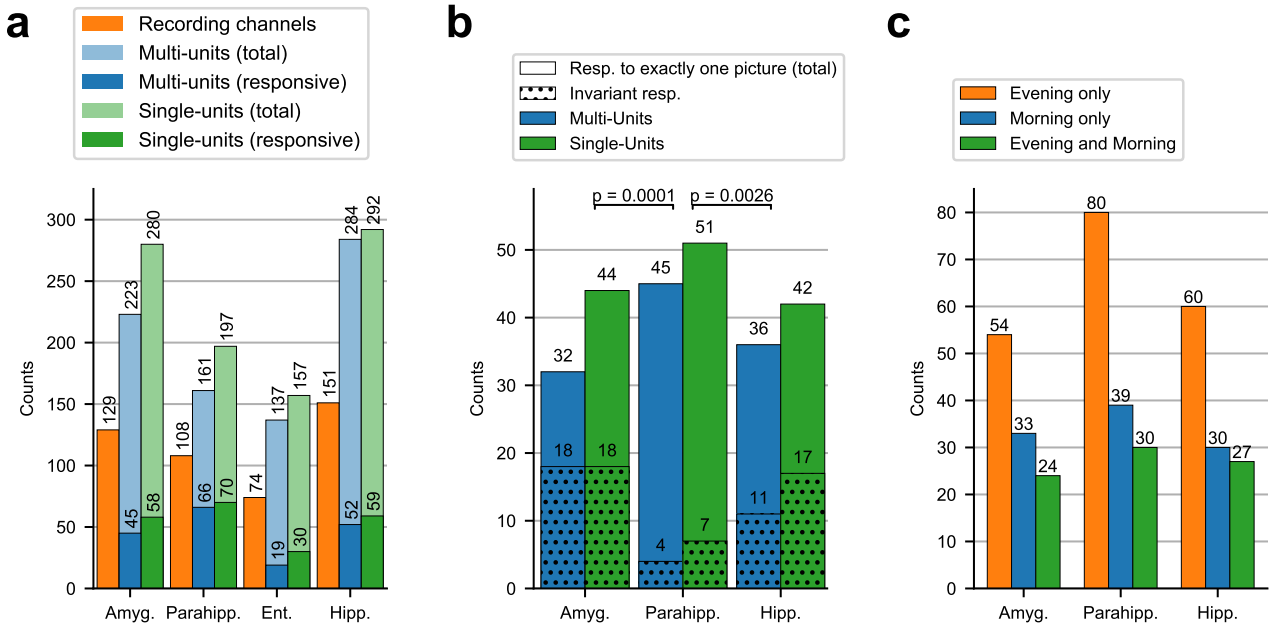

Figure 4.2: **Units analyzed.** **a,** Counts of included recording channels, multi and single units, and responsive units. A unit is counted as responsive if it responds to at least one stimulus in at least one of the screening sessions in the evening or in the morning. The entorhinal cortex was excluded from all further analyses because of the low number of responsive neurons. **b,** Displayed data corresponds to Screenings 1 and 2 only (evening, see Fig. 1 b). Displayed are counts of units responding to one picture but not its written name, and exactly one picture and its written name ("invariant neurons"). The fraction of invariant neurons is significantly higher in Hipp. and Amyg. than in Parahipp. (both $p < 0.01$; Fisher's exact test). **c,** Numbers of responses that were detected in the evening only, in the morning only, or both in the evening and morning. Amyg., amygdala; Parahipp., parahippocampal cortex; Ent., entorhinal cortex; Hipp., hippocampus.

4.2.2 Recording of concept neurons across entire nights

We recorded neuronal activity from 1437 single- and multi-units in 40 sessions throughout entire nights including sleep (regional distribution of units in Fig. 4.2 a; for methodology of whole-night unit analysis see Chapter 3; Niediek, Boström, et al. 2016). Polysomnography was recorded for sleep staging.

Fig. 4.1 b shows the activity of a concept neuron throughout a night, along with sleep stages. Selective responses of this neuron to its preferred stimulus "Professor Elger", presented as both a picture and written name, are displayed in Fig. 4.1 c along with another example of a neuron responding selectively to a picture of "Lois Griffin" and the corresponding written name. Short "screening sessions" were conducted at the beginning and end of each whole-night recording session to formally assess responses to pictures and names. A total of 350 single- and multi-units responded selectively to one or more of the pictures in the evening or in the morning (called "responsive" units in the following, other

units will be referred to as "non-responsive"). Of these responsive neurons, 97 responded also to the corresponding written name (called "invariant" units in the following). The proportion of invariant units was significantly higher in the amygdala and hippocampus than in the parahippocampal cortex (Fig. 4.2 b). The fraction of neuronal responses that were reliably detected both in the evening and next morning was 21.6% in the amygdala, 20.1% in the parahippocampal cortex, and 23.1% in the hippocampus (Fig. 4.2 c; see also Chapter 5).

4.2.3 Motivation for subsequent analyses

As outlined in Section 1.2, memory consolidation is a process by which declarative memories initially dependent on the hippocampus are transferred to cortical areas, thereby gradually becoming independent of the hippocampus. A possible mechanism of memory consolidation is the repeated reactivation of initially labile "memory traces" by the hippocampus, mostly during slow-wave sleep. However, the physiological substrate of these memory traces has remained elusive. Human hippocampal concept neurons have been proposed as building blocks of memory (Section 1.4; Quian Quiroga 2012).

This thesis tests the idea that the neurophysiological correlate of memory traces is the coordinated activity of concept neurons: as explained in Section 1.5, we suggest that during the original experience of a memory episode, the coordinated activity of hippocampal concept neurons rapidly encodes the memory episode in a labile form, and that the reactivation of the same ensemble of concept neurons during subsequent slow-wave sleep consolidates the memory.

4.2.4 Sleep-stage modulation of concept neurons

If memory traces are reactivated during slow-wave sleep and if concept neurons form memory traces, then concept neurons necessarily have to be active during slow-wave sleep. In fact, firing rates of concept neurons in the hippocampus during slow-wave sleep did, on average, not differ significantly from waking (Fig. 4.3 a; sleep-stage modulation quantified by Hedges' g; times when subjects were actively participating in the experiments were excluded from all analyses; see Section 4.1.9). Hedges' g for non-responsive (NR), responsive (R), and invariant (I) units were -0.08, 0.03, and 0.06, respectively (none significantly different from zero; two-sided Wilcoxon signed-rank test). Theories of memory consolidation do not associate REM sleep with declarative memory consolidation. In line with this view, concept neurons in the hippocampus were significantly inhibited during REM sleep compared to waking (Fig. 4.3 b); Hedges' g for NR, R, and I units

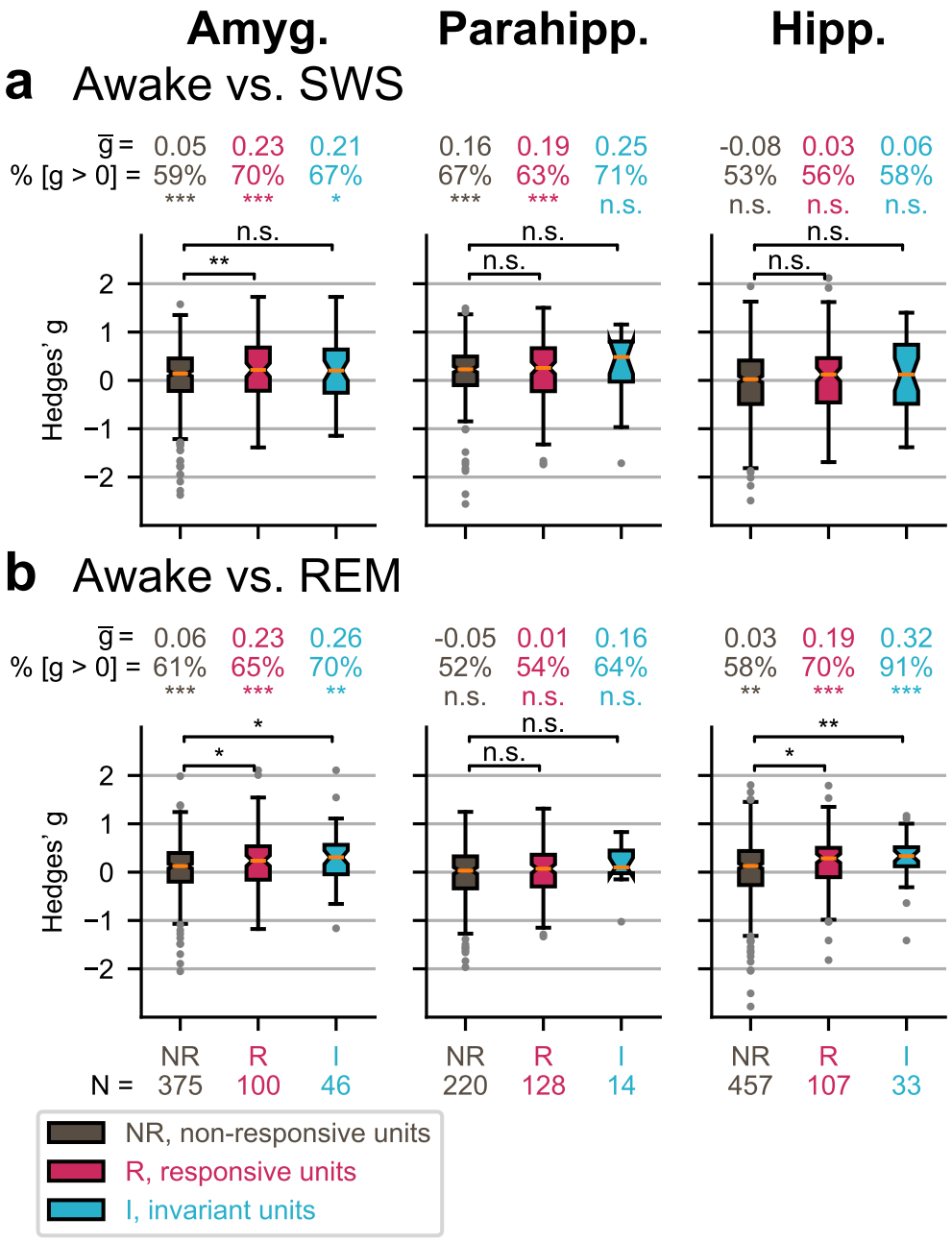

Figure 4.3: **Concept neurons are modulated by sleep stages. a,** Awake vs. SWS. In the amygdala and parahippocampal cortex, units were more active during waking than during SWS, as quantified by Hedges' g. This effect was larger for responsive and invariant neurons than for non-responsive neurons (the difference was significant only for non-responsive versus responsive units in the amygdala). Hippocampal neurons did not significantly differ between waking and SWS. **b,** Awake vs. REM. In the amygdala and hippocampus, units were significantly more active during waking than REM. This effect was significantly larger for responsive and invariant units than for non-responsive neurons. Parahippocampal units did not significantly differ between waking and REM. Amyg., amygdala; Parahipp., parahippocampal cortex; Hipp., hippocampus.

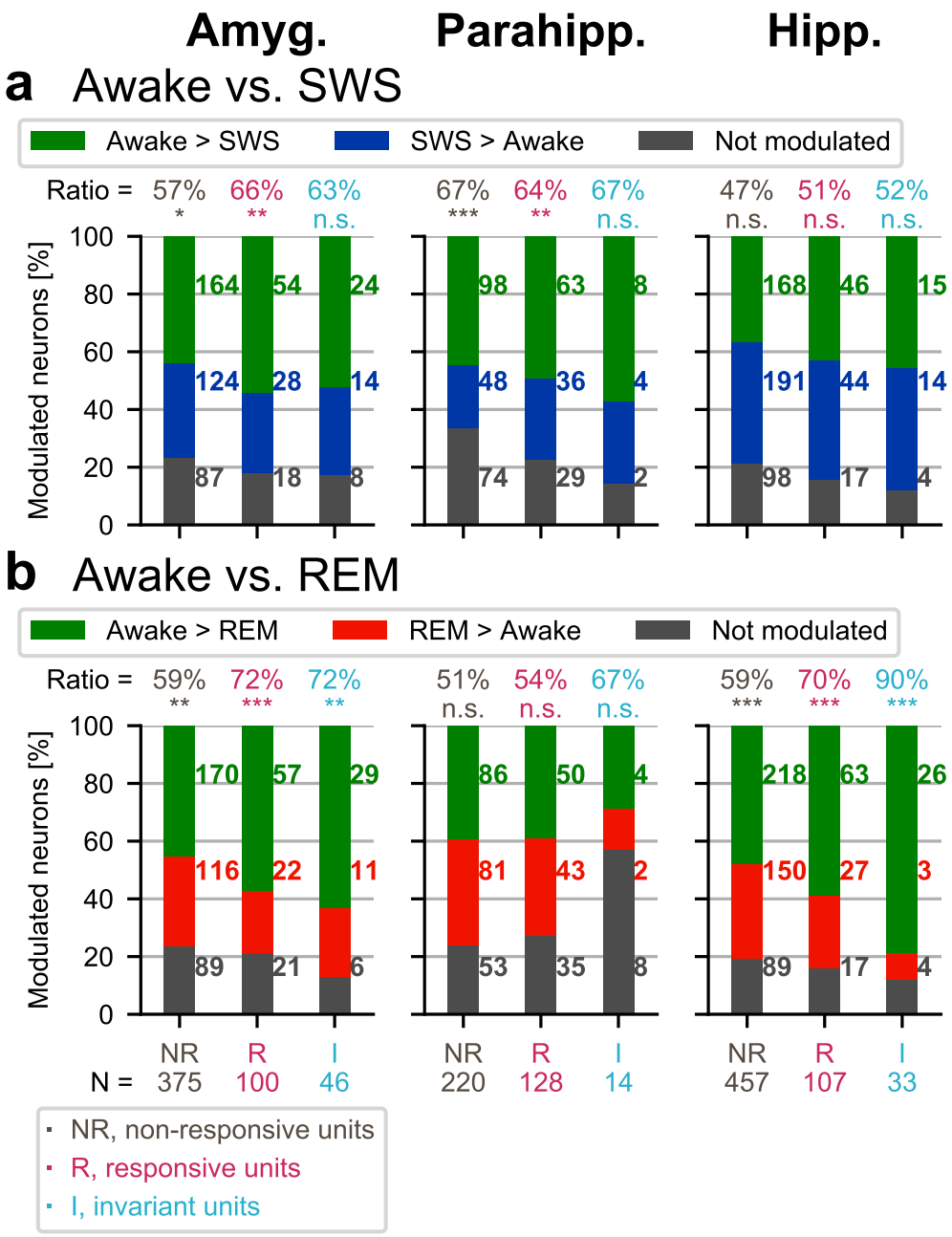

Figure 4.4: **Counts of sleep-stage-modulated concept neurons.** Displayed are counts of modulated and non-modulated units (related to Fig. 4.3). **a,** Awake vs. SWS. In the amygdala and parahippocampal cortex, more units exhibited increased activity during waking vs. SWS than vice versa. In the hippocampus, counts of modulated units did not significantly differ between waking and SWS. Above each bar, the proportion of units with "Awake > SWS"-modulation out of all modulated units is displayed. Asterisks/n.s. correspond to a two-sided binomial test (chance level 50%) of the number of units with "Awake > SWS" among all modulated units. **b,** Awake vs. REM. In the amygdala and hippocampus, more units exhibited increased activity during waking vs. REM than vice versa. In the parahippocampal cortex, counts of modulated units did not significantly differ between waking and REM. Information above each bar as in a, but for "Awake > REM"-modulated units. Amyg., amygdala; Parahipp., parahippocampal cortex; Hipp., hippocampus.

were 0.03, 0.19, and 0.32, respectively (all $p < 0.01$; two-sided Wilcoxon signed-rank test). This modulation was significantly stronger both for invariant and responsive neurons than for non-responsive neurons (NR vs. R, $p < 0.05$; NR vs. I, $p < 0.01$; two-sided Mann–Whitney U test). In the amygdala, neurons were less active both during slow-wave sleep and REM sleep compared to waking, whereas neurons in the parahippocampal cortex were less active during slow-wave sleep but not during REM sleep compared to waking (Fig. 4.3 a and b). The same picture emerged when, instead of quantifying the strength of modulation, we analyzed counts of units, categorized operationally as either sleep-stage modulated or not (Fig. 4.4).

4.2.5 Sharp-wave ripples

Spatial memory consolidation in rodents is believed to take place mostly during sharp-wave ripples in slow-wave sleep (Section 1.3.3; Buzsáki 1989, 2015). Although hippocampal ripples have been described in humans (Bragin, Engel, et al. 1999; Nir, Staba, et al. 2011; Staresina, Bergmann, et al. 2015), their relation to concept neurons (to our knowledge) has never been explored. Fig. 4.5 a shows a sample ripple event in the hippocampus with an action potential of a concept neuron fired concurrently (ripple detection methods are described in Section 4.1.8). As expected, ripple rates were lower during REM sleep than during waking and slow-wave sleep (Fig. 4.5 b). Fig. 4.5 c shows action potentials of the invariant units from Fig. 4.1 c during ripples. Firing of NR, R, and I units was strongly linked to ripples: we used Hedges' g to quantify the increase of firing during vs. before ripples (Fig. 4.5 d). NR, R, and I units had an average Hedges' g of 0.23, 0.26, and 0.32, respectively, for modulation by awake ripples, and 0.39, 0.44, and 0.47, respectively, for modulation by ripples in slow-wave sleep (all $p < 10^{-6}$; two-sided Wilcoxon signed-rank test). During waking, both R and I neurons were significantly more strongly linked to ripples than NR neurons (both $p < .05$; two-sided Mann–Whitney U test). However, during slow-wave sleep, the modulation by ripples exhibited higher variance, and the strength of modulation did not significantly differ for NR vs. R/I units.

4.2.6 Spike-count correlations

Next, we tested whether ensembles of concept neurons linked through a common memory episode (here, the Fotonovela) were *concurrently* reactivated during sleep after learning. We defined the spike-count correlation of a pair of concept neurons in a given time-window as the Pearson correlation coefficient of vectors of spike-counts, obtained by counting spikes in bins subdividing the time-window (Section 4.1.9; Cohen and Kohn

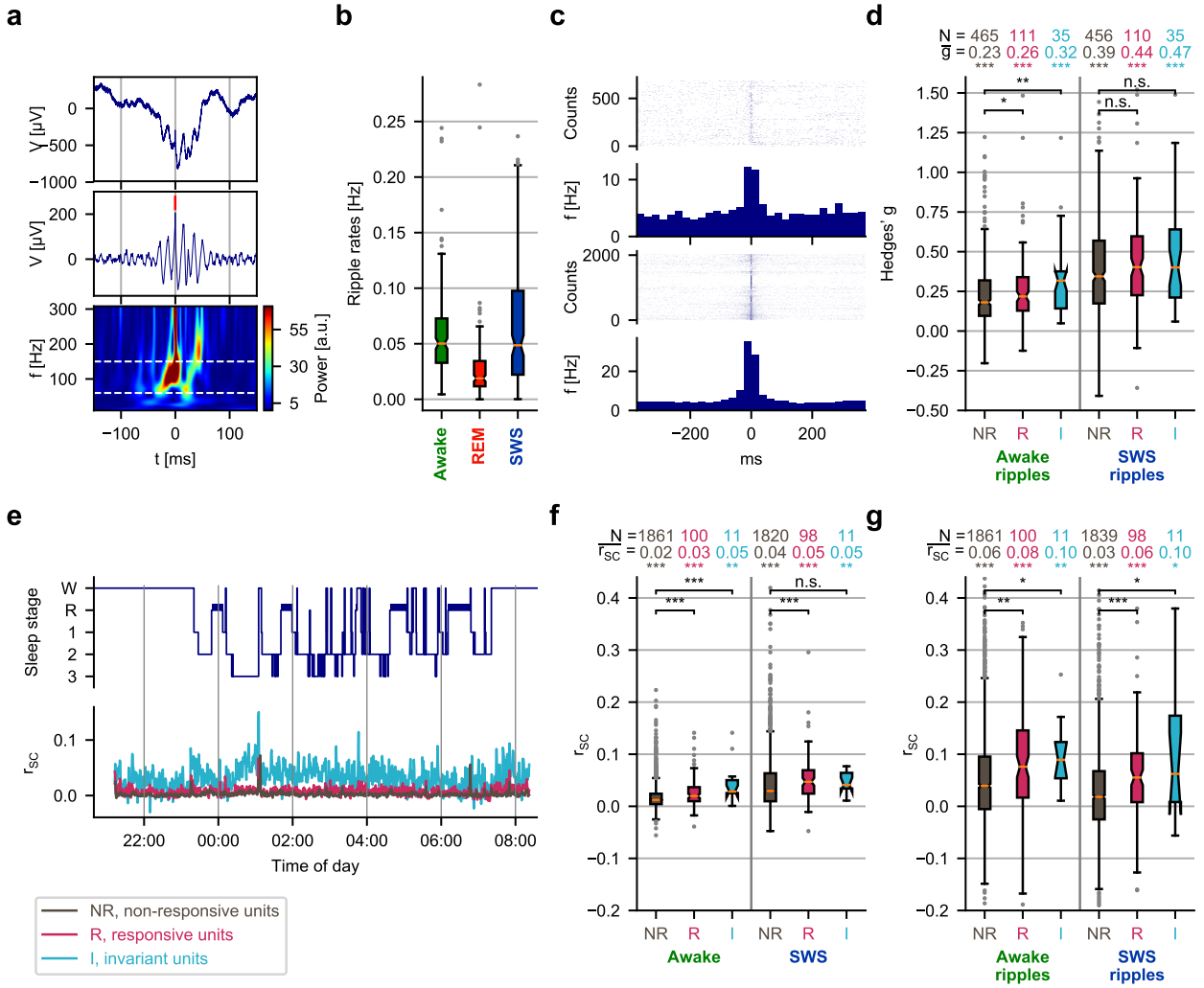

Figure 4.5: **Concept neurons are reactivated during ripples and reflect episodic memory. a,** Sample ripple event. Top, unfiltered data; center, filtered for display (bandpass, 80 Hz to 200 Hz); bottom, time-frequency analysis by Stockwell transform. **b,** Ripple rates in the hippocampus during waking, REM sleep, and SWS. **c,** Raster plots of two concept neurons (same as in Fig. 1 c) time-locked to ripples. Firing rates were elevated during ripples. **d,** Firing rate increase of non-responsive, responsive, and invariant units during awake ripples and SWS ripples. Hedges' g was calculated for "during ripple" (−125 ms to 125 ms relative to ripple center) versus "before ripple" (−375 ms to −125 ms relative to ripple center). All types of units showed significantly increased firing during ripples (all $p < 10^{-6}$; two-sided Wilcoxon signed-rank test against 0). This increase was higher during SWS than during waking, higher for responsive units and highest for invariant units (Mann–Whitney U test). **e,** Spike-count correlations in the hippocampus from one experimental session. Displayed are the hypnogram along with mean spike-count correlations for all three types of units (5 min windows of 1 s bins; Parameter Set 3 in Table 4.1). **f,** Spike-count correlations during waking and SWS. Spike-count correlations were higher for both responsive and invariant units than for non-responsive units (Mann–Whitney U test). **g,** Spike-count correlations during ripples. Responsive and invariant units exhibited higher spike-count correlations during ripples than non-responsive units, both during waking and SWS (Mann–Whitney U test). In **d** and **g**, differences in unit counts for Awake ripples vs. SWS ripples arise because no SWS ripples were detected on some channels.

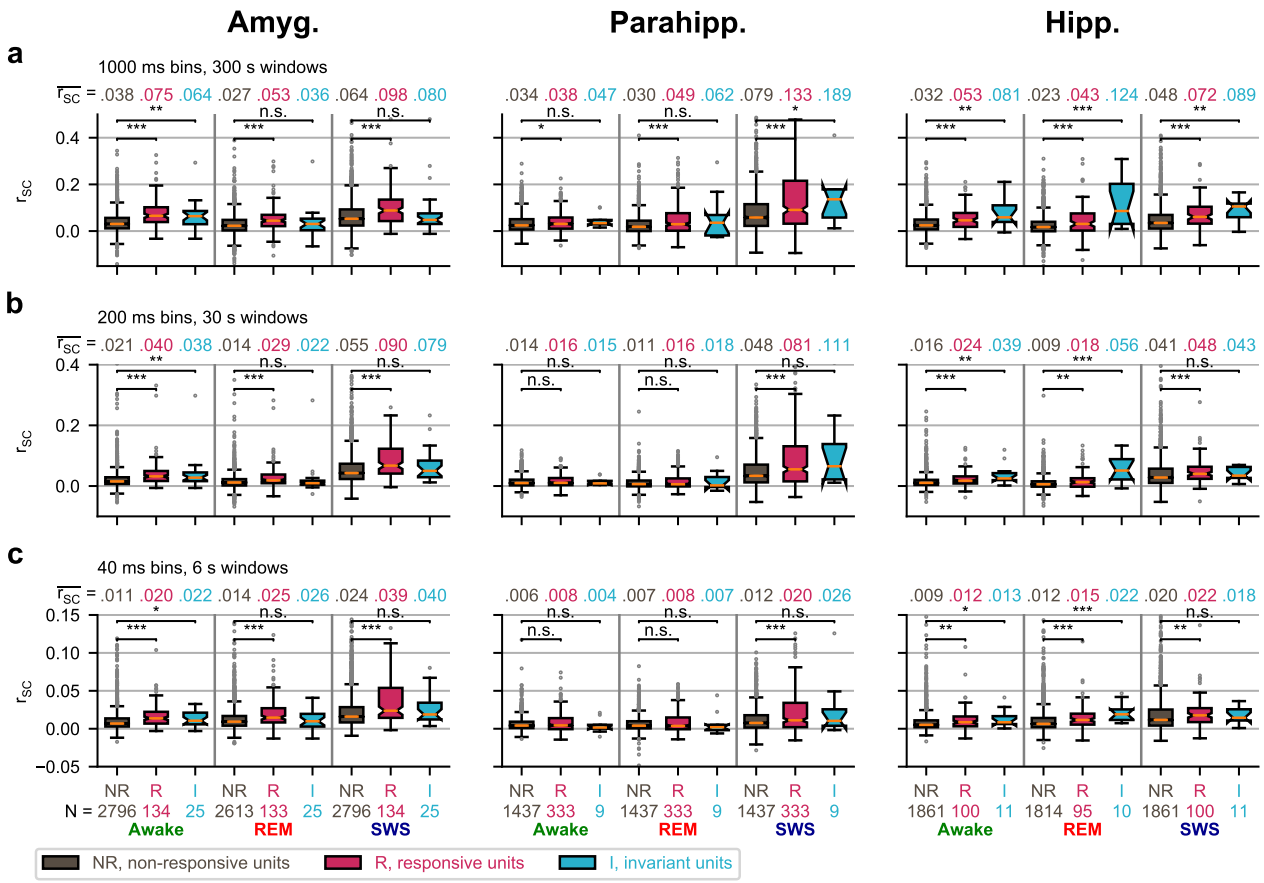

Figure 4.6: **Spike-count correlations for different analysis parameters. a,** Windows of 5 min duration consisting of non-overlapping 1 s bins. **b,** Windows of 30 s duration consisting of non-overlapping 200 ms bins. **c,** Windows of 6 s duration consisting of 40 ms bins with an overlap of 20 ms. Amyg., amygdala; Parahipp., parahippocampal cortex; Hipp., hippocampus.

2011; for a similar approach in rats see Wilson and McNaughton 1994). We computed average spike-count correlations for all pairs of non-responsive, responsive, and invariant neurons (separately for each region). A sample time course of spike-count correlations (computed in 5 min windows) in the hippocampus of one subject is displayed in Fig. 4.5 e along with sleep stages. Hippocampal spike-count correlations were significantly higher for responsive and invariant units compared to non-responsive units both during waking and slow-wave sleep (Fig. 4.5 f; average spike-count correlations for NR, R, and I units during waking, 0.03, 0.05, and 0.08, respectively; during slow-wave sleep, 0.05, 0.07, and 0.09 respectively; comparison NR vs. R and NR vs. I, all $p < 0.01$; two-sided Mann–Whitney U test). Spike-count correlations were generally higher during slow-wave sleep than during waking (NR units, $p < 0.0001$; R units, $p < 0.05$; I units, n.s.; two-sided Mann–Whitney U test). We also analyzed spike-count correlations during ripples by taking each ripple event as a time bin (Fig. 4.5 g). Because of varying ripple event rates across recordings, the lengths of the spike-count vectors also varied (lengths during waking, 233 to 9034 (median, 1109); during slow-wave sleep, 30 to 2407 (median, 664); see also Section 4.1.9). The average spike-count correlations during ripples during waking for NR, R, and I units were 0.06, 0.08, and 0.10, respectively, and during ripples during slow-wave sleep, 0.03, 0.06, and 0.10, respectively (NR vs. R, all $p < 0.01$; NR vs. I, all $p < 0.05$.; two-sided Mann–Whitney U test).

To understand at which temporal scale the reactivation of memory traces takes place, we analyzed spike-count correlations in windows of lengths varying from 6 s (40 ms bins) to 5 min (1 s bins; see Fig. 4.6 for results and Table 4.1 for all parameter values). We also performed the same analysis for pairs of neurons in the amygdala and in the parahippocampal cortex. We observed three general trends: first, in all three regions, spike-count correlations were generally smallest for bins of 40 ms duration, had intermediate values for bins of 200 ms duration, and were highest for bins of 1 s duration. Second, in all three regions, spike-count correlations were generally higher during slow-wave sleep than during waking and REM sleep. Third, in all three regions, both pairs of R units and pairs of I units generally had higher spike-count correlations than pairs of NR units.

In the following, we outline our results for each of the three regions; see also Fig. 4.6. All p-values reported for the three regions resulted from a two-sided Mann–Whitney U test.

In the amygdala, we observed higher spike-count correlations for pairs of R units compared to pairs of NR units at all temporal scales and during all sleep stages (all $p < 0.001$). Pairs of I units also had higher spike-count correlations than pairs of NR units at all temporal scales and during all sleep stages, but this difference was significant only during

waking ($p < 0.05$ at all temporal scales).

In the parahippocampal cortex, pairs of R units had significantly higher spike-count correlations than pairs of NR units at all temporal scales during slow-wave sleep (all $p < 0.001$), but during waking and REM sleep, this difference was significant only for bins of 1 s duration (Parameter Set 3 in Table 4.1; both $p < 0.05$). Spike-count correlations of pairs of I units were significantly higher compared to pairs of NR units only during slow-wave sleep for bins of 1 s duration (Parameter Set 3 in Table 4.1).

In the hippocampus, pairs of R units had significantly higher spike-count correlations than pairs of NR units at all temporal scales and during all sleep stages (all $p < 0.01$). Pairs of I units had significantly higher spike-count correlations than pairs of NR units at all temporal scales during waking and REM sleep (all $p < 0.05$). During slow-wave sleep, spike-count correlations of pairs of I units were significantly higher compared to pairs of NR units only for bins of 1 s duration (Parameter Set 3 in Table 4.1; $p < 0.01$).

To summarize, these results show that concept neurons related through a common memory episode featuring their preferred stimuli were concurrently reactivated during subsequent sleep, indicating consolidation of the "what" component of episodic memories through reactivation of concept neurons.

4.2.7 Temporal order: cross-correlations

We next turned to the temporal order of events – the "when" component of episodic memory. In rats, the temporal order of neuronal firing during behavior is preserved during subsequent rest and sleep (Section 1.3.4; this "neuronal replay" is considered a hallmark of memory consolidation; Skaggs and McNaughton 1996; Lee and Wilson 2002). By the analogy between rodent place cells and human concept neurons, we hypothesized that in humans, the temporal order of concepts in a memory episode could be represented by the temporal order of concept neuron firing during consolidation.

The Fotonovela defined a specific temporal order among concepts for which concept neurons had been identified. To identify temporal order in concept neuron firing after learning, we computed cross-correlograms between all pairs of responsive neurons (separately for each region; Section 4.1.9). Asymmetries of cross-correlograms were elevated during slow-wave sleep compared to waking, indicating the emergence of stereotypically ordered firing among many pairs of concept neurons during slow-wave sleep (Fig. 4.7 a shows an example; Fig. 4.7 b shows comparisons; awake vs. slow-wave sleep, $p < 0.0001$ in each region; two-sided Mann–Whitney U test; for the definition of asymmetry, see Section 4.1.9). These asymmetries were most pronounced during ripples (Fig. 4.7 b; asym-

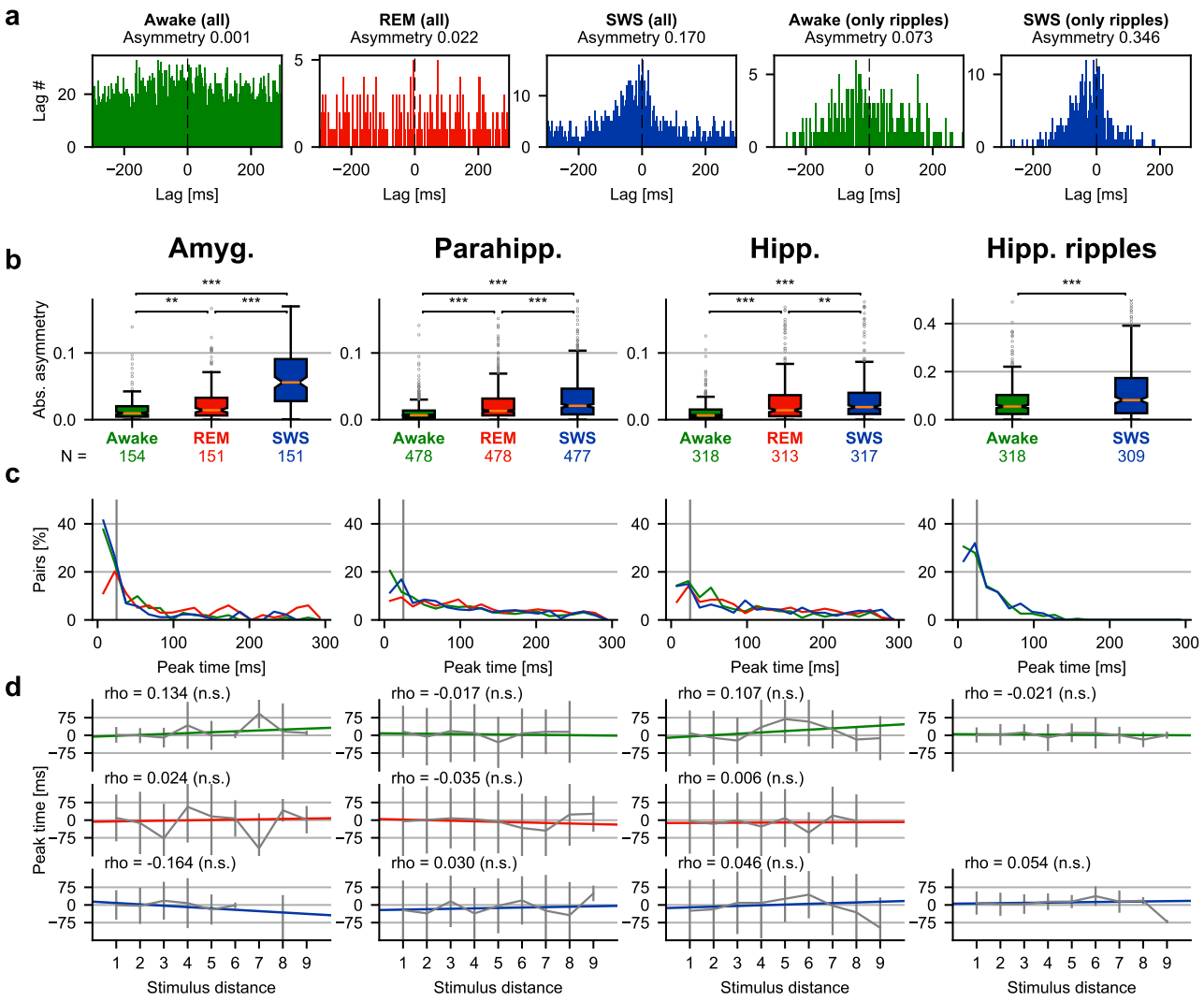

Figure 4.7: **Cross-correlation times of concept neurons do not reflect temporal order of stimuli. a,** Sample cross-correlograms for a pair of concept neurons in the hippocampus. The cross-correlation was more asymmetric during SWS than during REM sleep and waking, and most asymmetric during ripples (for methods, see Section 4.1.9). **b,** Asymmetries in different sleep stages. Absolute values of asymmetry were significantly higher during SWS than during REM sleep and waking. Asymmetries were highly elevated during ripples. N, counts of cross-correlograms included in the analysis. Small differences in N between sleep stages arise because asymmetry is not defined for empty cross-correlograms. **c,** Peak cross-correlation times in different sleep stages. Many peak cross-correlation times are on the order believed to be relevant for spike-timing-dependent plasticity. Vertical lines at 25 ms. **d,** Cross-correlation times by stimulus distance. The stimulus distance was defined by the Fotonovela learning experiment. Sign of peak times was normalized by relative stimulus position (see Section 4.1.9). Contrary to what the analogy between rat place cells and human concept neurons would suggest, stimulus distance and cross-correlation peak times were not systematically correlated. rho, Pearson's correlation coefficient; gray errorbars, standard deviation.

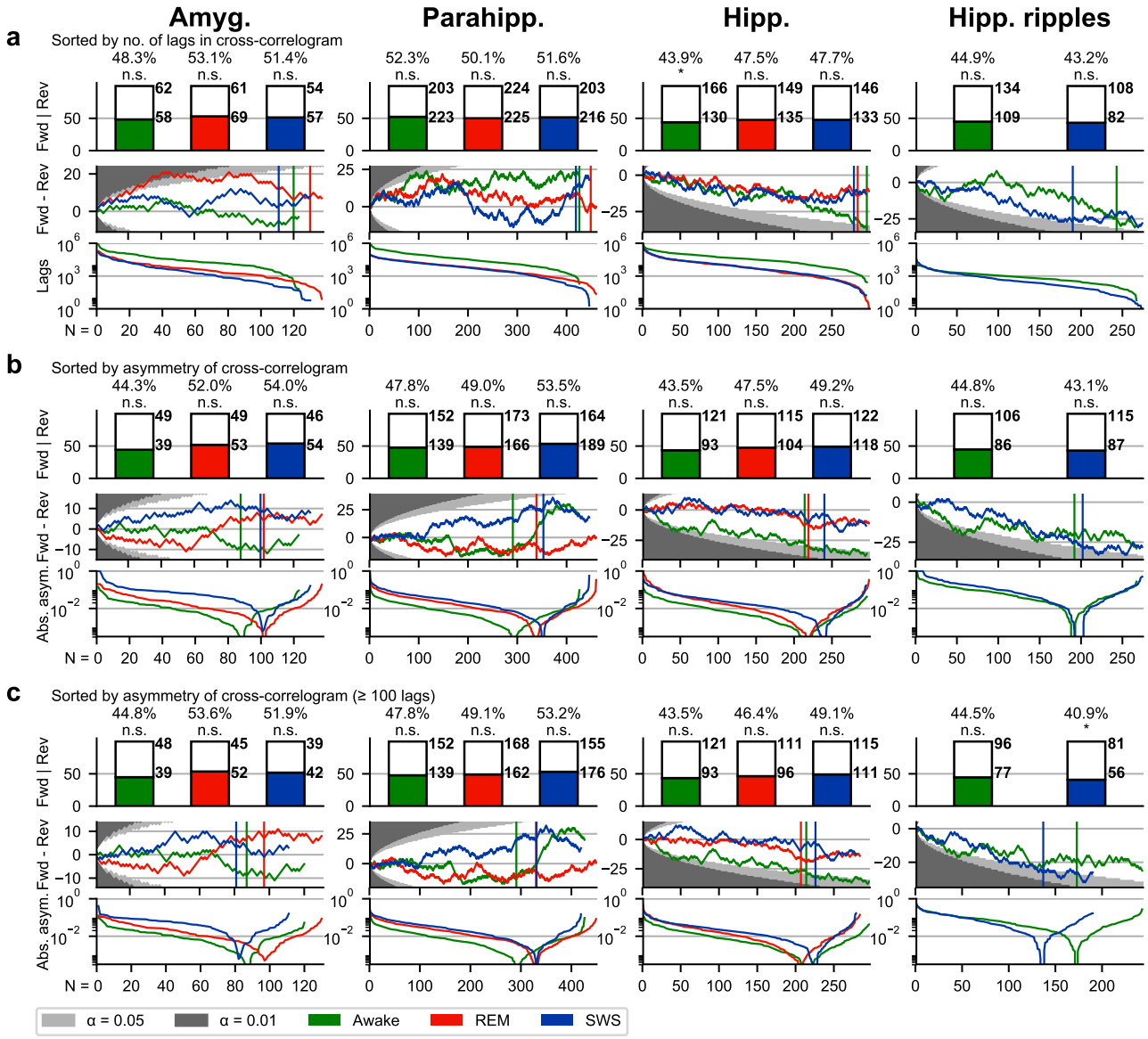

Figure 4.8: **Stimulus order and firing order, sorted by "number of lags" and "asymmetry".** A pair of responsive units was defined as 'forward' (Fwd) if the order of the units' preferred stimuli in the Fotonovela and the firing order (defined by peak cross-correlation time) coincided, and as 'reverse' (Rev) otherwise. Top panels in **a**–**c** depict numbers of forward pairs (colored bars) and reverse pairs (empty bars; significant deviation from chance determined by two-sided binomial test with chance level 50%). Numbers correspond to the points marked by vertical lines in the middle panels. Middle panels depict the difference 'Fwd minus Rev' for subsets of the most populated (**a**) or most asymmetric (**b**, **c**) cross-correlograms. Bottom panels depict the sorting criterion used in the corresponding middle panels. **a,** Pairs of units sorted by number of lags in cross-correlogram. Vertical lines denote the last pair with a cross-correlogram containing at least 100 lags. Reverse pairs prevailed in the hippocampus during waking ($p < 0.05$). **b,** Pairs sorted by asymmetry of cross-correlogram. Vertical lines denote the last pair with non-negative asymmetry: cross-correlograms to the right of the vertical line are inconsistent (i.e., the signs of their peak time and prevailing constituent lags differ; see Section 4.1.9). **c,** Similar to b, but only for cross-correlograms with at least 100 lags. Vertical lines denote the last pair with non-negative asymmetry. Reverse pairs prevailed in the hippocampus during ripples during slow-wave sleep ($p < 0.05$).

metries in the hippocampus during all times vs. during ripples only, $p < 0.0001$ for both waking and slow-wave sleep; two-sided Mann–Whitney U test), and more pronounced during ripples in slow-wave sleep compared to ripples during waking ($p < 0.0001$; two-sided Mann–Whitney U test).

Asymmetric cross-correlations with short peak times potentially hint at synapse modifications, as action potentials fired in sequence with a sufficiently short lag have been shown to modify synaptic efficacy, a phenomenon known as *Hebbian learning* or *spike-timing-dependent plasticity* (Section 1.3.5; Hebb 1949; Bliss and Lømo 1973; Levy and Steward 1983; Markram, Lübke, et al. 1997). In turn, the formation of long-lasting memories is believed to be based on synapse modifications (Bliss and Collingridge 1993; Kandel, Dudai, et al. 2014). We computed the cross-correlation peak times for all pairs of responsive neurons (Fig. 4.7 c). Peak times were shorter during slow-wave sleep and waking compared to REM sleep (fraction of peak cross-correlation times below 25 ms for waking/REM sleep/slow-wave sleep: amygdala, 59.4%/26.3%/66.7%; parahippocampal cortex, 30.8%/15.0%/25.7%; hippocampus, 28.3%/18.7%/26.9%; for waking/slow-wave sleep during hippocampal ripples, 53.2%/51.0%).

In rats, the activity of place cells during rest or sleep reproduces trajectories from earlier running (Lee and Wilson 2002; Davidson, Kloosterman, et al. 2009). In the Fotonovela, concepts appear in a fixed order. For each pair of responsive neurons, we computed the Pearson correlation coefficient between the relative position numbers of the neurons' preferred stimuli in the Fotonovela and their peak cross-correlation time, normalized by the sign of the stimuli's relative position. Surprisingly, this correlation was not significant in any region or sleep stage (Fig. 4.7 d; methods in Section 4.1.9).

The exact values of peak cross-correlation times likely depend on numerous factors, e.g., the number of synapses between indirectly connected neurons. To analyze the temporal order of activity of responsive units regardless of the exact times of peak cross-correlation, we classified each pair of responsive units as either a 'forward pair' if the sign of their peak cross-correlation time and the order of their preferred stimuli coincided, or a 'reverse pair' otherwise (Section 4.1.9 and Fig. 4.8). Investigation across a range of analysis parameters revealed a significant prevalence of reverse pairs compared to forward pairs in the hippocampus during waking (Fig. 4.8 a; 43.9% forward pairs) and during ripples in slow-wave sleep (Fig. 4.8 c; 40.9% forward pairs). However, since these effects were very unstable across analysis parameters (as displayed in Fig. 4.8), we conclude that no reliable, systematic effect of stimulus order on the temporal order of activity of concept neurons could be observed in our data. All results are discussed more broadly in Chapter 5.

Chapter 5

Discussion

We set out to identify a mechanism of human episodic memory consolidation during sleep at the level of concept neurons. Epilepsy patients implanted with micro-electrodes in their medial temporal lobes performed a story-learning task that defined a specific sequential order among visual stimuli. We developed and evaluated a complete framework for the analysis of whole-night single-unit recordings. We recorded from concept neurons tuned to these stimuli during entire nights after learning.

These were our main findings:

1. Concept neurons provided a stable and invariant representation of semantic content across entire nights including sleep.

2. In the hippocampus, the activity of concept neurons was systematically modulated by sleep stages, with similar activity levels during waking and slow-wave sleep and marked inhibition during REM sleep.

3. Concept neurons were more active during ripples than outside of ripples.

4. Concept neurons activated during learning were more correlated than non-responsive neurons. Correlations were highest during slow-wave sleep. Correlations were also elevated during ripples.

5. Concept neurons had asymmetric cross-correlograms. These cross-correlograms were most asymmetric during slow-wave sleep. Many peak cross-correlation times were on the order believed to be relevant for synapse modification.

6. Asymmetric cross-correlations did not systematically correspond to the order of stimuli in the episodic learning task.

How do these results contribute to the understanding of memory consolidation? The standard view of systems memory consolidation posits that during memory encoding, memory traces are rapidly formed in the hippocampus, and that memory consolidation takes place by the reactivation of these hippocampal memory traces during subsequent slow-wave sleep (Frankland and Bontempi 2005).

We propose that the coordinated activity of concept neurons in the hippocampus is a physiological correlate of the hippocampal memory trace.

Specifically, we argue that hippocampal concept neurons represent the content of memory episodes in a compact manner, and that the coordinated reactivation of content-specific ensembles of hippocampal concept neurons during slow-wave sleep (especially during ripples) leads to the creation of a long-lasting association (i.e., episodic memory) between the concepts represented by the individual concept neurons. We also suggest that concept neurons in the amygdala and parahippocampal cortex play a similar albeit not identical role.

In the following, we will outline how our data support our model proposition, relate our data to our Hypotheses 1–5 outlined in Section 1.5, and discuss possible limitations of our study.

Invariance and constancy of concept neurons

If concept neurons indeed represent content in memory consolidation, the representation has to be semantically invariant (otherwise it could not represent *content*) and stable over the time course of consolidation (otherwise consolidation could not take place by reactivation of the same neurons). This is the content of our Hypothesis 1 in Section 1.5. The results we presented in Section 3.3.3 and Fig. 4.2 b show that a substantial portion of concept neurons indeed represents concepts invariantly and after an entire night of sleep. More technical aspects of this point are discussed further below.

Sleep-stage modulation

Concept neurons in the hippocampus were as active during slow-wave sleep as during waking (Section 4.2.4 and Figs. 4.3 and 4.4). Activity during slow-wave sleep is a necessary requirement if the claim holds that hippocampal memory traces formed from concept neurons are reactivated (Hypothesis 2 in Section 1.5). On the other hand, the marked inhibition of hippocampal units during REM sleep fits the view that declarative memory consolidation does not take place during REM sleep.

The significantly stronger relative inhibition of responsive and invariant neurons versus non-responsive neurons during REM sleep could result from an elevated activity of responsive and invariant neurons during waking prior to sleep (e.g., as part of memory consolidation or potential "rehearsal" already during waking; for the notion that consolidation by reactivation can begin already during rest after learning before the onset of sleep see e.g., Davidson, Kloosterman, et al. 2009; Foster and Wilson 2006). Alternatively, the observed effect could result from the presence of non-concept neurons in the non-responsive population.

In rats, Mizuseki and Buzsáki (2013) reported decreased activity in REM sleep versus waking and only slightly increased activity in slow-wave sleep versus waking for principal cells in CA1, CA3, and in the dentate gyrus, a picture highly similar to our finding in human concept neurons. It remains open how this picture relates to Pavlides and Winson (1989), who reported significant increases in firing rates in both slow-wave and REM sleep compared to waking for place cells in CA1 that were active during pre-sleep behavior, and small increases for those that were inactive.

In the parahippocampal cortex, we found a strong inhibition of concept neurons during slow-wave sleep versus waking, but no inhibition during REM sleep. This fits the notion that the parahippocampal cortex is better described as a high-level sensory area than as core part of the declarative memory system. Our observation that significantly fewer units in the parahippocampal cortex were invariant than in the other two regions also points towards a sensory function of the parahippocampal cortex.

In the amygdala, concept neurons were inhibited during both slow-wave and REM sleep compared to waking. Several lesion studies concluded that the amygdala is not as relevant as the hippocampus for declarative memory (Section 1.1.3; Zola-Morgan and Squire 1993). Other studies have shown a role for the amygdala in emotional memory consolidation (Girardeau, Inema, et al. 2017). The visual stimuli in our episodic memory task were generally neutral and not controlled for emotional content, a gap to be filled by future studies.

Ripples

In rodents, there is convincing evidence that the reactivation of hippocampal memory traces is strongly linked to ripples, and that ripples are necessary for normal memory consolidation (Girardeau, Benchenane, et al. 2009; Ego-Stengel and Wilson 2010).

In line with the notion that reactivations of memory traces happen mostly during ripples, our data showed an elevated activity of hippocampal concept neurons during ripples

(Section 4.2.5; this is Hypothesis 3 in Section 1.5). This elevation was greater during slow-wave sleep than during waking. The difference could result from an alternation between two states during waking: the *encoding state* without ripples, where concept neurons are active as part of memory trace formation, and the *consolidation state* with ripples, where concept neurons are active as part of memory trace reactivation. During slow-wave sleep, the encoding state does not exist, leading to a higher net difference in concept neuron activity between epochs with ripples and without ripples.

During waking, the modulation of firing by ripples was significantly stronger for responsive and invariant neurons than for non-responsive neurons. A possible interpretation is that the non-responsive neurons did not participate as much in consolidation because the content potentially represented by them may not have been present in any recently encoded memory episode.

Spike-count correlations

In rats, Wilson and McNaughton (1994) showed that – as predicted by models of memory consolidation – pairs of neurons concurrently active during exploration were concurrently reactivated during subsequent slow-wave sleep. Our data demonstrate the same mechanism in humans: responsive and invariant neurons (i.e., the neurons activated during learning) had higher spike-count correlations than non-responsive neurons, during both waking and slow-wave sleep (Section 4.2.6; Fig. 4.5 e, g and Fig. 4.6; this is Hypothesis 4 in Section 1.5). This can be interpreted as concurrent reactivations of exactly those neuronal ensembles that were concurrently activated already during learning, which is the essence of our proposition that learning-related ensembles of concept neurons are a neurophysiological correlate of hippocampal memory traces. The same effect was also present during ripples (Fig. 4.5 f). The smaller absolute values for spike-count correlations during ripples versus all times can possibly be attributed to the different analysis parameters such as the number of bins and the bin duration.

The following (as of yet hypothetical) situation could also explain the observed effects regarding spike-count correlations: if concept neurons formed a network with moderate to strong correlations among its members, while the non-responsive population also encompassed non-concept neurons whose activity only weakly correlated with any other neurons, then concept neurons would exhibit elevated spike-count correlations compared to non-responsive neurons, similar to our observations, without any meaning to content-specific memory consolidation. While there is no concrete evidence for this scenario, targeted experiments are required for a definite conclusion. Such experiments could, for

example, include only some of a pool of identified responsive neurons in a learning task, and compare reactivations of the included vs. non-included responsive neurons.

Cross-correlations

We found highly asymmetric cross-correlations of concept neurons during slow-wave sleep, and less asymmetric cross-correlations during waking and REM sleep. Surprisingly, neither cross-correlation peak times nor the direction of asymmetries were systematically related to the order of stimuli in the episodic memory task (Section 4.2.7; Figs. 4.7 and 4.8). Our Hypothesis 5 (Section 1.5) was not confirmed.

Skaggs and McNaughton (1996) showed in rats that asymmetric cross-correlations during sleep reflect sequential neuronal activity during pre-sleep experience. Since then, memory for sequences has been theorized to be encoded by the sequential activity of place cells (strong supporting evidence was given by e.g., Lee and Wilson 2002; Davidson, Kloosterman, et al. 2009). Our data suggest that human episodic memory is not as simple: apparently human episodic learning cannot be modeled as a simple chain of sequentially firing content-coding concept neurons, with sequential reactivation serving as a consolidation mechanism.

What is the reason for this difference? Already during encoding, human concept neurons and rodent place cells are not perfectly analogous: a spatial overlap of rodent place fields leads to a temporal overlap of place cell firing, while human concept neurons were reported to inhibit one another during sequential presentation of visual stimuli (Kornblith, Quian Quiroga, et al. 2017). Similarly, while rodent place cells have been reported to be phase-locked to an oscillation of the local field potential in the theta range during exploration, no such phase-locking of concept neurons has been reported in humans (the study by Rutishauser, Ross, et al. (2010) reported phase-locking of human hippocampal neurons to an oscillation in the 3 Hz to 7 Hz range, but the study did not test if phase-locked neurons were concept neurons – on the contrary, the population for which phase-locking was reported was described in Rutishauser, Ye, et al. (2015) to be independent of another, visually selective population). However, theta phase-locking during encoding might be a prerequisite for sequential reactivation during consolidation.

A simpler reason for our failure to observe robust sequential reactivation might stem from the fact that the concept neurons we observed were located in various parts of the medial temporal lobe. Especially in the hippocampus, neurons in different subfields might at the same time behave very similarly during visual stimulus presentation, and very differently during memory consolidation.

Another possible explanation for the absence of a robust prevalence of 'forward pairs' in our data is the simple behavioral observation that humans tend to form associations between memory items in both directions, forward and reverse (Kahana 1996; Howard, Fotedar, et al. 2005).

Finally, both forward and reverse "neuronal replay" have been reported in rodents (Section 1.3.4; Foster and Wilson 2006; Diba and Buzsáki 2007; Ambrose, Pfeiffer, et al. 2016). It is thus conceivable that the absence of a clear preference of 'forward pairs' in our data results from concurrently existing forward and reverse "neuronal replay". To further investigate this possibility, future studies will have to consider combinations of three or more concept neurons simultaneously, possibly using decoding algorithms (Davidson, Kloosterman, et al. 2009).

Nevertheless, it remains valid to interpret asymmetric cross-correlations (especially with peaks below 25 ms) as evidence hinting at possible synapse modification, as outlined in Section 1.3.5. We emphasize that cross-correlations with a short peak do not necessarily indicate direct synaptic coupling of the observed neurons (instead, concurrent input with slightly differing delays could underlie the observed cross-correlations). Regardless of this caveat, almost synchronous firing of two or more neurons could potentially induce synaptic changes in a common target neuron, which highlights the relevance of peaked (compared to flat, uniform) cross-correlograms *regardless of asymmetry*.

Invariance and constancy of the representation: technical aspects

Only a subset of visually selective neurons in the hippocampus and amygdala responded to both its preferred stimulus picture and the corresponding written name (Fig. 4.2 b). At least three reasons could explain why not all neurons responded to the written name. First, the part of a picture relevant to a responsive neuron could differ from what we chose as written name (e.g., the neuron could respond to "hand bag" when we wrote "the Queen"). Second, despite the prevalence of invariantly responding neurons, a subset of the visually selective neurons in the hippocampus and amygdala could still be tuned to physical stimulus parameters. Third, the response to the written name could simply be weaker than the response to the picture, leading to a false-negative invariance classification. Support for this idea comes from the fact that the response magnitude for the written name of the preferred picture was significantly higher than to the other written names even in neurons that were not invariant according to the operational definition used here (data not shown).

Two studies have described invariant responses in the parahippocampal cortex: Quian Quiroga, Reddy, et al. (2005) reported that 11 out of 20 responsive units in the parahip-

pocampal cortex responded to multiple pictures depicting the same semantic content, and Quian Quiroga, Kraskov, et al. (2009) found that 10 out of 19 responsive units in the parahippocampal cortex responded invariantly (using three different pictures depicting the same semantic content), and that none of these units responded to a written name or sound representing the same content. We found that out of the 96 parahippocampal units that responded to exactly one picture (in the evening screening sessions), 11 responded to the corresponding written name (Fig. 4.2 b). These neurons could either be truly semantically invariant, or they could simply respond in a graded manner to many stimuli (as described by Mormann, Kornblith, et al. 2017). Such a graded response could result in a small percentage of the neurons responding to both a picture and its corresponding written name by chance, without true semantic invariance.

Similarly, are those responses that were found only in the evening or only in the morning nonexistent at the other time point (see Fig. 4.2 c)? In principle, a neuron could be lost from recording, or its visual tuning could undergo changes. Both reasons could lead to a change in response magnitude between evening and morning and are difficult to disentangle. However, the response magnitude for preferred stimuli from one time (evening or morning) was significantly higher than for non-preferred stimuli even at time points where no response was detected by the formal response criterion (data not shown). This means that the proportion of preserved responses was higher than evident from the counts of neurons that responded both in the evening and morning.

Concept neurons in anesthesia

Sleep and general anesthesia both entail periods of unconsciousness. We analyzed the activity of single neurons in the human medial temporal lobe during general anesthesia induced by propofol, one of the most common anesthetic agents (Niediek, Navratil, et al. 2013). The activity of concept neurons during sleep differs from the activity during anesthesia. Fig. 5.1 shows the activity of a neuron in the parahippocampal cortex during anesthesia at varying concentrations of propofol. The activity ceased completely at sufficiently high concentrations of propofol. We observed this pattern in all neurons in the amygdala, entorhinal cortex, hippocampus, and parahippocampal cortex, ($n = 506$, 17 sessions; manuscript in preparation). Thus, the effect of high concentrations of propofol on neuronal firing in the MTL was more extreme than the effect of any sleep stage: while sleep exerted modulatory effects on concept neurons (Section 4.2.4), the changes in firing during sleep never encompassed all neurons, and rarely included a complete cessation of firing.

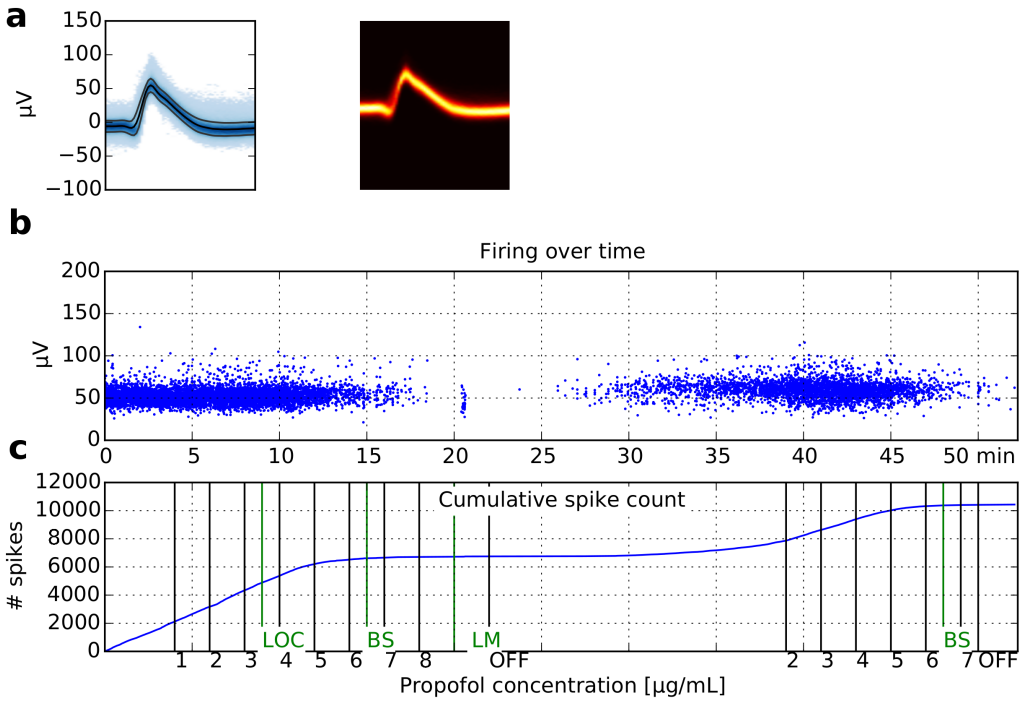

Figure 5.1: **Sample time course of neuronal activity during propofol anesthesia.** Displayed are data from a neuron in the left parahippocampal cortex. **a,** Mean action potential wave form, and density plot of action potentials. **b,** Action potentials over time. Each small dot corresponds to the time point and maximum amplitude of one action potential. The complete cessation and re-onset of firing are visible. See **c** for propofol concentrations on the same time axis. **c,** Cumulative spike counts over time. Time axis is the same as in **b**. Propofol concentrations are indicated below the plot. LOC, loss of consciousness; BS, burst suppression; LM, larynx mask; OFF, propofol infusion stopped.

Investigating the effect of propofol on concept neurons is motivated by the fact that already small (0.9 µg mL^{-1}) concentrations of propofol have been reported to induce profound impairments of declarative memory (Veselis, Pryor, et al. 2008, 2009).

Future questions

A shortcoming of our study is that we can not directly report possible changes in neuronal activity patterns as a result of learning, because we did not measure neuronal activity before learning. Future single-neuron studies on human memory consolidation should overcome this problem by using an appropriate experimental design.

In this study we have not investigated hippocampo–cortical or hippocampo–amygdalar interactions. As reported in the literature, such interactions are likely to play a major role in memory consolidation (Ji and Wilson 2007; Maingret, Girardeau, et al. 2016; Girardeau, Inema, et al. 2017). Our data allow for a future investigation addressing these questions.

Conclusion: a *mechanism* of memory consolidation

In conclusion, our data constitute converging support for reactivation of hippocampal concept neuron ensembles during slow-wave sleep (especially ripples) as a fundamental mechanism of episodic memory consolidation: concept neurons invariantly represent concepts across an entire night; activity is inhibited during REM but not slow-wave sleep; concept neurons are strongly linked to ripples; spike-count correlations are higher for learning-related neurons than for unrelated neurons; and these correlations are highest during slow-wave sleep. Furthermore, asymmetric cross-correlations during slow-wave sleep, especially during ripples, point at a temporal structure possibly enabling synapse modifications among concept neurons (and their target structures) during slow-wave sleep. Nevertheless, the observed temporal structure does not simply reflect stimulus sequences. Because subjects recalled the sequential order of stimuli very well, the sequential order of stimuli must be encoded in a different way than simple neuronal firing sequences.

Appendix A

Installation instructions and user guide for Combinato

This appendix contains brief instructions on how to install and use the spike sorting software package Combinato. The installation instructions and the user guide are maintained as a Wiki at `https://github.com/jniediek/combinato/wiki`. A previous version of this appendix has been published as "Supporting Text" in Niediek, Boström, et al. (2016).

A.1 Installation instructions for Combinato

A.1.1 Installation on a Linux computer

Getting the code

If you use git, clone the repository:

```
git clone https://github.com/jniediek/combinato.git
```

If you do not use git, download Combinato from

`https://github.com/jniediek/combinato/archive/master.zip`.

Installing dependencies

Combinato depends on `scipy`, `pywt`, `matplotlib`, `pytables`, and `pyqt`. Most modern Linux distributions have these packages installed by default. If you miss any of these packages, use your distribution's package manager to install them. For example, in Ubuntu and Debian

```
sudo apt-get install python-scipy python-matplotlib python-pywt
python-tables python-qt4
```

installs all dependencies.

Setting up the environment

Choosing the right clustering backend Combinato uses a compiled executable file as backend for clustering. To automatically select the correct file for your operating system, navigate your shell to the Combinato repository and run

`python setup_options.py`.

Setting Paths Combinato is organized as a collection of executable scripts. These are the files named `css-*` in the repository's main folder. To be able to execute these scripts, add the repository's folder to your `$PATH` as shown below.

For some of the tools in the subdirectories `signalviewer` and `tools`, it is necessary to add the repository's folder to `$PYTHONPATH` as well.

For example, if the Combinato repository is in `/home/username/combinato`, add the following to the shell's configuration (e.g., `/home/username/.bashrc`):

```
PATH=$PATH:/home/username/combinato
PYTHONPATH=$PYTHONPATH:/home/username/combinato
export PATH PYTHONPATH
```

Testing the Installation

1. Open a new shell
2. Navigate to the Combinato repository
3. Enter `python tools/test_installation.py`

If everything worked, you will see the following output:

```
Found Combinato
Found SPC binary
Your version of pytables is 3.3.0
Combinato clustering setup: no problems detected.
Found display
Found 'montage', plotting continuous data possible.
```

A.1.2 Installation on a Windows computer

General Remark

Combinato works on Windows, but it is primarily developed for Linux. Combinato is organized as a set of command line tools, which is optimal for remote servers and shell scripting, but might be cumbersome on Windows computers. So please consider using Combinato on Linux (or OS X). If you decide to use Windows, here are the instructions.

Installing Python

Any Python distribution should work. We use Combinato with Anaconda for Windows by Continuum. For now, please use the Python 2.7 version.

You can download Anaconda from `https://www.continuum.io/downloads`.

Anaconda contains all packages that Combinato depends on (`scipy`, `matplotlib`, `pytables`, `pywt`, `pyqt`).

Getting the Combinato code

If you use git, clone the repository:

`git clone https://github.com/jniediek/combinato.git`.

If you do not use git, download Combinato from

`https://github.com/jniediek/combinato/archive/master.zip`.

Save the repository to a convenient place, for example

`C:\Users\YourUsername\Anaconda\Lib\site-packages`.

Setting Paths

Combinato uses an executable file as backend for clustering. To automatically select the correct file for your operating system, navigate your shell to the Combinato repository and run

`python setup_options.py`.

Testing the Installation

1. Open a new shell
2. Navigate to the Combinato repository
3. Enter `python tools/test_installation.py`

If everything worked, you will see the following output:

```
Found Combinato
Found SPC binary
Your version of pytables is 3.3.0
Combinato clustering setup: no problems detected.
Found display
Found 'montage', plotting continuous data possible.
```

If you see `Plotting continuous data will not work`, don't worry. This feature requires ImageMagick, but it is not crucial.

Using the Combinato scripts on Windows

On Windows, you cannot simply run the scripts named `css-*`, but you have to prepend `python` to each command. For example, to run `css-simple-clustering`, enter

`python css-simple-clustering`, or, if the current directory of your command prompt is different from the Combinato repository,

`python C:\Path\To\Combinato\css-simple-clustering`. This is cumbersome, and this problem does not exist on Linux and OS X. See the FAQ (`https://github.com/jniediek/combinato/wiki/FAQ`) to learn why Combinato is made this way.

A.1.3 Installation on an OS X computer

Installing Python

Any Python distribution should work. We use Combinato with Anaconda for OS X by Continuum. For now, please use the Python 2.7 version.

You can download Anaconda from `https://www.continuum.io/downloads`.

Anaconda contains all packages that Combinato depends on (`scipy`, `matplotlib`, `pytables`, `pywt`, `pyqt`).

Getting the Combinato code

If you use git, clone the repository:

`git clone https://github.com/jniediek/combinato.git` If you do not use git, download Combinato from

`https://github.com/jniediek/combinato/archive/master.zip`. Save the repository to a convenient place, for example

`/Applications/anaconda/lib/python2.7/site-packages`.

Setting Paths

Combinato uses an executable file as backend for clustering. To automatically select the correct file for your operating system, navigate your shell to the Combinato repository and run

`python setup_options.py`.

Combinato is organized as a collection of executable scripts. These are the files named `css-*` in the repository's main folder. To be able to execute these scripts, add the repository's folder to your `$PATH`: The path is set in the file `.bash_profile` in your user directory. For example, this file should contain a line like

`export PATH=$PATH:/Applications/anaconda/lib/python2.7/site-packages/combinato`.

For some of the tools in the subdirectories `signalviewer` and `tools`, it is necessary to add the repository's folder to `$PYTHONPATH` as well.

Testing the Installation

1. Open a new shell
2. Navigate to the Combinato repository
3. Enter `python tools/test_installation.py`

If everything worked, you will see the following output:

```
Found Combinato
Found SPC binary
Your version of pytables is 3.3.0
Combinato clustering setup: no problems detected.
Found display
Found 'montage', plotting continuous data possible.
```

If you see `Plotting continuous data will not work`, don't worry. This feature requires ImageMagick, but it is not crucial.

A.2 User guide for Combinato

This user tutorial introduces the individual steps of spike sorting with Combinato, progressing from synthetic to real data.

A.2.1 Working with synthetic data

Synthetic data

In this part of the tutorial, we will work with synthetic (simulated) data. We will work with the file

`http://bioweb.me/CPGJNM2012-dataset/simulation_5.mat`.

The simulated data is described in Pedreira, Martinez, et al. (2012).

Extracting spikes

After downloading the simulated data, move the command prompt to the folder where you stored it and enter

```
css-extract --matfile simulation_5.mat
```

There is now a folder `simulation_5`, containing one file `data_simulation_5.h5`.

If you would like to use your own Matlab file, store the data in a variable `data` and the sampling rate in a variable `sr`.

Clustering spikes

Just enter

```
css-simple-clustering --datafile simulation_5/data_simulation_5.h5
```

After a few seconds, the folder `simulation_5` contains the sorted data.

Checking results

Now we would like to see the output of the clustering procedure. There are two main ways for visualization: overview plots and the graphical user interface.

Using overview plots Enter

```
css-plot-sorted --label sort_pos_simple
```

There is now a folder `overview`, containing just one plot (Fig. A.1).

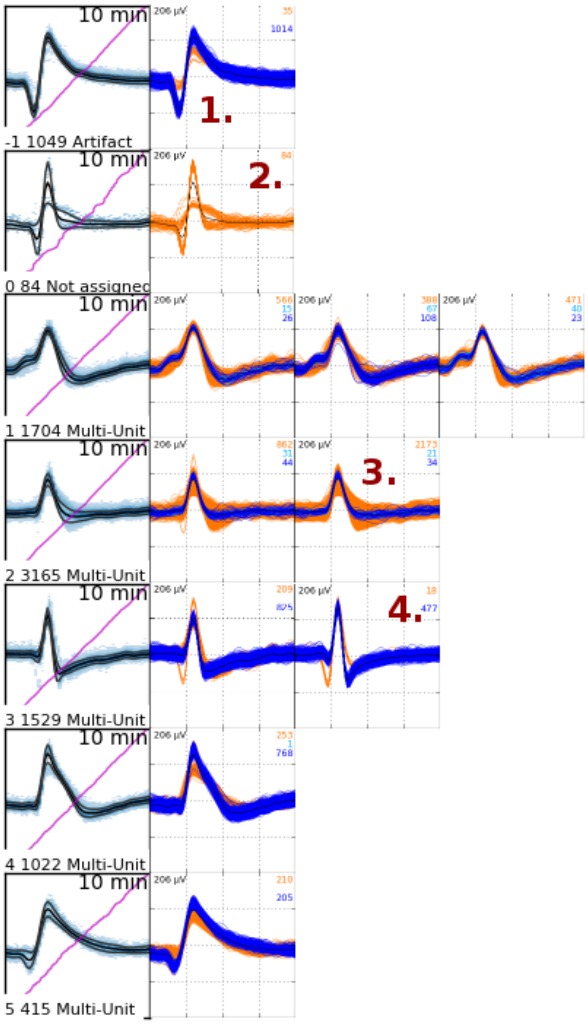

Figure A.1: **Clusters from Simulation 5.** Each row corresponds to one cluster, displayed as a density plot in the first column. The pink line shows the cumulative spike count over the time course of the recording. Each cluster's subclusters are displayed in the subsequent columns as line plots. The red numbers 1. through 4. point at a few problems with the clustering that will be solved in the next part of the tutorial (Appendix A.2.2).

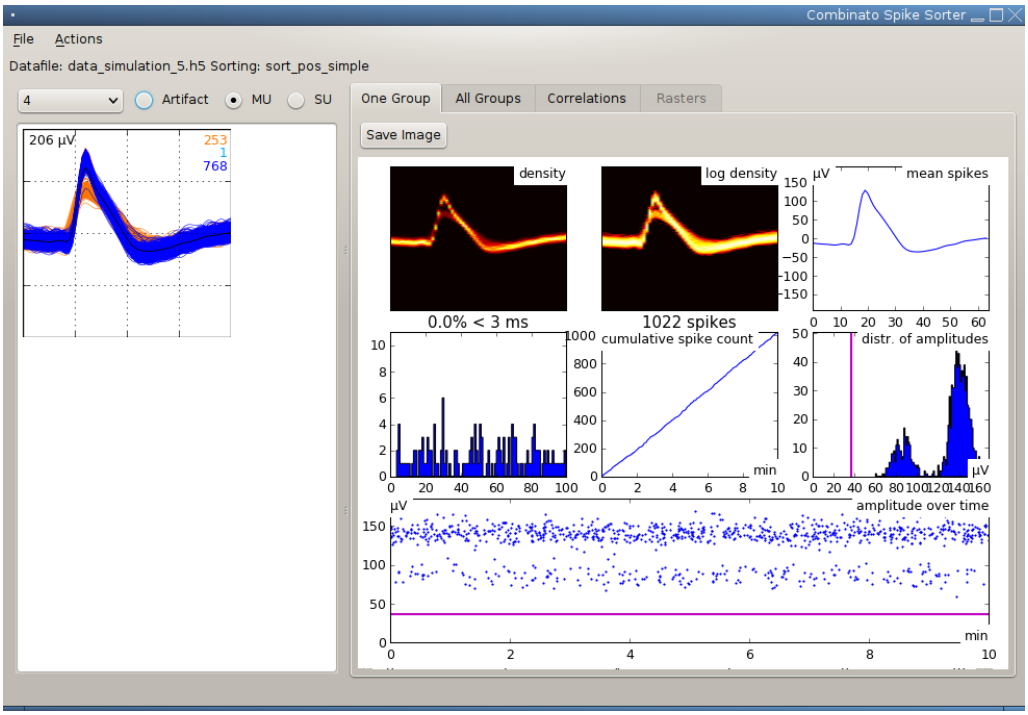

Figure A.2: **Screenshot of Combinato's GUI.** Displayed is cluster 4 from simulation 5, which is "under-clustered". We will solve this problem in Appendix A.2.2.

Using the graphical user interface Enter `css-gui` and click on File, Open. You will see a list containing just one file, our Simulation 5. Click on OK. You will see the screen shown in Fig. A.2.

Go through the individual cluster groups by using the pull down menu. The plots on the right hand side update automatically. In our screenshot you can see that the unit displayed is "under-clustered": it should be split apart further. We are going to solve this problem in the next part of the tutorial (Appendix A.2.2).

Now, click on the "All Groups" tab. You will see the screen shown in Fig. A.3, an overview of all cluster groups contained in Simulation 5. In some cases, clusters are grouped together in the wrong way. To solve this problem:

- First create a new group by clicking Actions, New Group.
- Then click on one of the clusters you would like to move to the new group (red 1. in Fig. A.3)
- The last step is to click into the new, empty group (red 2. in Fig. A.3).

You can save your modification by clicking File, Save.

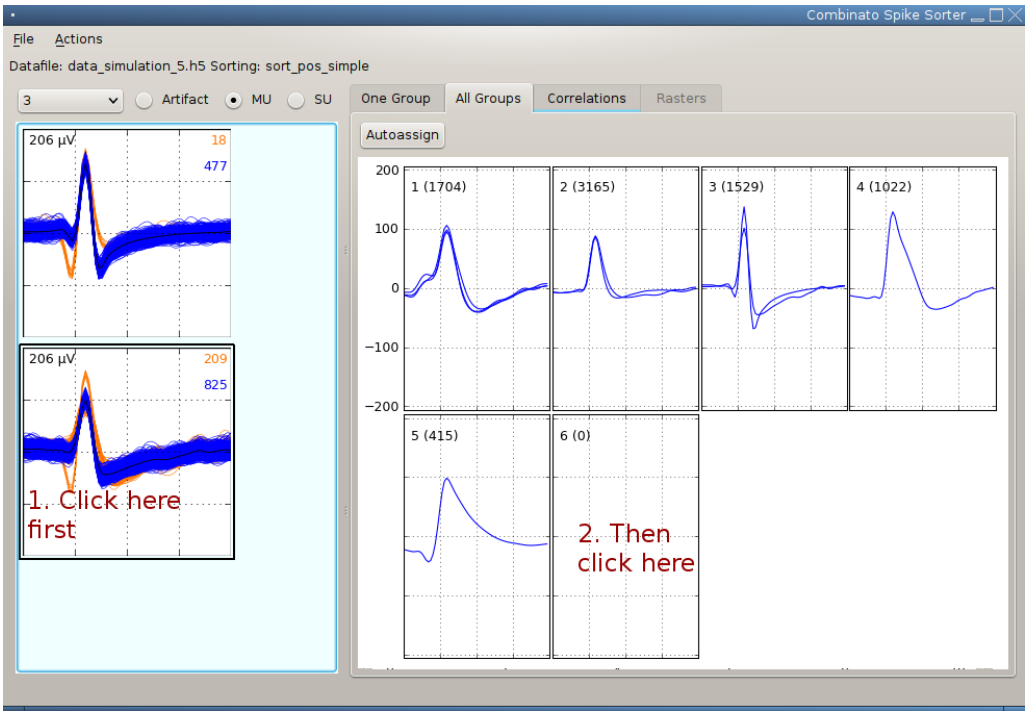

Figure A.3: **Overview of groups in Simulation 5.** The red 1. and 2. indicate where to click to modify the clustering result manually.

A.2.2 Setting parameters and improving automatic results

In this part of the tutorial we will tune some parameters to optimize the automatic sorting results.

What's the problem?

We saw in Fig. A.1 that Combinato created an acceptable but not optimal clustering result. The problems are (the numbers refer to the red numbers in Fig. A.1):

1. A cluster was wrongly designated an artifact.
2. Some spikes were not assigned to any cluster.
3. A multi-unit should be split apart further.
4. There are some spikes that do not really belong to the units they were assigned to.

Setting parameters to improve clustering results

Create a file called `local_options.py` in the same folder that contains the `simulation_5` folder. The content of the file is the following:

```
options = {'MaxClustersPerTemp': 7,
           'RecursiveDepth': 2,
           'MinInputSizeRecluster': 1000,
           'MaxDistMatchGrouping': 1.6,
           'MarkArtifactClasses': False,
           'RecheckArtifacts': False}
```

Then re-run the clustering procedure. At this point, you should use a different *label*. Labels are names under which the clustering results are stored. By using different labels, you can save different clustering results from the same data and compare them later. Enter

`css-simple-clustering --datafile simulation_5/data_simulation_5.h5 --label optimized`.

When processing is completed, enter

`css-plot-sorted --label sort_pos_optimized`.

The prefix `sort_pos_` is automatically prepended to the label. The improved sorting results are shown in Fig. A.4. We see that with the optimized options, Combinato generated ten units.

There are still some problems with the clustering, which you can fix manually with `css-gui` (the numbers refer to Fig. A.4):

1. Unit 1 consists of 8 subclusters. Probably the 5th and 7th subclusters should be made a different unit.

2. Unit 3 consists of 2 subclusters. These are very different and should be split into two units using `css-gui`.

3. Unit 7 consists of 2 subclusters. The first of these could be split further.

Manual optimization

As explained in Appendix A.2.1, use `css-gui` to further split apart under-clustered units. You can also set units to *Single Unit* in `css-gui` (all units are considered multi-units by default), see Fig. A.5.

If you save your modifications and re-plot the results by `css-plot-sorted --label sort_pos_optimized`, the result will be very similar to Fig. A.6.

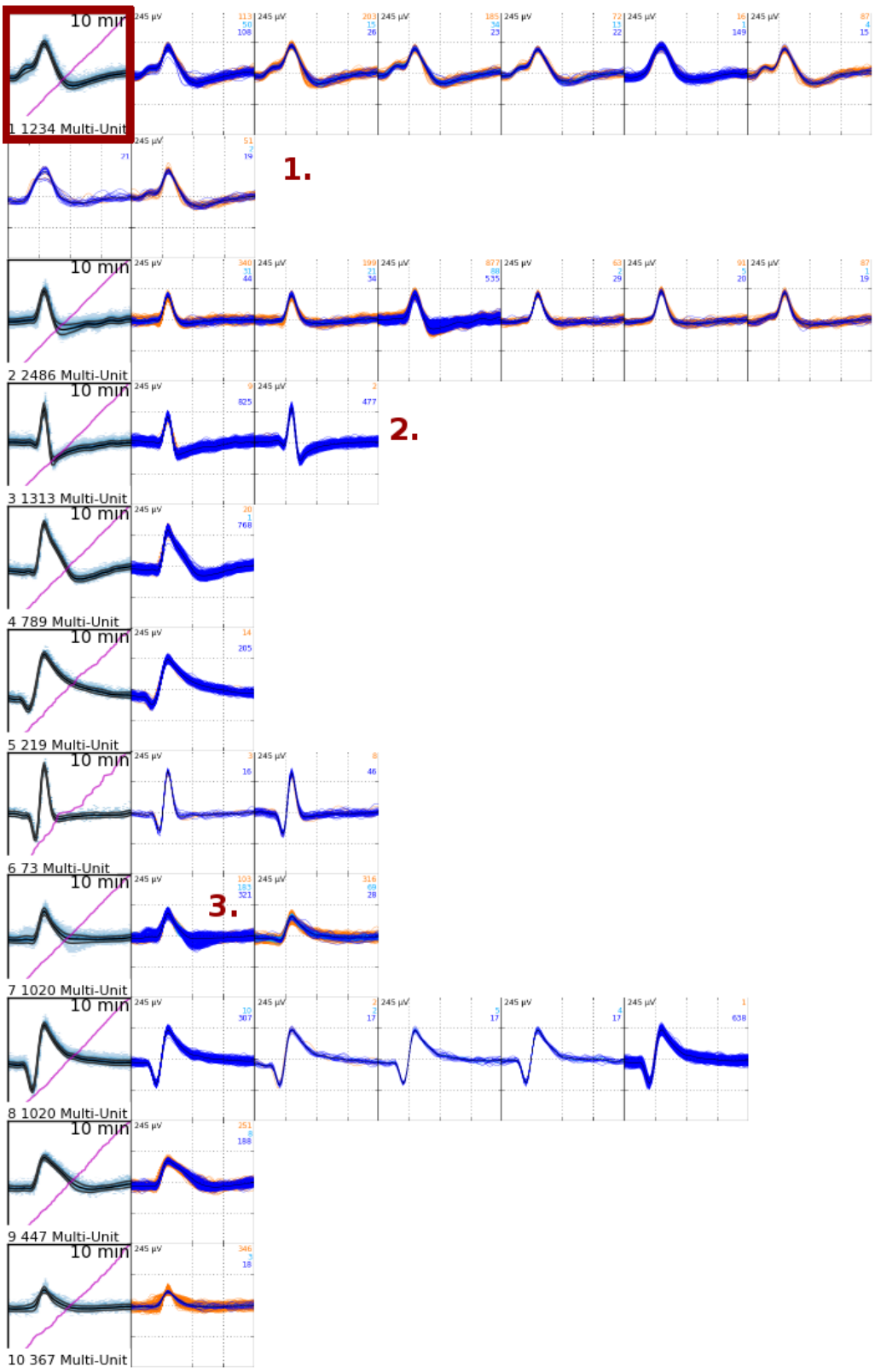

Figure A.4: **Optimized clustering results from Simulation 5.** Compared to the original result (Fig. A.1), the number of clusters has increased. The ground truth, which is available because this is simulated data, confirms that the new result is better, as visual inspection suggests.

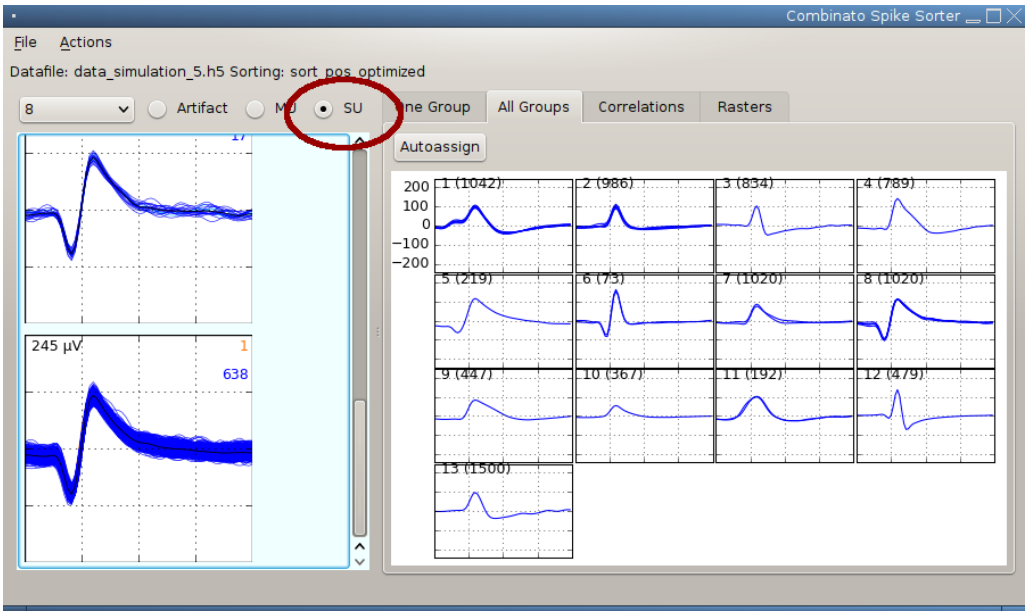

Figure A.5: **Setting units to single unit in the Combinato GUI.** The red ellipse indicates the button used to save a unit as *Single Unit*.

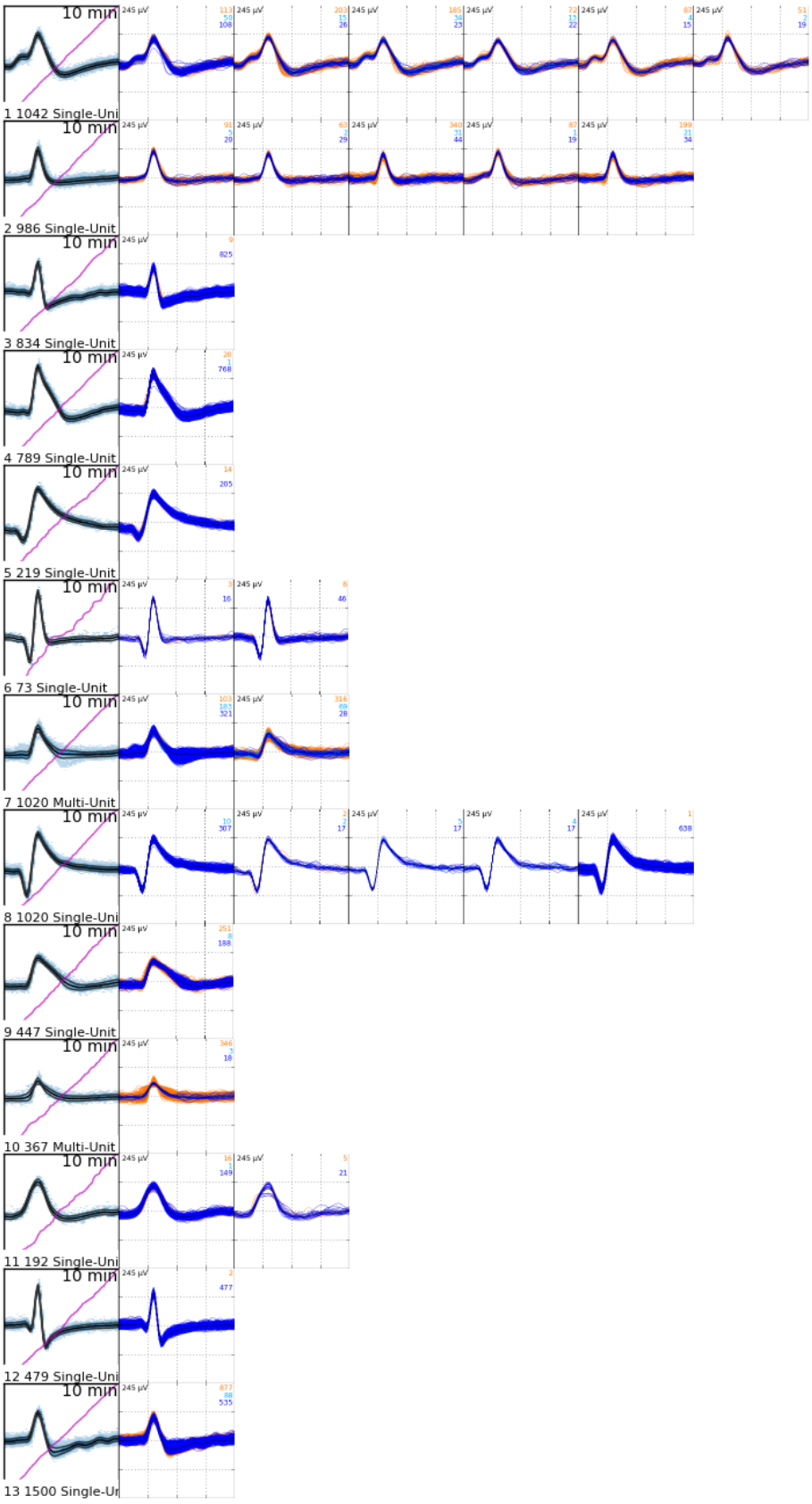

Figure A.6: **Manually optimized clustering results of Simulation 5.** The problems indicated in Fig. A.4 have been resolved.

A.2.3 Working with real data

In this part of the tutorial we will finally work with real data recorded from the right hippocampus.

Downloading the data

Download the file `CSC67.ncs` from

`https://uni-bonn.sciebo.de/index.php/s/K1NLbTjVmO1Hx19`.

The password is `combi_data`.

Extracting spikes and masking artifacts

First make sure to delete the files `local_options.py` and `local_options.pyc`, should they still be present from the previous parts of the tutorial.

Similar to before, run

`css-extract --files CSC67.ncs`.

to extract spikes. Then run

`css-mask-artifacts --datafile CSC67/data_CSC67.h5`

to mask artifacts before spike sorting.

Creating raw data graphics

- Run `css-plot-rawsignal` to create an overview plot of the raw signal (Fig. A.7).
- Run `css-plot-extracted --datafile CSC67/data_CSC67.h5` to create an overview plot of the extracted spikes before sorting (Fig. A.8).

Both plots are saved in the `overview` folder. You can use the program `css-overview-gui` to visualize summary statistics of all channels, and to quickly display the overview plots (see Fig. A.9 for a screenshot).

Clustering the data

Just as before, run

`css-simple-clustering --datafile CSC67/data_CSC67.h5`.

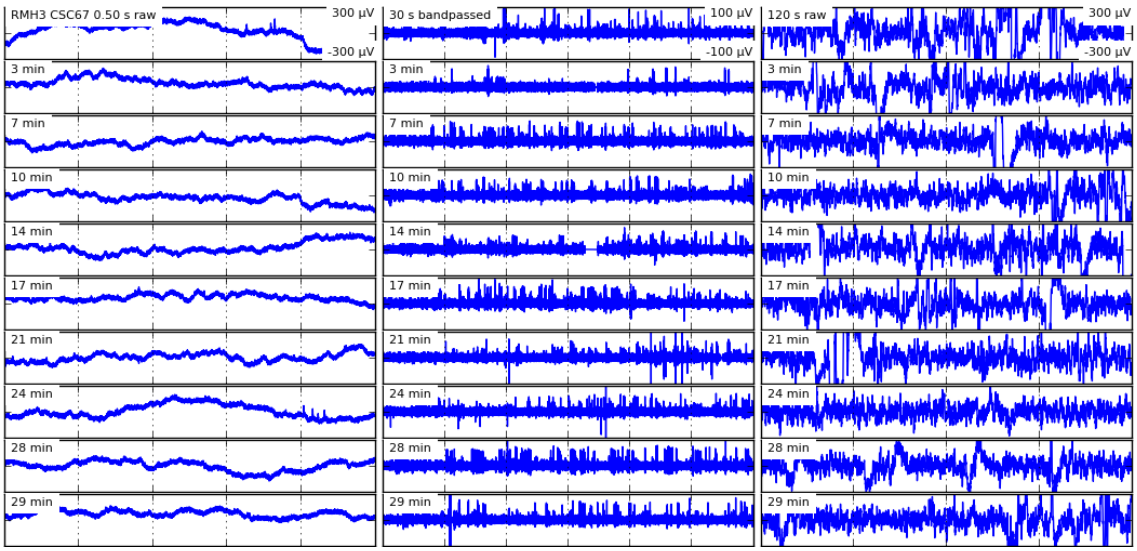

Figure A.7: **Plot of raw signal.** Each of the three columns shows the same data at a different temporal resolution: window durations are 500 ms, 30 s, and 2 min, respectively. Data in the middle column are bandpass filtered for display (elliptic filter, passband 300 Hz to 1000 Hz). Individual action potentials are visible in the left and middle columns.

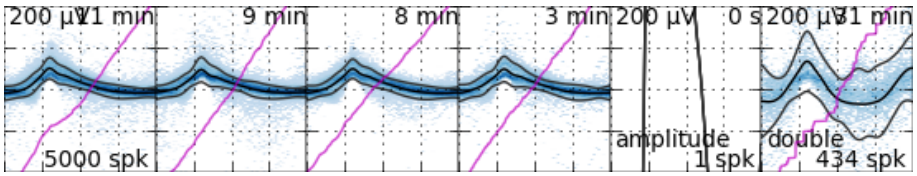

Figure A.8: **Plot of extracted spikes *before* spike sorting.** Each box contains a density plot of up to 5000 spikes. Pink lines indicate the cumulative spike count over the duration indicated. Boxes marked "amplitude" or "double" show spikes marked as artifacts due to the "high amplitude" or "double detection" artifact criteria (see Section 3.2 for details).

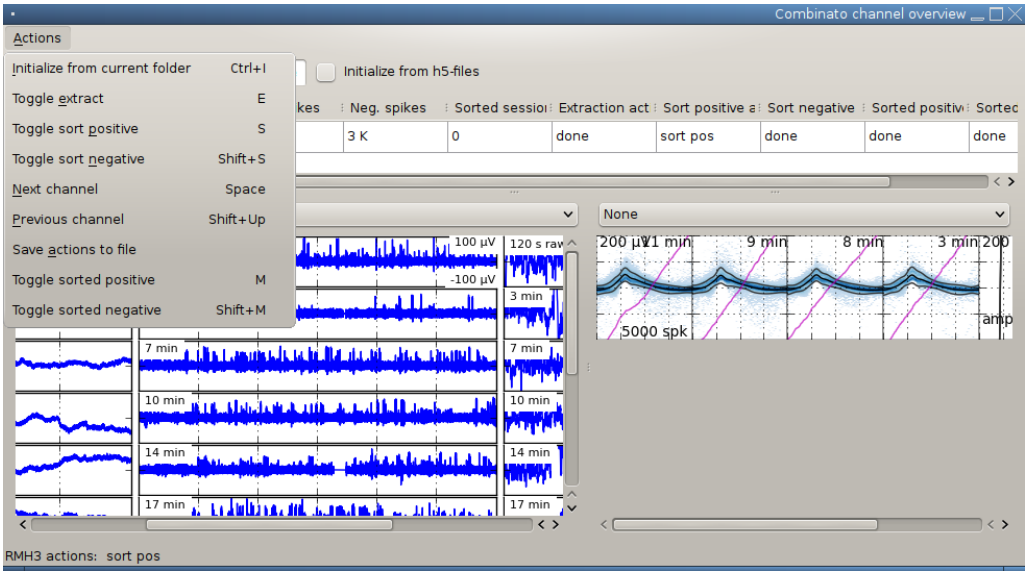

Figure A.9: **Screenshot of the Combinato Overview GUI.** This program displays the information contained in Figs. A.7 and A.8 in a convenient way.

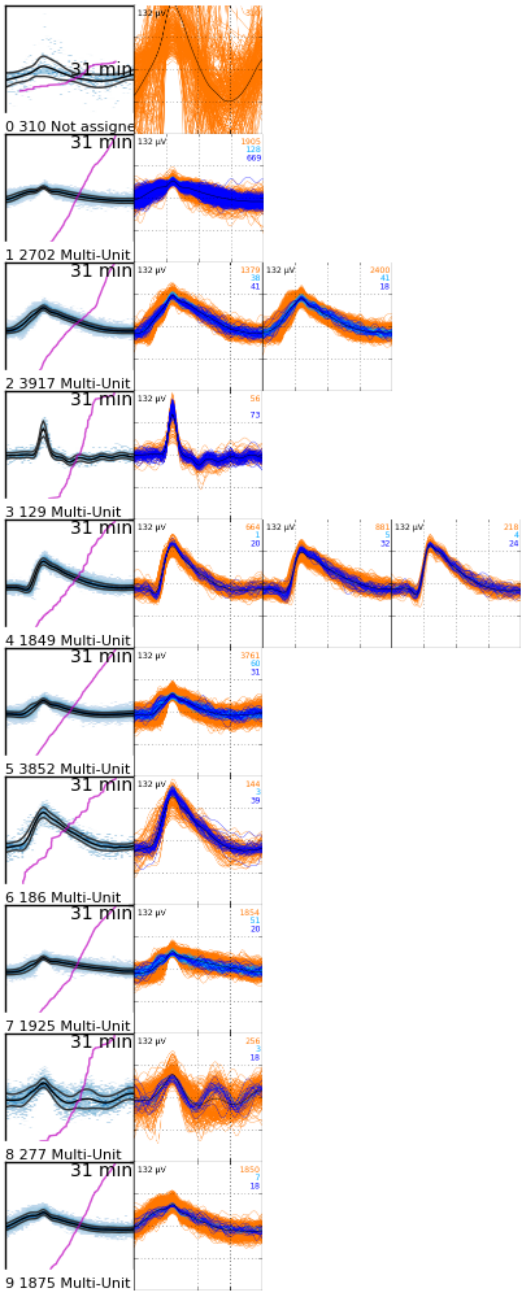

Figure A.10: **Plot of sorted spikes from CSC67.** Units 3 and 8 are artifacts. Units 5 and 7 should be merged.

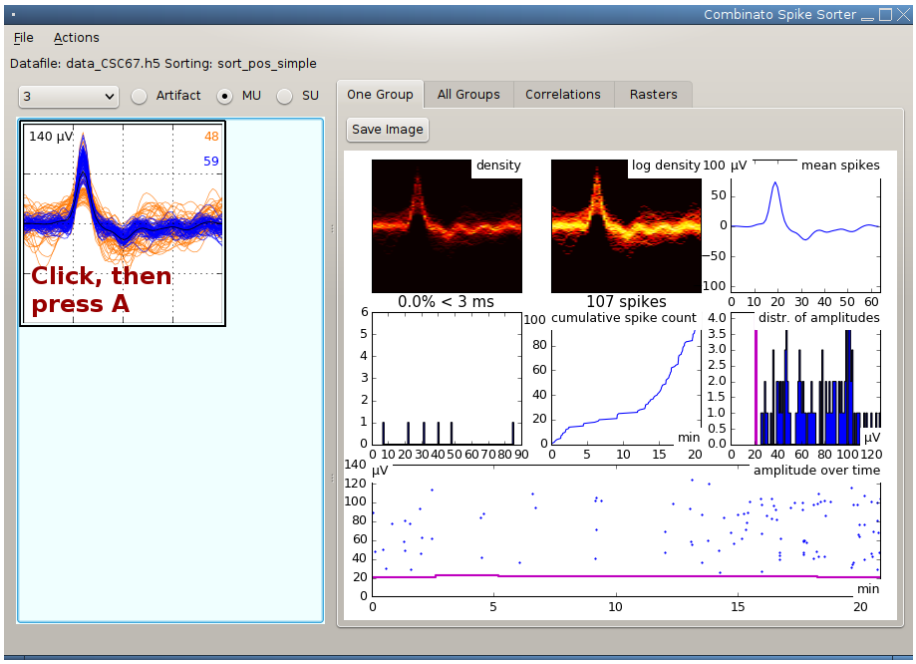

Figure A.11: **Marking artifacts.** The key `A` denotes a cluster as artifact.

Checking the spike sorting results

Using overview plots Run `css-plot-sorted --datafile CSC67/data_CSC67.h5 --label sort_pos_simple` to create the overview plot shown in Fig. A.10. You can display this overview plot within `css-overview-gui`, which is useful especially if you work with *job files* (not part of the tutorial). Fig. A.10 reveals a few points that can be optimized:

- Units 3 and 8 are artifacts,
- Units 5 and 7 look similar and should be merged.

We will use the `css-gui` to fix these problems.

Using the graphical user interface Open `css-gui` and load `CSC67` (File, Open). Then find the artifacts in the pull down menu. To move a cluster to the group *Artifacts*, just click on it and press `A` (see Fig. A.11). To decide whether to merge units 5 and 7 or not, use the Tab *Correlations*, as shown in Fig. A.12.

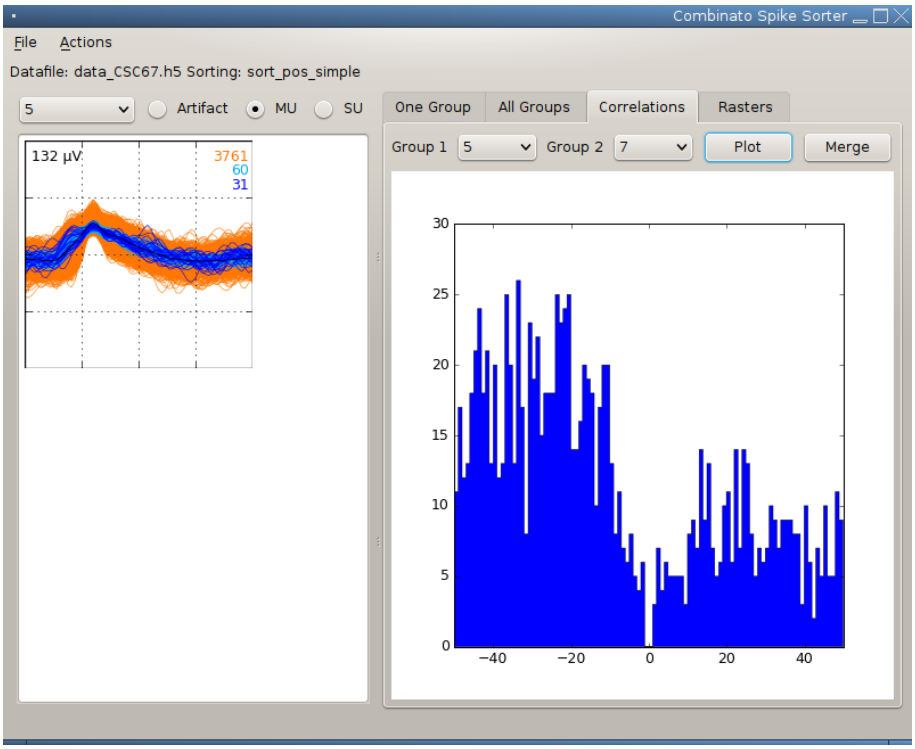

Figure A.12: **Cross-correlogram displayed in the Combinato GUI.** Cross-correlograms are very useful in deciding if two given clusters contain spikes from the same neuron.

Outlook

Combinato offers many possibilities not discussed in the tutorial. Among these are

- Splitting the clustering–merging procedure into individual steps for fine-tuning,
- Working with job files created in `css-overview-gui`,
- Extracting or sorting only parts of data files, indicated by time ranges,
- Excluding time ranges from the sorting procedure (e.g., to avoid known periods of signal contamination),
- And many more.

Also use `--help` as an option to all `css-*` programs to obtain more detailed information.

Working with raster plots

One very handy feature of Combinato are its automatically updating raster plots in `css-gui`. As you can see in Fig. A.13, unit 4 responded to the tie (both to the image and the written name in German), and unit 5 responded to the strawberry (picture only).

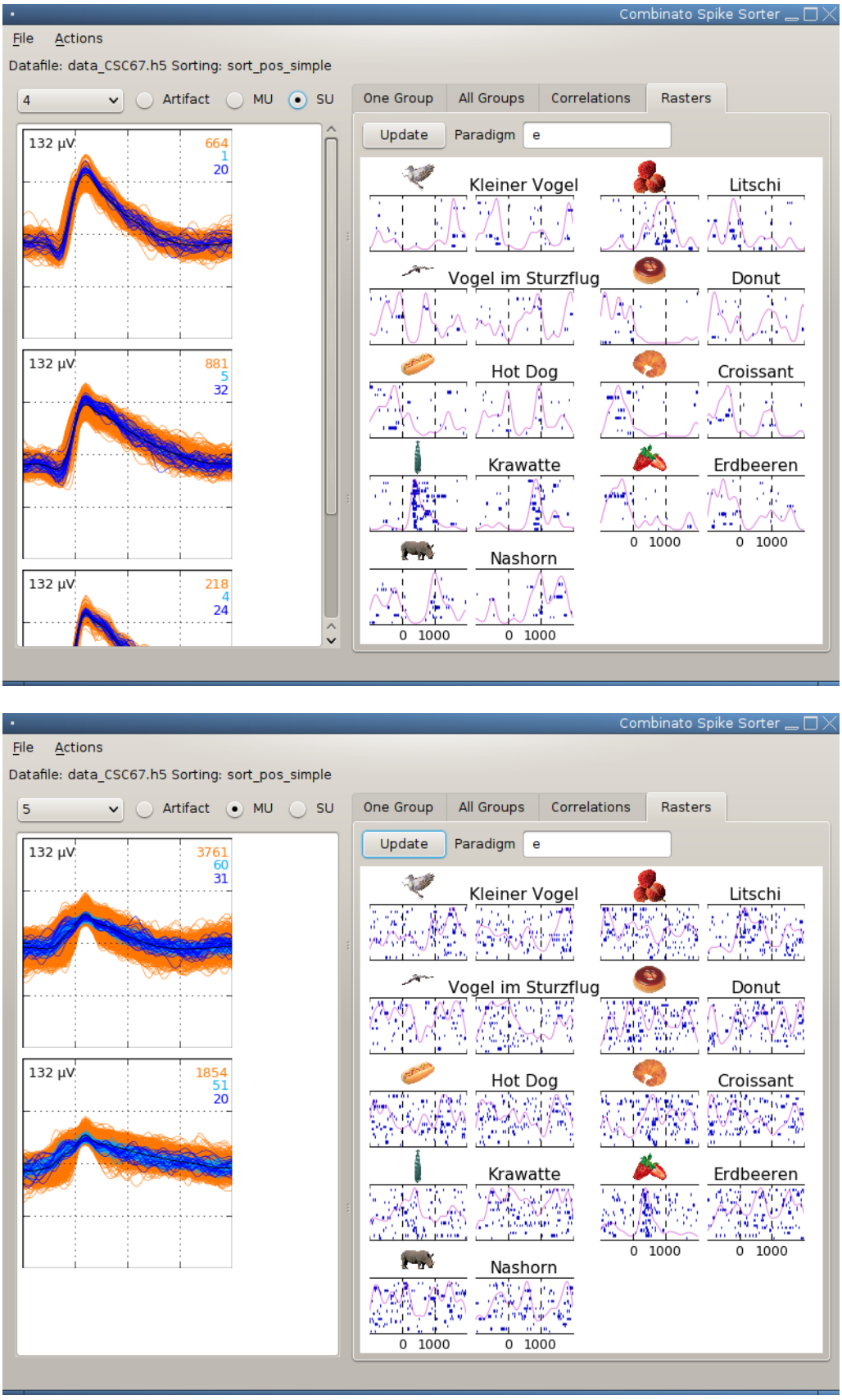

Figure A.13: **The Combinato GUI contains updating raster plots for visually presented stimuli. Top,** unit 4 responded to the tie (picture and written name). **Bottom,** unit 5 responded to the strawberry (picture only).

Appendix B

Contributions

Surgical procedures and handling of microwires

All surgical procedures (see Section 2.2) were performed by Prof. Dr. Jan Boström (Department of Neurosurgery, University of Bonn), or Prof. Dr. Volker A. Coenen (Stereotaxy and MR based OR Techniques, Department of Neurosurgery, University of Bonn; now Department of Neurosurgery, University of Freiburg).

All handling of microwires during surgeries was performed by Prof. Dr. Dr. Florian Mormann (Department of Epileptology, University of Bonn).

Sleep staging

Sleep staging (see Section 4.1.2) was performed by the author, or, in some cases, by Dr. Heidemarie Gast (Department of Epileptology, University of Bonn; now Department of Neurology, Inselspital Bern, Switzerland).

Fotonovela experiments

The Fotonovela experiments (see Section 4.1.5) were performed by the author, or, in some cases, by Dr. Thomas P. Reber (Department of Epileptology, University of Bonn), Dr. Heidemarie Gast (Department of Epileptology, University of Bonn; now Department of Neurology, Inselspital Bern, Switzerland), and Prof. Dr. Dr. Florian Mormann (Department of Epileptology, University of Bonn).

CRediT category	Persons
Conceptualization	JN FM
Data curation	JN FM
Formal analysis	JN
Funding acquisition	FM CEE
Investigation	JN FM JB
Methodology	JN
Project administration	FM
Resources	CEE
Software	JN
Supervision	FM
Validation	JN
Visualization	JN FM
Writing – original draft	JN
Writing – review & editing	JN FM JB CEE

Table B.1: **Contributions to Niediek, Boström, et al. (2016) according to CRediT.** JB, Jan Boström; CEE, Christian E. Elger; FM, Florian Mormann; JN, Johannes Niediek.

Contributions to Niediek, Boström, et al. (2016) according to CRediT

We reproduce in Table B.1 the contributions to Niediek, Boström, et al. (2016) according to PLOS policy and the "contributer role taxonomy" (CRediT; Allen, Scott, et al. 2014; Brand, Allen, et al. 2015).

References

Allen L., Scott J., Brand A., Hlava M., Altman M. (2014). *Publishing: Credit where credit is due*. Nature 508 (7496):312.

Alted F. (2010). *Why Modern CPUs Are Starving and What Can Be Done about It*. Comput. Sci. Eng. 12 (2):68–71.

Alvarez P., Squire L. R. (1994). *Memory consolidation and the medial temporal lobe: a simple network model*. Proc. Natl. Acad. Sci. U.S.A. 91 (15):7041–7045.

Amaral D., Lavenex P. (2007). *Hippocampal Neuroanatomy*. The Hippocampus Book. Ed. by P. Andersen, R. Morris, D. Amaral, T. Bliss, J. O'Keefe. Oxford: Oxford University Press, pp. 37–114.

Ambrose R. E., Pfeiffer B. E., Foster D. J. (2016). *Reverse Replay of Hippocampal Place Cells Is Uniquely Modulated by Changing Reward*. Neuron 91 (5):1124–1136.

Anagnostaras S. G., Maren S., Fanselow M. S. (1999). *Temporally graded retrograde amnesia of contextual fear after hippocampal damage in rats: within-subjects examination*. J. Neurosci. 19 (3):1106–1114.

Baddeley A. D. (2001). *Is working memory still working?* Am. Psychol. 56 (11):851–864.

Baddeley A. D., Hitch G. (1975). *Working Memory*. Psychology of Learning and Motivation. Ed. by G. H. Bower. Vol. 8. New York: Academic Press, pp. 47–89.

Bayley P. J., Hopkins R. O., Squire L. R. (2006). *The Fate of Old Memories after Medial Temporal Lobe Damage*. J. Neurosci. 26 (51):13311–13317.

Benjamini Y., Hochberg Y. (1995). *Controlling the False Discovery Rate: A Practical and Powerful Approach to Multiple Testing*. J. Royal Stat. Soc. B 57 (1):289–300.

Berényi A., Somogyvári Z., Nagy A. J., Roux L., Long J. D., Fujisawa S., Stark E., Leonardo A., Harris T. D., Buzsáki G. (2014). *Large-scale, high-density (up to 512 channels) recording of local circuits in behaving animals*. J. Neurophysiol. 111 (5):1132–1149.

Bi G.-Q., Poo M.-M. (1999). *Distributed synaptic modification in neural networks induced by patterned stimulation*. Nature 401 (6755):792–796.

Blatt M., Wiseman S., Domany E. (1996). *Superparamagnetic clustering of data*. Phys. Rev. Lett. 76 (18):3251–3254.

Bliss T. V. P., Collingridge G. L. (1993). *A synaptic model of memory: long-term potentiation in the hippocampus*. Nature 361 (6407):31.

Bliss T. V. P., Lømo T. (1973). *Long-lasting potentiation of synaptic transmission in the dentate area of the anaesthetized rabbit following stimulation of the perforant path*. J. Physiol. 232 (2):331–356.

Bondar I. V., Leopold D. A., Richmond B. J., Victor J. D., Logothetis N. K. (2009). *Long-Term Stability of Visual Pattern Selective Responses of Monkey Temporal Lobe Neurons*. PLOS ONE 4 (12):e8222.

Bragin A., Engel J., Wilson C. L., Fried I., Buzsáki G. (1999). *High-frequency oscillations in human brain*. Hippocampus 9 (2):137–142.

Brand A., Allen L., Altman M., Hlava M., Scott J. (2015). *Beyond authorship: attribution, contribution, collaboration, and credit*. Learn. Publ. 28 (2):151–155.

Bright P., Buckman J., Fradera A., Yoshimasu H., Colchester A. C., Kopelman M. D. (2006). *Retrograde amnesia in patients with hippocampal, medial temporal, temporal lobe, or frontal pathology*. Learn. Mem. 13 (5):545–557.

Burnos S., Hilfiker P., Sürücü O., Scholkmann F., Krayenbühl N., Grunwald T., Sarnthein J. (2014). *Human Intracranial High Frequency Oscillations (HFOs) Detected by Automatic Time-Frequency Analysis*. PLOS ONE 9 (4):e94381.

Buzsáki G. (1986). *Hippocampal sharp waves: their origin and significance*. Brain Res. 398 (2):242–252.

— (1989). *Two-stage model of memory trace formation: A role for "noisy" brain states*. Neuroscience 31 (3):551–570.

— (1996). *The Hippocampo-Neocortical Dialogue*. Cereb. Cortex 6 (2):81–92.

— (2015). *Hippocampal sharp wave-ripple: A cognitive biomarker for episodic memory and planning*. Hippocampus 25 (10):1073–1188.

Buzsáki G., Horváth Z., Urioste R., Hetke J., Wise K. (1992). *High-frequency network oscillation in the hippocampus*. Science 256 (5059):1025–1027.

Clark R. E., West A. N., Zola-Morgan S., Squire L. R. (2001). *Rats with lesions of the hippocampus are impaired on the delayed nonmatching-to-sample task*. Hippocampus 11 (2):176–186.

Cohen J. (1960). *A Coefficient of Agreement for Nominal Scales*. Educ. Psychol. Meas. 20 (1):37–46.

Cohen M. R., Kohn A. (2011). *Measuring and interpreting neuronal correlations*. Nat. Neurosci. 14 (7):811–819.

Cohen N. J., Squire L. R. (1980). *Preserved learning and retention of pattern-analyzing skill in amnesia: dissociation of knowing how and knowing that*. Science 210 (4466):207–210.

Corkin S. (2002). *What's new with the amnesic patient H.M.?* Nat. Rev. Neurosci. 3 (2):153–160.

Corkin S., Amaral D. G., González R. G., Johnson K. A., Hyman B. T. (1997). *H. M.'s Medial Temporal Lobe Lesion: Findings from Magnetic Resonance Imaging*. J. Neurosci. 17 (10):3964–3979.

Dan Y., Poo M.-M. (2006). *Spike Timing-Dependent Plasticity: From Synapse to Perception*. Physiol. Rev. 86 (3):1033–1048.

Davidson T. J., Kloosterman F., Wilson M. A. (2009). *Hippocampal Replay of Extended Experience*. Neuron 63 (4):497–507.

Diba K., Buzsáki G. (2007). *Forward and reverse hippocampal place-cell sequences during ripples*. Nat. Neurosci. 10 (10):1241–1242.

Diekelmann S., Born J. (2010). *The memory function of sleep*. Nat. Rev. Neurosci. 11:114–126.

Ebbinghaus H. (1885). *Über das Gedächtnis. Untersuchungen zur experimentellen Psychologie.* Leipzig: Duncker & Humblot.

— (1913). *Memory: A Contribution to Experimental Psychology*. Trans. by H. A. Ruger, C. E. Bussenius. New York: Teachers College, Columbia University.

Ego-Stengel V., Wilson M. A. (2010). *Disruption of ripple-associated hippocampal activity during rest impairs spatial learning in the rat*. Hippocampus 20 (1):1–10.

Einevoll G. T., Franke F., Hagen E., Pouzat C., Harris K. D. (2012). *Towards reliable spike-train recordings from thousands of neurons with multielectrodes*. Curr. Opin. Neurobiol. 22 (1):11–17.

Ekstrom A. D., Kahana M. J., Caplan J. B., Fields T. A., Isham E. A., Newman E. L., Fried I. (2003). *Cellular networks underlying human spatial navigation*. Nature 425 (6954):184–188.

Fisher R. S., Acevedo C., Arzimanoglou A., Bogacz A., Cross J. H., Elger C. E., Engel J., Forsgren L., French J. A., Glynn M., Hesdorffer D. C., Lee B., Mathern G. W., Moshé S. L., Perucca E., Scheffer I. E., Tomson T., Watanabe M., Wiebe S. (2014). *ILAE Official Report: A practical clinical definition of epilepsy*. Epilepsia 55 (4):475–482.

Fisher R. S., Cross J. H., French J. A., Higurashi N., Hirsch E., Jansen F. E., Lagae L., Moshé S. L., Peltola J., Roulet Perez E., Scheffer I. E., Zuberi S. M. (2017). *Operational classification of seizure types by the International League Against Epilepsy: Position Paper of the ILAE Commission for Classification and Terminology*. Epilepsia 58 (4):522–530.

Foster D. J., Wilson M. A. (2006). *Reverse replay of behavioural sequences in hippocampal place cells during the awake state*. Nature 440 (7084):680–683.

Frankland P. W., Bontempi B. (2005). *The organization of recent and remote memories*. Nat. Rev. Neurosci. 6 (2):119–130.

Fried I. (2014). *The Neurosurgical Theater of the Mind*. Single Neuron Studies of the Human Brain: Probing Cognition. Ed. by I. Fried, U. Rutishauser, M. Cerf, G. Kreiman. Cambridge, MA: The MIT Press, pp. 19–25.

Fried I., MacDonald K. A., Wilson C. L. (1997). *Single Neuron Activity in Human Hippocampus and Amygdala during Recognition of Faces and Objects*. Neuron 18 (5):753–765.

Fried I., Wilson C. L., Maidment N. T., Engel J., Behnke E., Fields T. A., Macdonald K. A., Morrow J. W., Ackerson L. (1999). *Cerebral microdialysis combined with single-neuron and electroencephalographic recording in neurosurgical patients*. J. Neurosurg. 91 (4):697–705.

Friedman A., Keselman M. D., Gibb L. G., Graybiel A. M. (2015). *A multistage mathematical approach to automated clustering of high-dimensional noisy data*. Proc. Natl. Acad. Sci. U.S.A. 112 (14):4477–4482.

Gast H., Niediek J., Schindler K., Boström J., Coenen V. A., Beck H., Elger C. E., Mormann F. (2016). *Burst firing of single neurons in the human medial temporal lobe changes before epileptic seizures*. Clin. Neurophysiol. 127 (10):3329–3334.

Gazzaniga M., Ivry R. B., Mangun G. R. (2013). *Cognitive Neuroscience: The Biology of the Mind*. 4th ed. New York: W. W. Norton & Company.

Gelbard-Sagiv H., Mukamel R., Harel M., Malach R., Fried I. (2008). *Internally Generated Reactivation of Single Neurons in Human Hippocampus During Free Recall*. Science 322 (5898):96–101.

Girardeau G., Benchenane K., Wiener S. I., Buzsáki G., Zugaro M. B. (2009). *Selective suppression of hippocampal ripples impairs spatial memory*. Nat. Neurosci. 12 (10):1222–1223.

Girardeau G., Inema I., Buzsáki G. (2017). *Reactivations of emotional memory in the hippocampus–amygdala system during sleep*. Nat. Neurosci. 20 (11):1634.

Graf P., Schacter D. L. (1985). *Implicit and explicit memory for new associations in normal and amnesic subjects.* J. Exp. Psychol. Learn. Mem. Cogn. 11 (3):501–518.

Gramfort A., Luessi M., Larson E., Engemann D. A., Strohmeier D., Brodbeck C., Goj R., Jas M., Brooks T., Parkkonen L., Hämäläinen M. (2013). *MEG and EEG data analysis with MNE-Python*. Front. Neurosci. 7:267.

Gramfort A., Luessi M., Larson E., Engemann D. A., Strohmeier D., Brodbeck C., Parkkonen L., Hämäläinen M. S. (2014). *MNE software for processing MEG and EEG data*. Neuroimage 86 (Supplement C):446–460.

Hagen E., Ness T. V., Khosrowshahi A., Sørensen C., Fyhn M., Hafting T., Franke F., Einevoll G. T. (2015). *ViSAPy: a Python tool for biophysics-based generation of virtual spiking activity for evaluation of spike-sorting algorithms*. J. Neurosci. Methods 245:182–204.

Harris K. D., Henze D. A., Csicsvari J., Hirase H., Buzsáki G. (2000). *Accuracy of Tetrode Spike Separation as Determined by Simultaneous Intracellular and Extracellular Measurements*. J. Neurophysiol. 84 (1):401–414.

Hebb D. O. (1949). *The Organization of Behavior: a Neuropsychological Theory*. New York: Wiley. Reprint edition: Lawrence Erlbaum Associates, Mahwah, NJ, 2002.

Hedges L. V. (1981). *Distribution Theory for Glass's Estimator of Effect Size and Related Estimators*. J. Educ. Stat. 6 (2):107.

Heit G., Smith M. E., Halgren E. (1988). *Neural encoding of individual words and faces by the human hippocampus and amygdala*. Nature 333 (6175):773–775.

Hill D. N., Mehta S. B., Kleinfeld D. (2011). *Quality Metrics to Accompany Spike Sorting of Extracellular Signals*. J. Neurosci. 31 (24):8699–8705.

Howard M. W., Fotedar M. S., Datey A. V., Hasselmo M. E. (2005). *The Temporal Context Model in Spatial Navigation and Relational Learning: Toward a Common Explanation of Medial Temporal Lobe Function Across Domains.* Psychol. Rev. 112 (1):75–116.

Iber C., Ancoli-Israel S., Chesson A., Quan S. F. (2007). *The AASM Manual for the Scoring of Sleep and Associated Events: Rules, Terminology and Technical Specifications*. Darien, IL: American Academy of Sleep Medicine.

Ison M. J., Mormann F., Cerf M., Koch C., Fried I., Quian Quiroga R. (2011). *Selectivity of pyramidal cells and interneurons in the human medial temporal lobe*. J. Neurophysiol. 106 (4):1713–1721.

Ison M. J., Quian Quiroga R., Fried I. (2015). *Rapid Encoding of New Memories by Individual Neurons in the Human Brain*. Neuron 87 (1):220–230.

Jacobs J., Kahana M. J., Ekstrom A. D., Mollison M. V., Fried I. (2010). *A sense of direction in human entorhinal cortex*. Proc. Natl. Acad. Sci. U.S.A. 107 (14):6487–6492.

Ji D., Wilson M. A. (2007). *Coordinated memory replay in the visual cortex and hippocampus during sleep*. Nat. Neurosci. 10 (1):100–107.

Kadir S. N., Goodman D. F. M., Harris K. D. (2014). *High-Dimensional Cluster Analysis with the Masked EM Algorithm*. Neural Comput. 26 (11):2379–2394.

Kahana M. J. (1996). *Associative retrieval processes in free recall*. Mem. Cogn. 24 (1):103–109.

Kamiński J., Sullivan S., Chung J. M., Ross I. B., Mamelak A. N., Rutishauser U. (2017). *Persistently active neurons in human medial frontal and medial temporal lobe support working memory*. Nat. Neurosci. 20 (4):590.

Kandel E. R., Dudai Y., Mayford M. R. (2014). *The Molecular and Systems Biology of Memory*. Cell 157 (1):163–186.

Kim J. J., Fanselow M. S. (1992). *Modality-specific retrograde amnesia of fear*. Science 256 (5057):675–677.

Kirchner H., Thorpe S. J. (2006). *Ultra-rapid object detection with saccadic eye movements: Visual processing speed revisited*. Vis. Res. 46 (11):1762–1776.

Kleiner M., Brainard D., Pelli D. (2007). *What's new in Psychtoolbox-3?* Perception 36 ECVP Abstract Supplement.

Knieling S., Niediek J., Kutter E., Boström J., Elger C. E., Mormann F. (2017). *An online adaptive screening procedure for selective neuronal responses*. J. Neurosci. Methods 291:36–42.

Knieling S., Sridharan K. S., Belardinelli P., Naros G., Weiss D., Mormann F., Gharabaghi A. (2015). *An Unsupervised Online Spike-Sorting Framework*. Int. J. Neural Syst. 26:1550042.

Kopelman M. D., Wilson B. A., Baddeley A. D. (1989). *The autobiographical memory interview: A new assessment of autobiographical and personal semantic memory in amnesic patients*. J. Clin. Exp. Neuropsychol. 11 (5):724–744.

Kornblith S., Quian Quiroga R., Koch C., Fried I., Mormann F. (2017). *Persistent Single-Neuron Activity during Working Memory in the Human Medial Temporal Lobe*. Curr. Biol. 27 (7):1026–1032.

Kreiman G., Koch C., Fried I. (2000). *Category-specific visual responses of single neurons in the human medial temporal lobe*. Nat. Neurosci. 3 (9):946–953.

Kudrimoti H. S., Barnes C. A., McNaughton B. L. (1999). *Reactivation of Hippocampal Cell Assemblies: Effects of Behavioral State, Experience, and EEG Dynamics*. J. Neurosci. 19 (10):4090–4101.

Lee A. K., Wilson M. A. (2002). *Memory of Sequential Experience in the Hippocampus during Slow Wave Sleep*. Neuron 36 (6):1183–1194.

Levy W. B., Steward O. (1983). *Temporal contiguity requirements for long-term associative potentiation/depression in the hippocampus*. Neuroscience 8 (4):791–797.

Louie K., Wilson M. A. (2001). *Temporally Structured Replay of Awake Hippocampal Ensemble Activity during Rapid Eye Movement Sleep*. Neuron 29 (1):145–156.

Maingret N., Girardeau G., Todorova R., Goutierre M., Zugaro M. (2016). *Hippocampo-cortical coupling mediates memory consolidation during sleep*. Nat. Neurosci. 19 (7):959–964.

Manns J. R., Hopkins R. O., Squire L. R. (2003). *Semantic memory and the human hippocampus*. Neuron 38 (1):127–133.

Markram H., Lübke J., Frotscher M., Sakmann B. (1997). *Regulation of Synaptic Efficacy by Coincidence of Postsynaptic APs and EPSPs*. Science 275 (5297):213–215.

Marr D. (1970). *A theory for cerebral neocortex*. Proc. Royal Soc. B 176 (1043):161–234.

— (1971). *Simple memory: a theory for archicortex*. Philos. Trans. Royal Soc. B 262 (841):23–81.

Marshall L., Helgadóttir H., Mölle M., Born J. (2006). *Boosting slow oscillations during sleep potentiates memory*. Nature 444 (7119):610.

Martinez J., Pedreira C., Ison M. J., Quian Quiroga R. (2009). *Realistic simulation of extracellular recordings*. J. Neurosci. Methods 184 (2):285–293.

McClelland J. L., McNaughton B. L., O'Reilly R. C. (1995). *Why there are complementary learning systems in the hippocampus and neocortex: insights from the successes and failures of connectionist models of learning and memory*. Psychol. Rev. 102 (3):419–457.

Miller J. F., Neufang M., Solway A., Brandt A., Trippel M., Mader I., Hefft S., Merkow M., Polyn S. M., Jacobs J., Kahana M. J., Schulze-Bonhage A. (2013). *Neural Activity in Human Hippocampal Formation Reveals the Spatial Context of Retrieved Memories*. Science 342 (6162):1111–1114.

Mishkin M. (1978). *Memory in monkeys severely impaired by combined but not by separate removal of amygdala and hippocampus*. Nature 273 (5660):297–298.

Misra A., Burke J. F., Ramayya A. G., Jacobs J., Sperling M. R., Moxon K. A., Kahana M. J., Evans J. J., Sharan A. D. (2014). *Methods for implantation of micro-wire bundles and optimization of single/multi-unit recordings from human mesial temporal lobe*. J. Neural. Eng. 11 (2):026013.

Mizuseki K., Buzsáki G. (2013). *Preconfigured, Skewed Distribution of Firing Rates in the Hippocampus and Entorhinal Cortex*. Cell Rep. 4 (5):1010–1021.

Mormann F., Andrzejak R. G., Elger C. E., Lehnertz K. (2007). *Seizure prediction: the long and winding road*. Brain 130 (2):314–333.

Mormann F., Dubois J., Kornblith S., Milosavljevic M., Cerf M., Ison M., Tsuchiya N., Kraskov A., Quian Quiroga R., Adolphs R., Fried I., Koch C. (2011). *A category-specific response to animals in the right human amygdala*. Nat. Neurosci. 14 (10):1247–1249.

Mormann F., Kornblith S., Cerf M., Ison M. J., Kraskov A., Tran M., Knieling S., Quian Quiroga R., Koch C., Fried I. (2017). *Scene-selective coding by single neurons in the human parahippocampal cortex*. Proc. Natl. Acad. Sci. U.S.A. 114 (5):1153–1158.

Mormann F., Kornblith S., Quian Quiroga R., Kraskov A., Cerf M., Fried I., Koch C. (2008). *Latency and Selectivity of Single Neurons Indicate Hierarchical Processing in the Human Medial Temporal Lobe*. J. Neurosci. 28 (36):8865–8872.

Mormann F., Niediek J., Tudusciuc O., Quesada C. M., Coenen V. A., Elger C. E., Adolphs R. (2015). *Neurons in the human amygdala encode face identity, but not gaze direction*. Nat. Neurosci. 18 (11):1568–1570.

Morris R., Anderson E., Lynch G. S., Baudry M. (1986). *Selective impairment of learning and blockade of long-term potentiation by an N-methyl-D-aspartate receptor antagonist, AP5*. Nature 319 (6056):774.

Morris R. (2007). *Theories of Hippocampal Function*. The Hippocampus Book. Ed. by P. Andersen, R. Morris, D. Amaral, T. Bliss, J. O'Keefe. Oxford: Oxford University Press, pp. 581–713.

Nadel L., Moscovitch M. (1997). *Memory consolidation, retrograde amnesia and the hippocampal complex*. Curr. Opin. Neurobiol. 7 (2):217–227.

Nadel L. (1994). *Multiple Memory Systems: What and Why, an Update*. Memory Systems 1994. Ed. by D. L. Schacter, E. Tulving. Cambridge, MA: MIT Press, pp. 39–63.

Ngugi A. K., Bottomley C., Kleinschmidt I., Sander J. W., Newton C. R. (2010). *Estimation of the burden of active and life-time epilepsy: A meta-analytic approach*. Epilepsia 51 (5):883–890.

Ngugi A. K., Kariuki S. M., Bottomley C., Kleinschmidt I., Sander J. W., Newton C. R. (2011). *Incidence of epilepsy: a systematic review and meta-analysis*. Neurology 77 (10):1005–1012.

Niediek J., Bain J. (2014). *Human single-unit recordings reveal a link between place-cells and episodic memory*. Front. Syst. Neurosci. 8:158.

Niediek J., Boström J., Elger C. E., Mormann F. (2016). *Reliable Analysis of Single-Unit Recordings from the Human Brain under Noisy Conditions: Tracking Neurons over Hours*. PLOS ONE 11 (12):e0166598.

Niediek J., Navratil M., Coenen V. A., Elger C. E., Söhle M., Mormann F. (2013). *Single units in the human medial temporal lobe during propofol anesthesia*. Program No. 570.16. 2013 Neuroscience Meeting Planner. San Diego, CA: Society for Neuroscience.

Nieuwenhuys R., Voogd J., van Huijzen C. (2007). *The Human Central Nervous System: A Synopsis and Atlas*. 4th ed. Berlin: Springer.

Nir Y., Staba R. J., Andrillon T., Vyazovskiy V. V., Cirelli C., Fried I., Tononi G. (2011). *Regional Slow Waves and Spindles in Human Sleep*. Neuron 70 (1):153–169.

O'Keefe J. (1976). *Place units in the hippocampus of the freely moving rat*. Exp. Neurol. 51 (1):78–109.

O'Keefe J., Dostrovsky J. (1971). *The hippocampus as a spatial map. Preliminary evidence from unit activity in the freely-moving rat*. Brain Res. 34 (1):171–175.

Pavlides C., Winson J. (1989). *Influences of hippocampal place cell firing in the awake state on the activity of these cells during subsequent sleep episodes*. J. Neurosci. 9 (8):2907–2918.

Pedreira C., Martinez J., Ison M. J., Quian Quiroga R. (2012). *How many neurons can we see with current spike sorting algorithms?* J. Neurosci. Methods 211 (1):58–65.

Peigneux P., Laureys S., Fuchs S., Collette F., Perrin F., Reggers J., Phillips C., Degueldre C., Fiore G. D., Aerts J., Luxen A., Maquet P. (2004). *Are Spatial Memories Strengthened in the Human Hippocampus during Slow Wave Sleep?* Neuron 44 (3):535–545.

Plihal W., Born J. (1997). *Effects of early and late nocturnal sleep on declarative and procedural memory*. J. Cogn. Neurosci. 9 (4):534–547.

Qin Y.-L., McNaughton B. L., Skaggs W. E., Barnes C. A. (1997). *Memory reprocessing in corticocortical and hippocampocortical neuronal ensembles*. Philos. Trans. Royal Soc. B 352 (1360):1525–1533.

Quian Quiroga R., Reddy L., Kreiman G., Koch C., Fried I. (2005). *Invariant visual representation by single neurons in the human brain*. Nature 435 (7045):1102–1107.

Quian Quiroga R. (2012). *Concept cells: the building blocks of declarative memory functions*. Nat. Rev. Neurosci. 13 (8):587–597.

Quian Quiroga R., Kraskov A., Koch C., Fried I. (2009). *Explicit Encoding of Multimodal Percepts by Single Neurons in the Human Brain*. Curr. Biol. 19 (15):1308–1313.

Quian Quiroga R., Nadasdy Z., Ben-Shaul Y. (2004). *Unsupervised Spike Detection and Sorting with Wavelets and Superparamagnetic Clustering*. Neural Comput. 16 (8):1661–1687.

Rama A. N., Cho S. C., Kushida C. A. (2006). *Normal Human Sleep*. Sleep: A Comprehensive Handbook. Ed. by T. Lee-Chiong. Hoboken, NJ: John Wiley & Sons, pp. 3–9.

Rasch B., Büchel C., Gais S., Born J. (2007). *Odor Cues During Slow-Wave Sleep Prompt Declarative Memory Consolidation*. Science 315 (5817):1426–1429.

Reber T. P., Faber J., Niediek J., Boström J., Elger C. E., Mormann F. (2017). *Single-Neuron Correlates of Conscious Perception in the Human Medial Temporal Lobe*. Curr. Biol. 27 (19):2991–2998.e2.

Rempel-Clower N. L., Zola-Morgan S., Squire L. R., Amaral D. G. (1996). *Three cases of enduring memory impairment after bilateral damage limited to the hippocampal formation*. J. Neurosci. 16 (16):5233–5255.

Rey H. G., Pedreira C., Quian Quiroga R. (2015). *Past, present and future of spike sorting techniques*. Brain Res. Bull. 119, Part B:106–117.

Ribot T. (1881). *Les maladies de la mémoire*. Paris: Librairie Germer Ballière.

Roediger H. L., Zaromb F. M., Goode M. K. (2008). *A Typology of Memory Terms*. Learning Theory and Behavior. Ed. by J. H. Byrne. Vol. 1. Learning and Memory: A Comprehensive Reference. New York: Academic Press, pp. 11–24.

Rossant C., Kadir S. N., Goodman D. F. M., Schulman J., Hunter M. L. D., Saleem A. B., Grosmark A., Belluscio M., Denfield G. H., Ecker A. S., Tolias A. S., Solomon S., Buzsáki G., Carandini M., Harris K. D. (2016). *Spike sorting for large, dense electrode arrays*. Nat. Neurosci. 19 (4):634–641.

Rudoy J. D., Voss J. L., Westerberg C. E., Paller K. A. (2009). *Strengthening Individual Memories by Reactivating Them During Sleep*. Science 326 (5956):1079–1079.

Rutishauser U., Mamelak A. N., Schuman E. M. (2006). *Single-Trial Learning of Novel Stimuli by Individual Neurons of the Human Hippocampus-Amygdala Complex*. Neuron 49 (6):805–813.

Rutishauser U., Ross I. B., Mamelak A. N., Schuman E. M. (2010). *Human memory strength is predicted by theta-frequency phase-locking of single neurons*. Nature 464 (7290):903–907.

Rutishauser U., Schuman E. M., Mamelak A. N. (2006). *Online detection and sorting of extracellularly recorded action potentials in human medial temporal lobe recordings, in vivo*. J. Neurosci. Methods 154 (1):204–224.

Rutishauser U., Tudusciuc O., Neumann D., Mamelak A. N., Heller A. C., Ross I. B., Philpott L., Sutherling W. W., Adolphs R. (2011). *Single-Unit Responses Selective for Whole Faces in the Human Amygdala*. Curr. Biol. 21 (19):1654–1660.

Rutishauser U., Ye S., Koroma M., Tudusciuc O., Ross I. B., Chung J. M., Mamelak A. N. (2015). *Representation of retrieval confidence by single neurons in the human medial temporal lobe*. Nat. Neurosci. 18 (7):1041–1050.

Ryle G. (1945). *Knowing how and knowing that: The presidential address*. Proceedings of the Aristotelian Society. Vol. 46. London: Wiley, pp. 1–16.

Sagar H. J., Cohen N. J., Corkin S., Growdon J. H. (1985). *Dissociations among processes in remote memory*. Ann. N. Y. Acad. Sci. 444:533–535.

Schacter D. L., Tulving E. (1994). *What are the Memory Systems of 1994?* Memory Systems 1994. Ed. by D. L. Schacter, E. Tulving. Cambridge, MA: MIT Press, pp. 2–38.

Schmitzer-Torbert N., Jackson J., Henze D., Harris K. D., Redish A. D. (2005). *Quantitative measures of cluster quality for use in extracellular recordings*. Neuroscience 131 (1):1–11.

Scoville W. B., Milner B. (1957). *Loss of Recent Memory after Bilateral Hippocampal Lesions*. J. Neurol. Neurosurg. Psychiatry 20 (1):11–21.

Shiffrin R. M., Atkinson R. C. (1969). *Storage and retrieval processes in long-term memory.* Psychol. Rev. 76 (2):179.

Skaggs W. E., McNaughton B. L. (1996). *Replay of Neuronal Firing Sequences in Rat Hippocampus During Sleep Following Spatial Experience*. Science 271 (5257):1870–1873.

Squire L. R. (1992). *Memory and the Hippocampus: A Synthesis From Findings With Rats, Monkeys, and Humans*. Psychol. Rev. 99 (2):195–231.

Squire L. R., Genzel L., Wixted J. T., Morris R. (2015). *Memory Consolidation*. Cold Spring Harb. Perspect. Biol. 7 (8):a021766.

Squire L. R., Wixted J. T. (2011). *The Cognitive Neuroscience of Human Memory Since H.M.* Annu. Rev. Neurosci. 34 (1):259–288.

Squire L. R., Zola-Morgan S. (1988). *Memory: brain systems and behavior*. Trends Neurosci. 11 (4):170–175.

— (1991). *The medial temporal lobe memory system*. Science 253 (5026):1380–1386.

Squire L. R., Zola-Morgan S., Chen K. S. (1988). *Human amnesia and animal models of amnesia: performance of amnesic patients on tests designed for the monkey.* Behav. Neurosci. 102 (2):210.

Squire L. R., Alvarez P. (1995). *Retrograde amnesia and memory consolidation: a neurobiological perspective*. Curr. Opin. Neurobiol. 5 (2):169–177.

Staba R. J., Fields T. A., Behnke E. J., Wilson C. L. (2014). *Subchronic In Vivo Human Microelectrode Recording*. Single Neuron Studies of the Human Brain: Probing Cognition. Ed. by I. Fried, U. Rutishauser, M. Cerf, G. Kreiman. Cambridge, MA: The MIT Press, pp. 43–58.

Staresina B. P., Bergmann T. O., Bonnefond M., van der Meij R., Jensen O., Deuker L., Elger C. E., Axmacher N., Fell J. (2015). *Hierarchical nesting of slow oscillations, spindles and ripples in the human hippocampus during sleep*. Nat. Neurosci. 18 (11):1679.

Stefanacci L., Buffalo E. A., Schmolck H., Squire L. R. (2000). *Profound amnesia after damage to the medial temporal lobe: A neuroanatomical and neuropsychological profile of patient EP*. J. Neurosci. 20 (18):7024–7036.

Stockwell R. G., Mansinha L., Lowe R. P. (1996). *Localization of the complex spectrum: the S transform*. IEEE Trans. Signal Process. 44 (4):998–1001.

Téllez-Zenteno J. F., Hernández-Ronquillo L. (2012). *A Review of the Epidemiology of Temporal Lobe Epilepsy*. Epilepsy Res. Treat. 2012:Article ID 630853.

Tolias A. S., Ecker A. S., Siapas A. G., Hoenselaar A., Keliris G. A., Logothetis N. K. (2007). *Recording Chronically From the Same Neurons in Awake, Behaving Primates*. J. Neurophysiol. 98 (6):3780–3790.

Tse D., Langston R. F., Kakeyama M., Bethus I., Spooner P. A., Wood E. R., Witter M. P., Morris R. (2007). *Schemas and Memory Consolidation*. Science 316 (5821):76–82.

Tulving E. (1972). *Episodic and Semantic Memory*. Organization of memory. Ed. by E. Tulving, W. Donaldson. Oxford: Academic Press, pp. 381–402.

— (1985). *Elements of Episodic Memory*. Oxford: Oxford University Press.

— (2002). *Episodic Memory: From Mind to Brain*. Annu. Rev. Psychol. 53 (1):1–25.

Veselis R. A., Pryor K. O., Reinsel R. A., Li Y., Mehta M., Johnson R. (2009). *Propofol and midazolam inhibit conscious memory processes very soon after encoding: an event-related potential study of familiarity and recollection in volunteers*. Anesthesiol. 110 (2):295–312.

Veselis R. A., Pryor K. O., Reinsel R. A., Mehta M., Pan H., Johnson R. (2008). *Low-dose propofol-induced amnesia is not due to a failure of encoding: left inferior prefrontal cortex is still active*. Anesthesiol. 109 (2):213–224.

Viskontas I. V., Quian Quiroga R., Fried I. (2009). *Human medial temporal lobe neurons respond preferentially to personally relevant images*. Proc. Natl. Acad. Sci. U.S.A. 106 (50):21329–21334.

Waydo S., Kraskov A., Quian Quiroga R., Fried I., Koch C. (2006). *Sparse Representation in the Human Medial Temporal Lobe*. J. Neurosci. 26 (40):10232–10234.

Wigström H., Gustafsson B., Huang Y.-Y., Abraham W. C. (1986). *Hippocampal long-term potentiation is induced by pairing single afferent volleys with intracellularly injected depolarizing current pulses*. Acta Physiol. Scand. 126 (2):317–319.

Wilson M. A., McNaughton B. L. (1994). *Reactivation of hippocampal ensemble memories during sleep*. Science 265 (5172):676–679.

Zola-Morgan S., Squire L. R., Amaral D. G. (1989a). *Lesions of the amygdala that spare adjacent cortical regions do not impair memory or exacerbate the impairment following lesions of the hippocampal formation*. J. Neurosci. 9 (6):1922–1936.

Zola-Morgan S., Squire L. R., Clower R. P., Rempel N. L. (1993). *Damage to the perirhinal cortex exacerbates memory impairment following lesions to the hippocampal formation*. J. Neurosci. 13 (1):251–265.

Zola-Morgan S., Squire L. R. (1986). *Memory impairment in monkeys following lesions limited to the hippocampus*. Behav. Neurosci. 100 (2):155.

— (1990). *The primate hippocampal formation: evidence for a time-limited role in memory storage*. Science 250 (4978):288–290.

— (1993). *Neuroanatomy of Memory*. Annu. Rev. Neurosci. 16 (1):547–563.

Zola-Morgan S., Squire L. R., Amaral D. G. (1986). *Human amnesia and the medial temporal region: enduring memory impairment following a bilateral lesion limited to field CA1 of the hippocampus*. J. Neurosci. 6 (10):2950–2967.

Zola-Morgan S., Squire L. R., Amaral D. G., Suzuki W. A. (1989b). *Lesions of perirhinal and parahippocampal cortex that spare the amygdala and hippocampal formation produce severe memory impairment*. J. Neurosci. 9 (12):4355–4370.

Zola-Morgan S., Squire L. R., Ramus S. J. (1994). *Severity of memory impairment in monkeys as a function of locus and extent of damage within the medial temporal lobe memory system*. Hippocampus 4 (4):483–495.

Zola-Morgan S., Squire L. R., Rempel N. L., Clower R. P., Amaral D. G. (1992). *Enduring memory impairment in monkeys after ischemic damage to the hippocampus*. J. Neurosci. 12 (7):2582–2596.